On the Effects of Moisture on Polymer-Based Electrochromic Devices

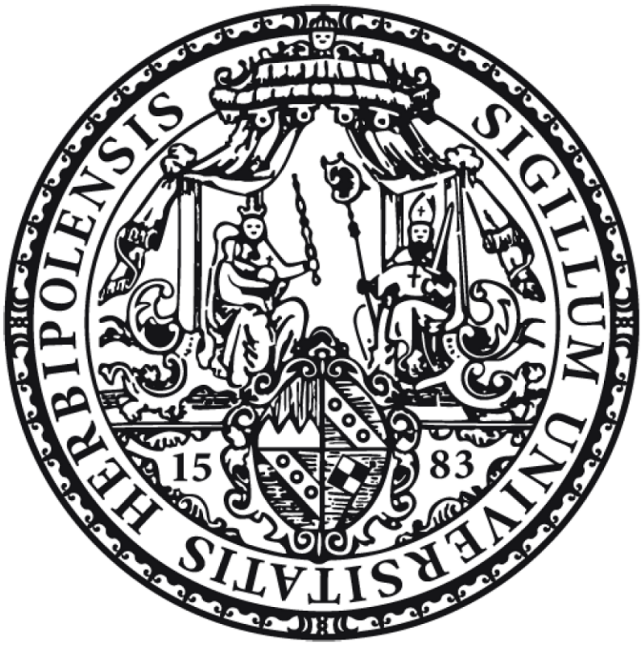

Kumulative Dissertation
zur Erlangung des naturwissenschaftlichen Doktorgrades
an der Fakultät für Chemie und Pharmazie der
Julius-Maximilians-Universität Würzburg

vorgelegt von

Sven Macher

aus Crailsheim

Würzburg, 2021

Eingereicht bei der Fakultät für Chemie und Pharmazie am

12.03.2021

Gutachter der Dissertation

1. Gutachter: Prof. Dr. Peer Löbmann
2. Gutachter: Prof. Dr. Christoph Lambert

Prüfer des öffentlichen Promotionskolloquiums

1. Prüfer: Prof. Dr. Matthias Lehmann
2. Prüfer: Prof. Dr. Peer Löbmann
3. Prüfer: Prof. Dr. Christoph Lambert
4. Prüfer: Prof. Dr. Tobias Hertel
5. Prüfer: Prof. Dr. Dirk Kurth

Datum des öffentlichen Promotionskolloquiums

20.07.2021

Doktorurkunde ausgehändigt am

_____

Die vorliegende Arbeit wurde in der Zeit vom 1. August 2017 bis zum 31. Dezember 2020 am *Fraunhofer-Institut für Silicatforschung ISC* in Würzburg unter der Leitung von Herrn Prof. Dr. Peer Löbmann angefertigt. Bei der vorliegenden kumulativen Dissertation handelt es sich um eine verkürzte Darstellung der Forschungsergebnisse. Die ausführlichen Ergebnisse sind Teil der folgenden Veröffentlichungen:

1. Macher, S., Schott, M., Sassi, M., Facchinetti, I., Ruffo, R., Patriarca, G., Beverina, L., Posset, U., Giffin, G. A., Löbmann, P., New Roll-to-Roll Processable PEDOT-Based Polymer with Colorless Bleached State for Flexible Electrochromic Devices, *Advanced Functional Materials* **2020**, 30, 1906254,

2. Macher, S., Schott, M., Dontigny, M., Guerfi, A., Zaghib, K., Posset, U., Löbmann, P., Large-area Electrochromic Devices on Flexible Polymer Substrates with High Optical Contrast and Enhanced Cycling Stability, *Advanced Materials Technologies* **2021**, 6, 2000836,

3. Macher, S., Rumpel, M., Schott, M., Posset, U., Giffin, G. A., Löbmann, P., Avoiding Voltage-Induced Degradation in PET-ITO-Based Flexible Electrochromic Devices, *ACS Applied Materials & Interfaces* **2020**, 12, 32, 36695-36705,

4. Macher, S., Sassi, M., Beverina, L., Posset, U., Schott, M., Giffin, G. A., Löbmann, P., Electrochromic Polymer Ink Derived from a Sidechain Modified EDOT for Electrochromic Devices with Colorless Bright State, *ChemElectroChem* **2021**, 8, 726-734,

5. Macher, S., Posset, U., Beverina, L., Sassi, M., Schott, M., Colloidal Coating Dispersion, **2020**, European Patent, EP3654094 A1.

Contents

List of Figures

List of Tables

List of Abbreviations

A^-	anion
a*	color value from green (-) to red (+) (CIELAB)
b*	color value from blue (-) to yellow (+) (CIELAB)
BG	Berlin Green
CE	counter electrode
CV	cyclic voltammetry
CR	contrast ratio
CSP	cross section polishing
EC	electrochromic
ECD	electrochromic device
ECM	electrochromic material
ECP	(conjugated) electrochromic polymer
EDOT	3,4-ethylendioxythiophene
EDX	electron dispersive X-ray spectroscopy
FTO	fluorine doped tin oxide
HOMO	highest occupied molecular orbital
IoT	internet of things
IR	infrared
ITO	indium doped tin oxide
L*	lightness value from black (0) to white (100) (CIELAB)
LCD	liquid crystal device
LiTFSI	lithium bis (trifluoromethanesulfonyl) imide
LUMO	lowest unoccupied molecular orbital
M^+	metal cation
MEPE	metallo-supramolecular polyelectrolytes
NIR	near infrared
PB	Prussian Blue
PC	propylene carbonate
PEDOT	poly(3,4-ethylenedioxythiophene)
PEG	polyethylene glycol
PEO	polyethylene oxide
PET	polyethylene terephthalate
PI	polydispersity index
PMMA	polymethyl methacrylate

ProDOT	poly(3,4-propylenedioxythiophene)
PSS	poly(styrenesulfonate)
PVDF	polyvinylidene fluoride
PW	Prussian White
PY	Prussian Yellow
R2R	roll-to-roll
RE	reference electrode
RT	room temperature
S2S	sheet-to-sheet
SEM	scanning electron microscopy
SPD	suspended particle device
UV	ultraviolet
Vis	visible light
WE	working electrode
WO_x	tungsten oxide
XRD	X-ray diffractometry

1 Introduction

By intensive use of fossil fuels in the energy sectors industry, transport, households as well as trade, commerce and services, humankind is increasingly influencing the climate on earth. Due to the increase of the greenhouse gas concentration in the atmosphere as a result of human activity, the greenhouse effect and thus global warming is intensifying.[1, 2] CO_2 is the most common greenhouse gas produced by humans, more than 60% of the anthropogenic global warming is attributed to it. The CO_2 concentration in the atmosphere today is 40% higher than before industrialization.[3, 4] As a consequence, the global average temperature is constantly increasing. An increase of 2 K compared to the pre-industrial average temperature is considered the threshold above which the risk of potentially catastrophic changes in the global environment increases massively.[1–4]

Regarding energy-efficiency, the building and construction sector is considered to be the largest single energy consumer in Europe. Buildings in the European Union consume approx. 40% of the final energy mainly for heating, cooling and ventilation demands. High CO_2 emissions due to the large energy consumption of buildings are therefore a main cause of global warming and climate change.[5, 6] As a consequence, energy conservation has become a major target of energy policies and is significantly influencing architectural design. Windows and glass fronts represent an integral element of modern buildings, as they offer daylight and natural ventilation, as well as a visible connection to the external environment. Large window and glazing areas and the therewith associated natural daylight penetration have been proven to stimulate work productivity and improve comfort and healthiness of the people living and working inside.[5–11] In terms of energy-efficiency, windows and glass fronts are thermally weak, as approx. 60% of the total energy loss of a building can be associated with conduction, convection and radiation through glazing areas.[5, 6, 12, 13]

Recently, modern and renovated buildings are equipped with high-performance insulation glazing systems. The next level of development is the widespread equipment of buildings with dynamic switchable glazing. It has been estimated that especially in hot climates, the trade-off between natural daylight and excessive solar heat gain is most efficiently regulated by switchable glazing.[5, 6, 11–14] Electrochromic Materials (ECMs), which change their optical properties due to an electrical voltage or current, are used in the form of energy-efficient switchable glazing to regulate the solar heat gain of buildings. Thus, ECMs can contribute to climate protection.[7, 15–21] Compared to other shading technologies such as suspended particle devices (SPD) or liquid crystal devices (LCD), electrochromic (EC) glazing is a flexible, low weight and low power dynamic shading solution.[7, 18, 21, 22]

Due to the relatively small fraction of engine power required for heating or cooling and the fact that heating is a convenient by-product of classic combustion engine driven vehicles, energy-efficient switchable glazing has received only little attention in the automotive sector in the past. As modern vehicles have to meet severe environmental specifications, air conditioning is identified today as a significant way to decrease CO_2 emissions and improve fuel economy of combustion engine driven vehicles or to extend the range of electrical vehicles.[23–28] Since EC glazing provides at least 2.5 times better results for solar radiation power loads, compared to state-of-the-art vehicle glazing, the opinion on EC glass for automotive application has changed completely.[25–28] By using EC glass, current air-conditioners may be downsized by 50% or more and still retain sufficient capacity to rapidly cool the interior and to sustain air-conditioning.[29, 30]

As the architectural and automotive application sectors show, there is a multi-purpose usage of EC materials and devices and therefore, this technology is considered to contribute to the societal challenge of climate change. However, the property performance required of ECDs is correspondingly high. For windshields, short response times and a visible light transmittance in the bright state of 70% in the US and 75% in the EU, respectively, must be achieved, for example.[23, 24] In addition, the color impression may not be falsified as a result of possible residual coloration in the bright state due to security risks in the automotive sector and essentially due to aesthetic reasons in the architectural sector. Commonly used conjugated electrochromic polymers do feature a wide range of vivid colors, short response times and high coloration efficiencies, but they often lack highly transmissive and fully colorless bright states. In addition, the compatibility to large area, low cost and high throughput manufacturing has not been shown conclusively.[21]

Furthermore, long-term performance and stability are major obstructions on the way to a successful commercialization of electrochromic devices (ECDs).[31] The requirements of device lifetime, measured in years and number of cycles, is rather high reaching up to 25 years or 10^5 cycles under harsh conditions for architectural applications. The durability of ECDs is affected by various environmental factors such as solar radiation (mainly UV), humidity, elevated or very low temperatures, mechanical stress as well as operational factors such as switching method or the magnitude of operating voltage and current. All these factors are strongly dependent on intrinsic device properties, its individual components and the actual application. Especially for automotive applications, stability requirements regarding environmental and operational factors are particularly severe.[17, 31–33] One factor that does not only affect device stability during operation, but can also cause later damage upon manufacture is air moisture. It is known from lithium-ion batteries that moisture has a significant influence on their performance. Since lithium ion-based electrolytes are used in ECDs as well, there are great similarities here. Even if these similarities may seem obvious to an expert in the art, in contrast to the lithium-ion battery sector, it is not yet generally accepted in the field of electrochromism that ECDs should ideally be manufactured in a dry atmosphere in order to guarantee long-term performance and durability.[34–36]

Against this background, the objectives of the present work arise. The establishment of an electrochromic system based on organic materials with short response times and highly transmissive and fully colorless bright states is extremely important, especially with regard to applications in the automotive sector. However, it is not only important to develop appropriate materials at the laboratory scale, but also to process them on a large scale and to harness the electrochromic effect in a full device. The large-scale and high-throughput processing of these devices and the establishment of a robust system are also major challenges.

A large influence of moisture on long-term performance and durability of ECDs is expected both during production and in later operation. Long-term performance and durability as well as possible degradation phenomena are strongly dependent on intrinsic device properties and its individual components. For this reason, it is crucially important to consider not only the materials themselves within the detailed investigation of possible degradation mechanism, but also the influence and interactions of the individual materials and components in the surrounding structure of an ECD.

Furthermore, it is important to focus not only on the pure understanding of the possible degradation phenomena, but also on suitable countermeasures in order to prevent ECDs from possible degradation. Of course, a thorough evaluation and testing of any change made to the ECDs under investigation is required, as well as the confirmation of the actual effect of the countermeasures to enhanced long-term performance and durability.

Ultimately, this doctoral thesis is intended to create a basis, with the help of scientific methodology, for assessing the requirements for ECDs themselves and the methods and processes used to manufacture them concerning long-term performance and durability. The more advanced the structure and components of an ECD are, and the more requirements to the corresponding manufacturing process have to be met, the higher are the expected costs of the technology. In this context, it will also be necessary to specify the trade-off between performance, costs and the respective application. It will be important to define the corresponding application-derived requirements for the appropriate device structure and process.

2 Fundamentals and State of the Art

2.1 Electrochromic Materials and Devices

Electrochromic materials (ECMs) exhibit a visual color change induced by the application of an external electrical voltage or an external electrical current. The EC effect is based on a reversible charge transfer process, i.e. a redox reaction, in which the ECM is involved in a battery-like assembly. If there are several stable and reversibly adjustable redox states, ECMs comprise one or more colored states, which ideally can be reversibly switched to an uncolored state. If an ECM changes color due to a reduction, it is called a cathodically-coloring material. If it colors due to an oxidation, it is called anodically coloring.[17, 37–40]

Electrochromic devices (ECDs) have so far been used as niche products such as the so-called "smart windows", which are used to regulate incoming light into buildings, and in automatically darkening vehicle rear view mirrors.[38, 41–43] A new trend - called "calm computing" - is a type of information technology, where networked systems create ambient intelligence, interacting in peoples periphery rather than taking center stage of attention. In comparison to smartphones, which often have high glare, optical head mounted displays and other similar portable devices communicate information more pleasantly.[44, 45] ECMs in particular are suitable for this purpose as a non-light emitting and low-power graphics and display solution. In addition, ECDs can be used in terms of "smart labels" on packaging, in the area of the "Internet of Things" (IoT) or as interactive design elements in the interior design or fashion sector.[45–48]

Due to their extremely low energy consumption and their non-light emitting nature, ECDs have advantages compared to similar switchable technologies such as suspended particle devices (SPD) or liquid crystal devices (LCD).[7, 18, 22] Nevertheless, there are a number of challenges that have to be addressed. Basically, an ECD combines electrochemical and optical technologies. In window applications, for example, ECDs are operated under harsh conditions for several decades and still have to meet the high requirements of optical products at the same time.[49] In order to compete with the technologies mentioned above, to achieve an extensive market penetration for EC products and to open up new technology fields for EC applications, the costs for the production of ECDs must be drastically reduced. Further challenges with regard to the achievement of marketability of EC products are in particular to improve the durability of the ECDs and to understand and control the failure mechanisms that occur due to electrochemical and environmental stress.[14, 50–52]

2.1.1 Set-up and Functionality of Electrochromic Devices

ECM can be divided into three material types.[17, 20, 38, 41] Type I ECMs are dissolved in an electrolyte and remain in solution in the ECD during operation. ECMs of this type show a high self-discharge. In order to maintain the colored or bright state, a constant current flow is necessary. The materials of type I include a wide variety of organic dyes or short-chain viologens.[17, 20, 38, 53] Long-chain viologens, on the other hand, are among the representatives of type II ECMs. In the appropriate set-up of an ECD, these materials are initially dissolved in an electrolyte as well. However, the color reaction leads to a reversible thin film deposition on one of the two electrode surfaces.[17, 20, 38, 41] Type III ECMs enable "all-solid-state" ECD. For this purpose, the active materials are deposited as thin films on the electrode surfaces. The active layers can be reversibly switched in the solid state and usually keep the addressed state for a certain time ("memory effect"). The materials of type III include Prussian Blue (PB) or conjugated conductive polymers.[17, 19, 20, 38, 41, 54–57]

Basically, the EC effect of the ECMs arises only within the set-up of an electrochemical cell.[38, 41] "All-solid-state" devices (type III) generally correspond to the vertical sandwich construction shown in Fig. 2.1, which in principle is comparable to a thin-film battery. The ECD is sandwiched in between two transparent, conductive plastic or glass substrate. An electrochromic layer and an ion-storage layer, which ideally has a complementary EC effect, are applied to the conductive layers of the two substrates. The layer stack comprising the transparent, conductive substrate and the EC film is called the working electrode and has usually the highest coloration efficiency in the system. The stack of the transparent, conductive substrate and the ion-storage or complementary-switching EC layer usually shows a lower coloration efficiency and is referred to as the counter electrode.[19, 55, 56] The two electrodes are separated by an ion-conducting but electrically insulating electrolyte, which ensures the charge carrier transport, when an external direct voltage is applied and enables the storage of ions for charge compensation in the respective layers.[38, 41]

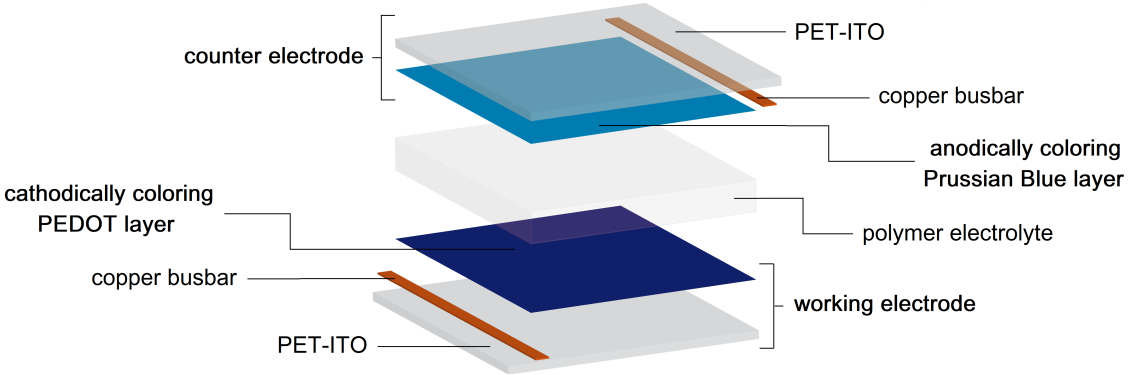

Figure 2.1: Set-up of an "all solid state" electrochromic device (ECD). The exemplary device is based on a cathodically-coloring poly(3,4-ethylenedioxythiophene) (PEDOT) film and an anodically-coloring Prussian Blue (PB) film. The two electrochromic layers are separated by a polymer electrolyte and are sandwiched in between two transparent, conductive PET-ITO sheets.

The color change of an ECD occurs during charging or discharging of the electrochemical cell, at which the two EC layers are mutually oxidized or reduced by an external direct voltage. Due to the oxidation or reduction at the two electrodes, an electrical current flows. At the same time, ions are transported through the electrolyte. By ion-storage into the EC layers, the oxidized or reduced layers are charge compensated. ECDs of the vertical "all-solid-state" type usually show only a slight self-discharge. Therefore, the respective state of the device can ideally be kept for several hours after the switching process even without the application of a constant direct voltage ("memory effect").[56] If the voltage is reversed, the electrical current flows in the opposite direction, the ions are appropriately removed from the EC layers and the ECD returns to its initial state. The switchability from the colored to the bright state and vice versa is reversible for many cycles.[38, 41, 56, 58]

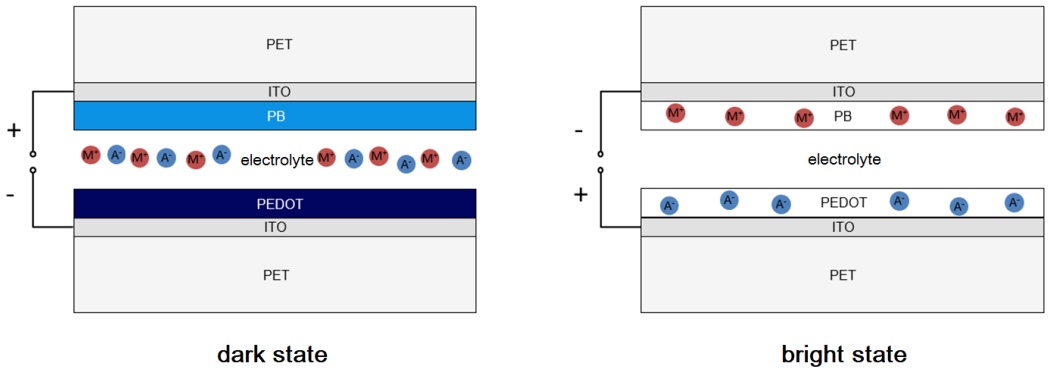

Figure 2.2: Functionality of an electrochromic device (ECD) based on poly(3,4-ethylenedioxythiophene) (PEDOT) and Prussian Blue (PB). The limiting dark and bright states are shown. A^- denotes anions and M^+ denotes metal cations for charge compensation during switching.

In Fig. 2.2 the described mode of operation is shown schematically using an ECD based on a cathodically-coloring poly(3,4-ethylenedioxythiophene) (PEDOT) and an anodically-coloring Prussian Blue (PB) electrode. Both electrodes are in an uncharged state, i.e. PEDOT is existent in its colored, reduced state and PB is also existent in its colored, but oxidized state. Therefore, no ions are initially stored in the EC films. By applying a positive direct voltage (Fig. 2.2, left) the uncharged polymer becomes completely charged (oxidized). For this purpose, electrons are removed from the polymer and anions A^- from the electrolyte are stored in the oxidized PEDOT layer for charge compensation. The PEDOT layer appears almost colorless (slight blue hue) in this state. The PB electrode becomes simultaneously charged (reduced) via uptake of the electrons emitted from the PEDOT electrode and the storage of metal cations M^+ from the electrolyte for charge compensation. The PB layer also brightens and the entire ECD appears in its bright state. When a negative direct voltage is applied (Fig. 2.2, right), the PEDOT electrode becomes reduced. The electrons get back into the PEDOT layer and the anions A^- are transferred back into the electrolyte. The polymer is in its deep blue state. The PB electrode becomes oxidized simultaneously, releases electrons and metal cations M^+ and also turns blue. The entire ECD appears in its dark state.[59–62]

2.1.2 Electrolytes for Electrochromic Devices

Besides the two electrodes, an ECD comprises a third important component, the electrolyte. Without a suitable electrolyte, a device cannot achieve the expected properties, no matter how well performing the used electrodes might be. Therefore, the electrolyte provides an essential role as the ionic conductor in between the electrodes. The most important properties that define a well performing electrolyte for ECDs are ionic conductivity, electric insulation, ion dissociation, the transport rate of the ions through bulk and interfaces as well as the thermal and electrochemical stability during operation.[57, 63–66]

Electrolytes can be divided into liquid, gel-like and solid electrolytes, which are comprised of solid polymer and inorganic or ceramic electrolytes. In liquid electrolytes, the charge exchange is conducted by salts dissociated in a suitable polar solvent, e.g. propylene carbonate (PC) or acetonitrile. Commonly used salts are, for example, lithium perchlorate ($LiClO_4$), lithium hexafluorophosphate ($LiPF_6$) or lithium bis (trifluoromethanesulfonyl) imide ($LiTFSI$).[67–72] Small ions are well suited for the ion storage in the electrochromic layers. Because of their small size, they are more mobile and therefore can diffuse into the electrochromic layer more easily than large ions.[73–76] In addition to the lithium salts mentioned, sodium, potassium, magnesium, aluminum or zinc salts with larger ion diameter, are also suitable and have advantages particularly in terms of raw material abundance and cost compared to lithium-ion technology.[77–80] Liquid electrolytes comprise the class with the highest ionic conductivity, but suffer from drawbacks due to electrolyte leakage and low chemical stability.[17, 63, 81, 82] Nevertheless, Gentex actually uses a liquid electrolyte system in it's EC rear-view mirrors.[43, 83, 84]

Gel polymer electrolytes are usually produced by adding the salts, liquid plasticizers and solvents to a polymer matrix such as polyethylene oxide (PEO), poly(methyl methacrylate) (PMMA) or poly(vinylidene fluoride) (PVDF). The two-phase system possesses cohesive properties of the solid polymer matrix and diffusive transport properties of the liquids entrapped into the polymer host.[17, 65] As plasticizers and solvents ethylene, propylene or dimetyl and dietyl carbonate are commonly used to adjust the ionic conductivity by increasing the amorphous phase concentration, dissociating possible ion aggregates, lowering the glass transition temperature and increasing the ionic mobility.[17, 65, 85] Compared to liquid electrolytes, the gel-like polymer electrolytes have a lower ambient-temperature ionic conductivity.[17, 68] Another disadvantage of this class of material are the poor mechanical properties, which are a result of the soft morphology of gels. Safety concerns related to electrolyte leakage, internal short circuits and material degradation upon extensive heating or ultaviolet irradiation remain an issue for gel electrolytes. Most of these drawbacks can be targeted by the addition of cross-linking materials in order to strengthen their mechanical properties. However, the cross-linking via ultraviolet (UV) or thermal curing results into a decrease of the ionic conductivity, since the conductivity is strongly influenced by the presence of immobilized solvent in the polymer network.[63, 66, 69, 72, 81, 86–88]

Solid polymer electrolytes typically consist of a salt, which is distributed in a polymer matrix. Commonly used salts include lithium perchlorate ($LiClO_4$), lithium hexafluorophosphate ($LiPF_6$) or lithium bis(trifluoromethanesulfonyl)imide ($LiTFSI$).[17, 65, 87] Polyvinylidene fluoride (PVDF), polymethyl methacrylate (PMMA) or polyethylene oxide (PEO) are frequently used as the polymer matrix. Solid polymer electrolytes score with chemical and electrochemical stability as well as mechanical flexibility and robustness. As mentioned earlier, the ionic conductivity takes place primarily in the free volume of the amorphous phase of the polymer matrix. However, the ionic conductivity of solid polymer electrolytes is too low for fast switching ECDs.[64, 65, 68, 70, 77, 87]

Commercially available polyethylene oxide (PEO) and polyethylene glycol (PEG) are the most established polymers used for polymer electrolytes and differ only in their chain length, i.e. their molecular mass, whereas PEO has a mass above and PEG a mass below $20\,000\,\mathrm{g\,mol^{-1}}$. PEO comprises ether groups and therefore a significant segmental ion mobility in the amorphous phase.[17, 63] The ether oxygen coordinates with the cations from the salt and hence compensates the lattice energy of the salt. To further increase the ion dissociation, polar plasticizers and microscopic fillers are usually added to inhibit the formation of crystalline polymer domains and to accelerate the ion transport within the polymer host. Additionally, LiTFSI and $LiClO_4$ are appended to PEO-based polymer electrolytes to enhance the ionic conductivity and to prevent the plasticizers from phase separation from the PEO. The main strength of PEO-based electrolytes is their good film forming characteristics, wettability and easy processing.[17, 65, 68, 77, 89] A well established alternative to PEO is amorphous polymethyl methacrylate (PMMA). PMMA has several advantages regarding its high light transmittance, ionic conductivity, environmental and chemical stability as well as low cost and its broad solvation of inorganic salts to form complexation between salt and polymer.[65, 68, 90] Another popular polymer introduced to electrolytes for ECDs is polyvinylidene fluoride (PVDF), which is regarded as highly processable with good durability as well as thermal and chemical stability. PVDF is favorable for ECDs application because of its high hydrophobicity and electrochemical stability. Despite this, PVDF is not stable towards lithium salts upon its fluorinated nature.[65, 68, 71, 77, 85, 88, 89, 91]

To enhance the performance of ECDs containing lithium salt electrolytes, the most effective and economically sound approach is to use electrolyte additives. An additive is a material that is added in small amounts (typically $<5\,\mathrm{wt.\%}$), which enhances the performance of the electrolyte. For example, an additive can reduce the irreversible loss of redox capacity and increase the long-term and thermal stability. Furthermore, physical parameters, such as ionic conductivity, viscosity or wettability, can be adjusted by the addition of electrolyte additives. Water scavengers, UV-absorbers, ion conductive fillers like zeolites and inorganic fillers to improve the mechanical properties are among the most frequently introduced additives for electrolytes used in ECDs.[85, 92, 93]

An electrolyte must fulfill a number of requirements if it is to be used in an ECD. First of all, the transference number of the ions is important. The transfer number is the part of an electric current that is transported by an ion type in a binary electrolyte. The transfer number is related to the ion concentration and ion mobility, ideally this should be as large as possible for EC applications.[17, 63] A guideline value to this is the ionic conductivity, which usually should be in the range between $10^{-4}\,\mathrm{S\,cm^{-1}}$ and $10^{-7}\,\mathrm{S\,cm^{-1}}$.[17, 94] Higher ionic conductivity leads to faster switching between the appropriate redox states of an ECD. Contrary to this, the electronic conductivity should be very low to prevent self-discharge as far as possible. Typical values are in the range of $10^{-12}\,\mathrm{S\,cm^{-1}}$.[17, 57, 94]

Furthermore, a porous separator is required to inhibit self-discharge and short circuits between the two electrodes. Polymer electrolytes can adopt the role of an extra separator, making the ECD lighter, more compact and less complex. Another aspect is good adherence and wettability to the nearby EC layers, improving the contact between electrolyte and EC layers.[17, 57, 94]

Another important requirement is a high optical transparency and transmittance in the required wavelength range, especially for see-through ECDs. To maximize transparency and color neutrality in the bright state of an ECD the electrolyte components and additives have to be colorless and must not generate light scattering, resulting in a hazy electrolyte layer.[17, 57, 94]

Mechanical, thermal, environmental as well as chemical, photochemical and electrochemical stability are major characteristics for high performance electrolytes for ECDs. Mechanical stability facilitates the handling and transport of ECDs and makes them more robust against mechanical impact. Superior thermal, environmental and photochemical stability ensures that heat, moisture or radiation released during operation does not result in degradation of the device. Electrochemical stability implies the suitability of the electrolyte to the operational voltage range during switching of the ECD. Chemical stability refers to the obviation of undesired chemical reactions of the electrolyte components and possibly the EC layers during device assembly and operation.[17, 57, 94]

Apart from that, synthesis and processability also play an important role, especially with regard to cost-effective continuous processes with high throughput. The volatility of the electrolyte components should be as low as possible to ensure long-term stability and reproducable processing. Furthermore, safety and environmental aspects have to be considered that are important for a successful commercialization and implementation of ECDs.[17, 57, 94, 95]

In this work, a UV-curable polymer electrolyte (HQ674), based on polyethylene oxide, developed by *Hydro-Québec* was used as electrolyte and separator in the devices. This electrolyte was optimized regarding the above mentioned requirements and is suitable for use in safe (no electrolyte leakage) all-solid-state ECDs.

2.1.3 Substrates for Electrochromic Devices

For opto-electronic applications such as ECDs but also thin-film solar cells or light-emitting diodes (LED), transparent conductive films are an essential component for device operation. In addition to a high light transmittance, the lowest possible surface sheet resistance is desirable for ECDs in order to keep ohmic voltage losses as low as possible. If the sheet resistance is too high, voltage losses result in longer response times and inhomogeneous coloration.[96–101] Due to the high demands on the transparent electrical conductors, the conductive substrates are the most expensive part of an electrochromic device. Even if these substrates do not constitute rare earth metals, the processes involved in producing these conductive substrates are both, complex and harsh, which results in high cost for large-scale production.[14, 17, 96, 97]

Thin films of heavily doped (several atom percent) semi-conductive oxides are often used for EC applications. These n-type semiconductors, for example, employ $In_2O_3{:}Sn$ (ITO) or $SnO_2{:}F$ (FTO), which, in addition to high light transmittance, have specific resistances in the range of approximately $1 \times 10^{-4}\,\Omega\,\mathrm{cm}$ on glass and approximately $4 \times 10^{-4}\,\Omega\,\mathrm{cm}$ on polyethylene terephthalate (PET).[17, 96–98] The low sheet resistance is achieved by broad conduction bands, which consist of overlapping s orbitals. Band gaps exceeding 3 eV ensure no interaction with the electromagnetic radiation in the range of visible and UV light. This ensures that the thin film appears transparent and nearly colorless. In the area of near infrared (NIR) radiation, on the other hand, the transmittance is very low. The NIR radiation is reflected to a great extent and the conductive layer also functions as a "low-e layer".[96–99] FTO layers are deposited to hot glass by chemical vapor deposition. In contrast, ITO layers can also be deposited on flexible substrates, such as PET by reactive direct current sputtering. The PET-ITO substrates are mechanically flexible, chemically and electrochemically stable and are suitable for continuous deposition of EC thin films by means of roll-to-roll (R2R) coating. A disadvantage of the deposition onto flexible substrates is the risk of cracking the conductive film upon bending and thereby lowering its conductivity.[17, 96–99]

Metal-based transparent conductive thin films show electrical conductivities that are up to two orders of magnitude higher than their oxidic counterparts. The extremely thin metal layers with typical thicknesses in the order of 10 nm made of copper, silver or gold show the ductility that is typical for metals and are therefore more mechanically robust than oxide thin films. The high reflection of the interfaces is disadvantageous, so that anti-reflective layers are necessary for suitable transmittance values. Nevertheless, silver-based coatings are commonly used in today's windows to minimize the solar radiation throughput ("low-e layer"). The electrochemical stability limits of the metal films are also restricted. Silver for example tends to oxidize as soon as appropriate potentials are present during ECD operation. Metal-based transparent conductive thin films are produced by means of vapor deposition or sputtering processes.[17, 96–98, 102–104]

To overcome the disadvantages of both, the oxide- and metal-based transparent conductive films, combinations in the shape of oxide-metal-oxide multilayer stacks, also known as insulator-metal-insulator stacks, are employed as an alternative in many application fields. Thermoplastic polymer foils that are commonly used in R2R-processes, don't withstand the temperatures needed to obtain oxidic semiconductors with low electrical resistivity and high light transmittance on the other hand. As mentioned above, single-layer metal electrodes show high reflection and thus have to be very thin. For example ITO/Au/ITO or ITO/Ag/ITO layer stacks grown by continuous R2R and low-temperature sputter processes show more robust mechanical properties as well as superior flexibility and conductivity compared to single-layer metal- or oxide based thin films. ITO/noble metal/ITO stacks are reported to obtain sheet resistances below $5\,\Omega\,\square$ and visible light transmittance above 85% with an overall thickness of the stack of less than 100 nm, whereas more than 400 nm of a single-layer ITO thin film with a specific resistance in the range of approximately $2 \times 10^{-4}\,\Omega\,\mathrm{cm}$ would be required to obtain the same sheet resistance.[105–108]

Another alternative are carbon-based thin films. For example, the deposition of graphene, fullerene or carbon nanotubes results in sheet resistances $<30\,\Omega\,\square$ and a visible light transmittance of $> 90\%$. Carbon nanotubes are single layers of carbon atoms which form a seamless cylinder. Carbon nanotubes have either metallic or semiconducting properties and are deposited by means of continuous R2R processes. Graphene consists of sp^2-hybridized carbon atoms arranged as a honeycomb lattice and is usually deposited by chemical vapor deposition. R2R, hot-press-lamination or ink-jet printing are alternative methods for large area deposition. Metallic nanowires made of copper or silver are also suitable, as they can be deposited by wet chemical methods and have conductivities comparable to those of the metallic thin films. However, the deposition of nanowires inevitably leads to a certain diffuse light scattering. Therefore, the thin films appear hazy.[96–99, 109–111]

Finally, organic conductive polymers, such as the commercially available PEDOT:PSS, can also be mentioned as transparent conductive layer materials. PEDOT:PSS shows significantly lower conductivities and visible light transmittance than the other materials, but is mechanically flexible and very cost-effective due to processing by means of wet chemical methods or printing processes and is therefore an alternative that is worth mentioning. Huge efforts in the field of conducting polymers were made by controlling the synthetic conditions, doping or functionalizing the backbone with substituent side chains. The lowest sheet resistance of PEDOT:PSS reported in literature is around $50\,\Omega\,\square$, combined with a visible light transmittance of around 90%.[96–98, 112–117]

However, since thin films of doped semi-conductive oxides offer far better performance in terms of electrical resistivity and transparency than their potential alternatives mentioned above, PET-ITO is still the material of choice to date for flexible, R2R-produced ECDs. The electrochromic materials used in this work are all deposited in thin film form on PET-ITO substrates.

2.1.4 Electrochromic Materials

Transition metal oxides are among the most important inorganic ECMs. Thin films are usually produced by vapor deposition, sputtering or sol-gel processes. The deposition of the appropriate nanoparticles is also possible.[17, 94] EC transition metal oxides are mainly used in EC windows. The EC oxides differ in cathodically- and anodically-coloring materials. In addition to the well-known tungsten oxide (WO_x), the oxides of titanium, niobium, tantalum and molybdenum also belong to the cathodically-coloring oxides. The oxides of chromium, manganese, iron, cobalt, rhodium, iridium and nickel are anodically coloring. Vanadium oxide shows both effects. Mixed metal oxides are frequently used as well because the EC properties can be improved by combining several oxides. For example, the cycle stability of tungsten oxide layers can be significantly improved by adding titanium oxide. Most inorganic-based ECDs are based on a cathodically-coloring layer as the working electrode, mainly WO_x, and an anodically-coloring layer as the counter electrode, often nickel or titanium vanadium oxide.[17, 41, 55, 90, 94, 118–124] The two most commonly used EC oxides, tungsten and nickel oxide, are examined in more detail below.[17, 94]

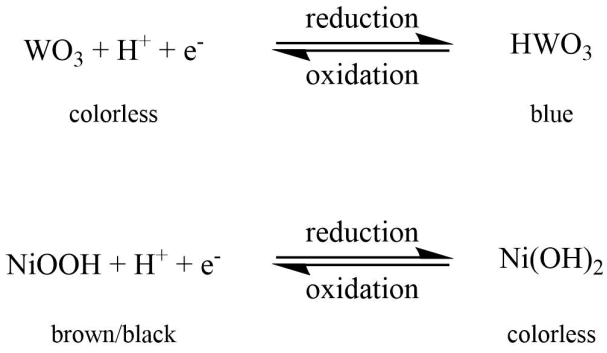

WO_x can be cathodically switched between a blue and an almost colorless state, nickel oxide switches anodically between a brown/black and an almost colorless, slightly yellowish colored state.[17, 94] The EC effect is based on an intervalence charge transfer. Due to the octahedral structure, there is a splitting of the *2p* bands of the oxygen and the *d* bands of the metals. A further splitting of the *d* bands into bands named e_g and t_{2g} is further observed. In the case of the cathodically-coloring tungsten(VI)oxide (WO_3) the *2p* band of the oxygen is occupied, while the *d* band of the metal is unoccupied. The band gap between them is large enough that there is no excitation and the layer appears colorless due to a lack of light absorption. In contrast, in the reduced state the *d* band of tungsten(V)oxide (HWO_3) is partially occupied by electrons and excitation occurs within the t_{2g} band. Thus, absorption in the visible range of the electromagnetic spectrum occurs, so that the WO_x layer turns blue. Anodically-coloring nickel(III)oxide ($NiOOH$) has unoccupied t_{2g} states and is therefore colored in the oxidized state. The t_{2g} band is completely occupied after the reduction to nickel(II)oxide ($Ni(OH)_2$). Due to the band gap between the t_{2g} and e_g band, the material in the reduced state becomes colorless.[17, 94, 125, 126]

Another non-oxidic inorganic ECM is Prussian Blue (PB). The mixed-valent complex compound with the molecular formula $Fe_4^{III}[Fe^{II}(CN)_6]_3 \cdot x\ H_2O$ (with $x = 14 - 16$) has several oxidation states, between which charge transfer is possible. The crystal structure of PB is cubic, with the Fe(II) octahedral coordinated by the carbon atoms of the cyanide ions and the Fe(III), alternating with the Fe(II), coordinated octahedral by the nitrogen atoms. Water is embedded in the spaces between the crystal structure. The blue color of PB results from a metal-to-metal charge transfer from Fe(II) to Fe(III). The reduction of PB leads to Prussian White (PW), which appears colorless when deposited as thin films. Anodically-coloring PB is often considered as a counter electrode material for cathodically-coloring EC layers. In the context of the present work, PB is used as a complementary-coloring counter electrode for a cathodically-coloring PEDOT working electrode. Therefore, PB is considered in more detail in 2.3.[17, 38, 41, 61, 94, 118, 127–133]

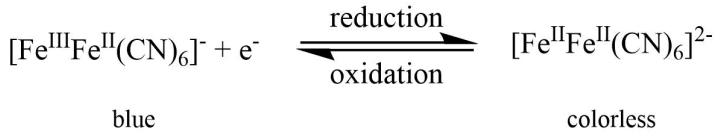

Organic electrochromic compounds i.a. include bipyridinium systems, also known as viologens. Most Viologens are colorless in their dicationic state. A reduction into the radical cationic state causes a coloration of the viologen corresponding to the substitution of the pyridine groups. A substitution with short alkyls leads to a blue color, as it is the case with methyl viologen, the best-known representative of its material class. Longer alkyl residues show a red color, while phenyl groups produce a greenish color.[17, 38, 53]

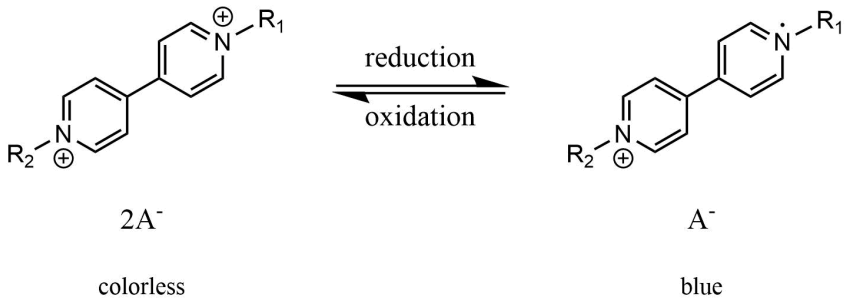

Other influencing factors on the potential window and the coloration of the viologens are the solvent, the type of counter ions, the electrode material and the substitution of the carbon atoms of the bipyridinium rings.[17, 38, 53, 134–136] The intense color of the cationic state is due to the conjugation of the unpaired electron and is considered as an intramolecular electron excitation. Viologens with short alkyls are usually type I ECM and are soluble in all their redox states in aqueous electrolytes. As the length of the alkyl chain increases, the solubility of the cationic state decreases, which is why these viologens can be assigned to type II ECM.[17, 38, 53]

The commercially most successful EC product is the viologen-based automatically darkening vehicle rear view mirror from *Gentex Corporation* (*Gentex* night-vision system NVS ®). The NVS® mirrors consist of an ITO-glass anode and a highly reflective metal cathode behind it. In the gap between the two electrodes are two viologen species, one of them is in the dicationic state (oxidized) and the other one is in its cationic state (reduced). At the cathode, the first species is reduced and thereby colored, while the second species is colored by oxidation at the anode. The darkening of the rear-view mirror remains only under a constant direct voltage. The ECD does not show a "memory effect", which is why the NVS® mirror is also referred to as a "self-erasing mirror". In the event of a power failure, it automatically returns to the bright state. [38, 41–43, 53, 83, 84]

Metallo-supramolecular polyelectrolytes (MEPE), also known as metallo or coordination polymers, belong to the organic ECM. As it is shown in Fig. 2.3, MEPEs consist of a metal ion surrounded by organic ligands. The structure can be built up using a self-assembly process induced by the metal ion.[137] The resulting chains are alternately made up of metal centers and terpyridine ligands. The structure of the MEPEs can be changed by varying the metal ions and the ligands, which means that ECMs of different colors can be realized. The color is related to a metal-to-ligand charge transfer, whereby electrons are transferred from the metal centers to the ligands. MEPE thin films can be easily produced using dip coating or layer-by-layer deposition. ECDs with MEPE working electrodes achieve a high EC contrast with short response times and low operating voltages. A multi-layer structure made of MEPEs with different metal centers can be used to produce broadband absorbing layers that are particularly in demand for application.[95, 137–153]

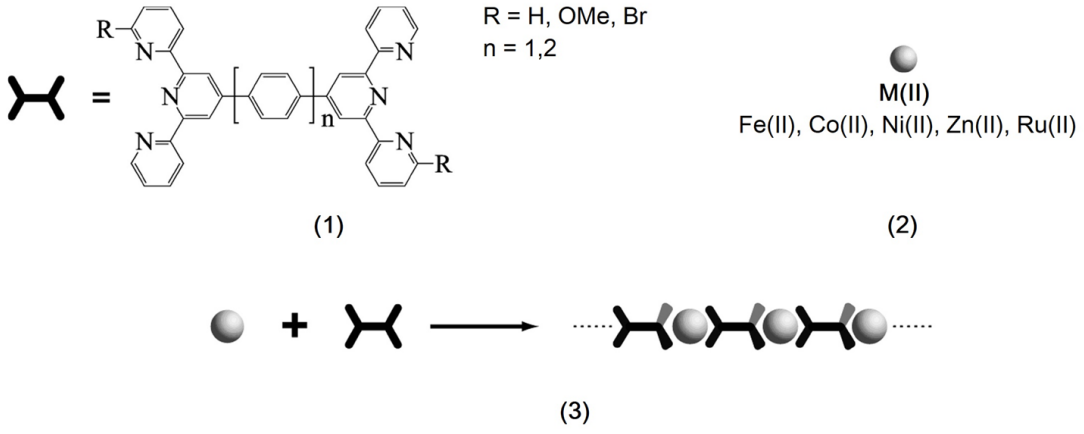

Figure 2.3: Self-assembly of metallo-supramolecular polyelectrolytes (MEPE) (3) from bis-terpyridine ligands (1) and divalent transition metal ions (2). Reprinted (adapted) with permission from the *American Chemical Society* according to reference [137]. Copyright 2020 American Chemical Society.

Another group of organic ECMs includes transition metal complexes such as hexacyanoferrates and phthalocyanines. The latter class of ECMs are composed of phthalocyanine ligands coordinated around a central transition metal ion. The EC properties of these materials are characterized by an intense coloration and a high redox activity. The color change is based on a metal-to-ligand charge transfer, an intervalence charge transfer, an intraligand excitation or electronic transitions in the visible range. Polymeric transition metal complexes can be prepared with multidentate chelate ligands such as bipyridine or terpyridine and show an intense metal-to-ligand charge transfer band in the reduced state, which disappears reversibly upon oxidation of the metal ion. EC thin films can be produced by reductive electropolymerization of complexes with vinyl- or halogen-substituted pyridyl ligands. The electrochemical reduction produces insoluble oligomers that can be deposited as a thin film on an electrode. Due to their low solubility, the transition metal complexes play a minor role for EC applications despite their excellent EC properties.[154–161]

Probably the most important group of ECMs is the class of the conjugated polymers. These inherently conductive polymers are also referred to as "synthetic metals" because of their electrical, magnetic and optical properties, which basically correspond to those of the metals. At the same time, these materials combine properties that are typical for plastics, for example mechanical flexibility or simple processing. In regards to their optical properties, all conductive polymers, in the form of thin films, potentially have an electrochromic effect. Conjugated polymers as such feature a wide range of vivid colors, response times in the range of seconds, and a light transmittance change over 60%.[19, 162–164] Furthermore, they are generally compatible with large area and high-throughput processes, e.g., R2R deposition and therefore are a low-cost solution for ECDs since they can be coated on flexible plastic substrates by means of wet chemical approaches.[21, 59, 165, 166] The most important representatives are drawn below.[17, 115, 167–171]

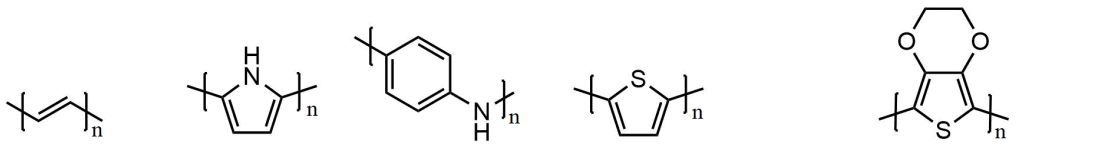

Heeger, MacDiarmid and Shirakawa, the discoverers of this material class, which also has enormous potential in the field of semiconductor components such as transistors, solar cells or diodes, were awarded the Nobel Prize in Chemistry in 2000. Heeger, MacDiarmid and Shirakawa published their studies on doped polyacetylene in 1977, which shows a particularly high conductivity due to doping. [172–174] With the invention of PEDOT and PEDOT:PSS in the late 1980s, the inherently conductive polymers finally gained technical significance.[14, 170, 172, 175–177] The present work is based on ECDs containing a sidechain-modified PEDOT working electrode (see 2.2 for more detailed information).

2.2 Conjugated Electrochromic Polymers

The electrochromic effect of conjugated polymers is linked to the nature of the charged states in conjugated polymers. Electrons of a conjugated π-system are able to move along the polyconjugated chains. One of the most striking examples of such a feature is the existence of the aromatic ring current in benzene. Furthermore, electrons can hop from chain to chain through occasional hopping processes, which enables translational charge transport even over longer distances.

The model of charge transport can be explained in detail by using the energy-band model. The basic electronic state of a solid is obtained by filling the electronic levels from low to high energies, taking into account the Pauli principle. The electronic properties of a solid depend in particular on the energy bands in the vicinity of the Fermi energy E_F. The highest occupied energy band is called the valence band, the lowest unoccupied band is the conduction band. Fig 2.4 shows the location of the Fermi energy and the occupation of the energy bands.

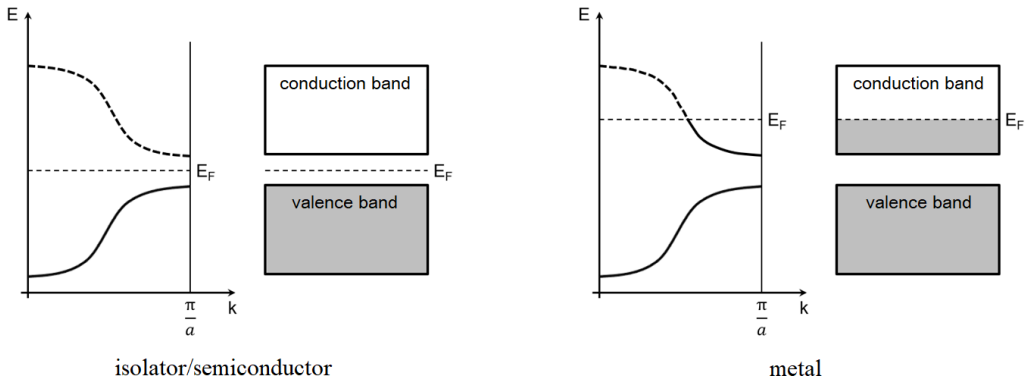

Figure 2.4: Fermi-Dirac distribution (l.) and the typical band structure (r.) of insulators, semiconductors and metals. The dashed horizontal line identifies the Fermi energy E_F.

In metals, one band is only partially occupied. At temperatures close to 0 K the highest occupied energy level corresponds to the Fermi level, which lies in the middle of an energy band. The excitation of the electrons in the conduction band creates positive charge carriers (holes) in the valence band. Both electrons and holes can migrate in an electric field. The charge transport is only influenced by scattering processes on the atomic cores of the solid. At higher temperatures it is not possible to distinguish exactly between occupied and unoccupied states because the electrons can be thermally excited. The orbital occupation is described by the Fermi-Dirac distribution. The conductivity of metals decreases with increasing temperature due to increased scattering of the electrons.[178–180]

In semiconductors and insulators, valence and conduction band are separated by a band gap. At temperatures close to 0 K the levels of the lower valence band are completely filled and the levels of the higher conduction band are completely empty. The Fermi edge lies exactly in the middle of the band gap. There are no mobile charge carriers in

the electronic basic state. There is no fundamental difference between insulators and semiconductors. However, semiconductors have a smaller band gap, so that some charge carriers can be excited into the unoccupied conduction band at room temperature. These electrons are mobile and can therefore contribute to the charge transport. The solid becomes conductive. In semiconductors, the conductivity increases with increasing temperature, which is a fundamental difference to metalls. For temperatures close to 0 K the conductivity disappears due to the lack of thermal excitation. Insulators have a much larger band gap, so there is no thermal excitation.[178–182]

The formation of the energy-band structure for conjugated polymers is explained in Fig. 2.5 using the example of polyacetylene, the simplest conjugated polymer.[182, 183] Polyacetylene is built up alternately from C-C single and C-C double bonds. The smallest building block of a polyacetylene chain is a sp^2-hybridized carbon atom. The orbitals of an ethylene molecule consist of the $1s$ orbitals of the hydrogen atoms and the $2s$, $2p_x$, $2p_y$ and $2p_z$ orbitals of the carbon atoms. Except for the $2p_z$ orbitals of the carbon atoms, all other orbitals are bonding and therefore have a lower energy. The $2p_z$ orbitals (A) have significantly higher energies and split into a bonding and an antibonding molecular orbital during the formation of the ethylene molecule. The low-energy bonding π orbital (highest occupied molecular orbital (HOMO)) contains the two electrons, while the high-energy, antibonding π*-orbital (lowest unoccupied molecular orbital (LUMO)) is not occupied (B). The energy band structure for polyacetylene is demonstrated for two (C), multiple (D) and an almost infinite chain (E) of ethylene polymeric units. All molecular orbitals, especially HOMO and LUMO, continue to split and come very close. Theoretically, as the π-electron system extends infinitely, the HOMO and LUMO merge resulting in a material with no band gap. An electron conductor with metal characteristics is created.[170, 178, 179, 181–184]

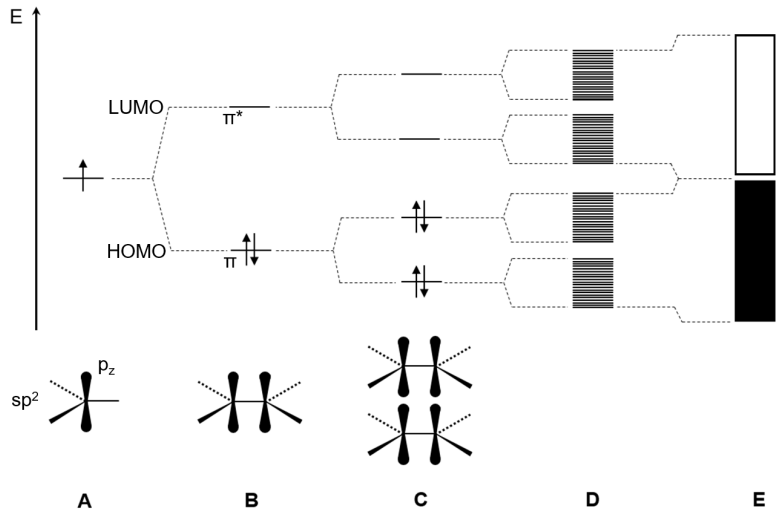

Figure 2.5: Formation of the energy-band structure using the example of polyacetylene. With increasing monomer building blocks, the splitting of the molecular orbitals is increasing. Individual molecular orbitals merge into continuous energy-bands.

A conjugated polymer with an almost infinitely extended π-electron system along the polymer backbone should have a metal-like conductivity. If all C-C bonds were of the same length, the π-electron would be divided into two orbitals, which would result in a half-filled band and the material would have metallic properties. However, conjugated polymers show an alternation in the bond length. Due to the bond length alternation, the π-electron system is not completely delocalized. The reason for this is a coupling of the wave functions of the π-electrons with the lattice vibration modes.[180, 181, 183]

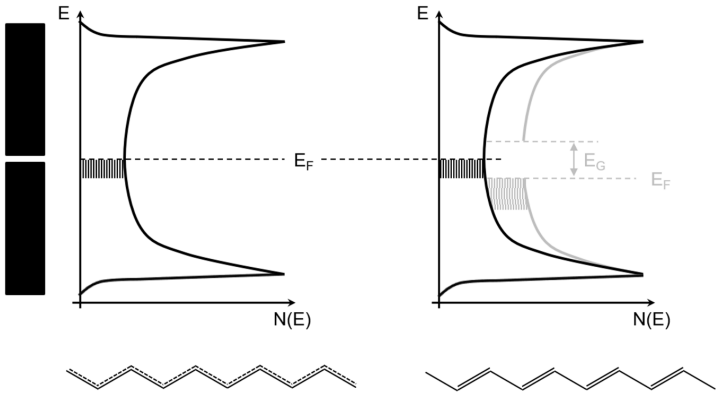

Figure 2.6: Band gap formation in conjugated polymers. The elimination of π-electron conjugation is shown as an example for polyacetylene. The band gap is represented by E_G.

Although the delocalization of π-electrons normally leads to an enormous energy gain (conjugation energy), in the case of conjugated polymers this energy gain is more than compensated by the formation of a band gap and the associated lowering of the Fermi energy. Fig. 2.6 shows the formation of the band gap for conjugated polymers. In the case of a fully conjugated system, some electrons occupy the black hatched area. Due to the abolishment of the bond length identity, the Fermi edge is energetically shifted downwards. Some of the electrons from the black hatched area occupy lower energetic levels in the grey hatched area. The energy gain achieved thereby more than compensates for the loss of conjugation energy. The stabilization of the molecule by the elimination of the π-electron conjugation is also called Peierls distortion. Since there are no half-filled bands, the solid shows typical properties of a semiconductor.[172, 178–180, 182, 183]

But still, the conductivity of organic semiconductors is very low and can only be significantly increased by oxidation or reduction of the polymer. This is also referred to as doping in analogy to inorganic semiconductors. Polyacetylene, as a degenerate conjugated polymer, has sites with an interrupted bond length alternation. An unpaired electron is located at a defect. This allyl radical is well stabilized by the neighboring double bonds. A single radical such as this is called a neutral soliton (Fig. 2.7). In the band model, a state occurs in the band gap that is occupied by an electron (spin $\frac{1}{2}$). Charge transport is facilitated by this neutral soliton state resulting in the excitation energy being halved and the electron being lifted into the conduction band with even less excitation energy. In the molecule, this means that the solitons can move very easily along the polymer chain.[168, 175, 179, 183]

Neutral solitons are easily extinguished by recombination, therefore the concentration of neutral solitons in a polymer is very low. The use of an oxidizing or reducing agent can remove the unpaired electron (oxidation) or add another electron (reduction) to a neutral soliton, thereby introducing either a positive or a negative charge into the polymer. Carbocationic or carbanionic structures are formed, which are referred to as positive or negative solitons. Positive or negative solitons are also stabilized by adjacent double bonds and can migrate along the polymer chain and thus contribute to the charge transport. The doping increases the number of free charge carriers in the polymer.[168, 175, 179, 183]

Another effect of the doping is the change in the band structure. As the doping progresses, the soliton state in the band gap becomes broader until gradually a broad soliton band is formed, as more and more soliton states are generated. The broad soliton band can even partially overlap with the valence and conduction band. In the case of positive solitons, the soliton band is empty and electrons can be lifted from the valence band into the soliton band. In the case of negative solitons, the soliton band is filled and electrons can be lifted into the conduction band. The newly created band creates a significantly smaller band gap between the soliton band and the valence or conduction band.[168, 183]

In polyaromatics, for example in polyparaphenylene, there are no degenerate states and therefore charge transport via solitons does not exist. The analog quasiparticle in polyaromatics is called the polaron and always represents a combination of charge carrier and lattice distortion due to the local polarization (Fig. 2.7). Because of the loss of the aromatization energy and its diradical character, there are no neutral polarons. Polarons can only be generated by oxidation or reduction. Polaron formation is countered by the loss of aromaticity, which is why strong oxidizing or reducing agents must be used.[175, 183, 185]

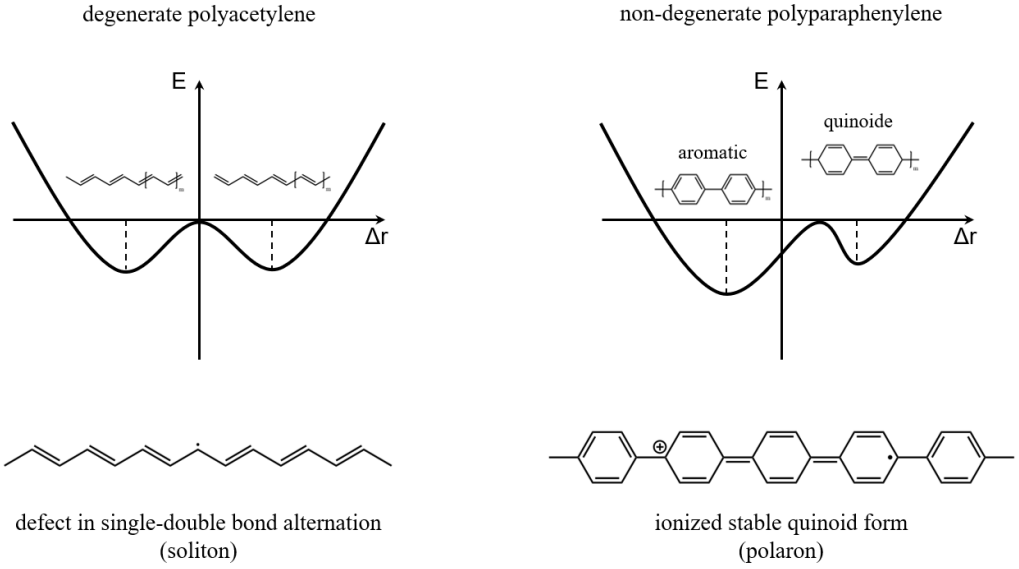

Figure 2.7: Potential energy E as a function of bond length alternation Δr and charge carrier formation for conjugated polymers with degenerate groundstate (polyacetylene) and non-degenerate groundstate (polyparaphenylene).

A polaron is formed by introducing or removing an electron in or from the polymer. This change results in chain deformation and a change in the energetic structure of the polymer. An electronic state is raised from the valence band into the band gap. Another state is reduced from the conduction band into the band gap. A negative polaron is created, if an electron is introduced to the previously empty state, reduced from the conduction band. A positive polaron is formed, if an electron is removed from the previously filled state raised from the valence band. In both cases, semi-filled states with spin $\frac{1}{2}$ arise.

A bipolaron can be created by adding or removing another electron. In the case of a negative bipolaron, two completely filled states arise in the band gap with spin 0. In the case of a positive bipolaron, two completely empty states arise, also with spin 0. New bands in the band gap also arise with further oxidation or reduction. Polaron and bipolaron are delocalized and can migrate in the electric field by shifting the double bonds in the conjugated π-system. The migration of polarons and bipolarons is the dominant charge transport mechanism in polyaromatics. Fig. 2.8 shows the polaron and bipolaron structures of PEDOT as an example.[59, 168, 175, 183, 185]

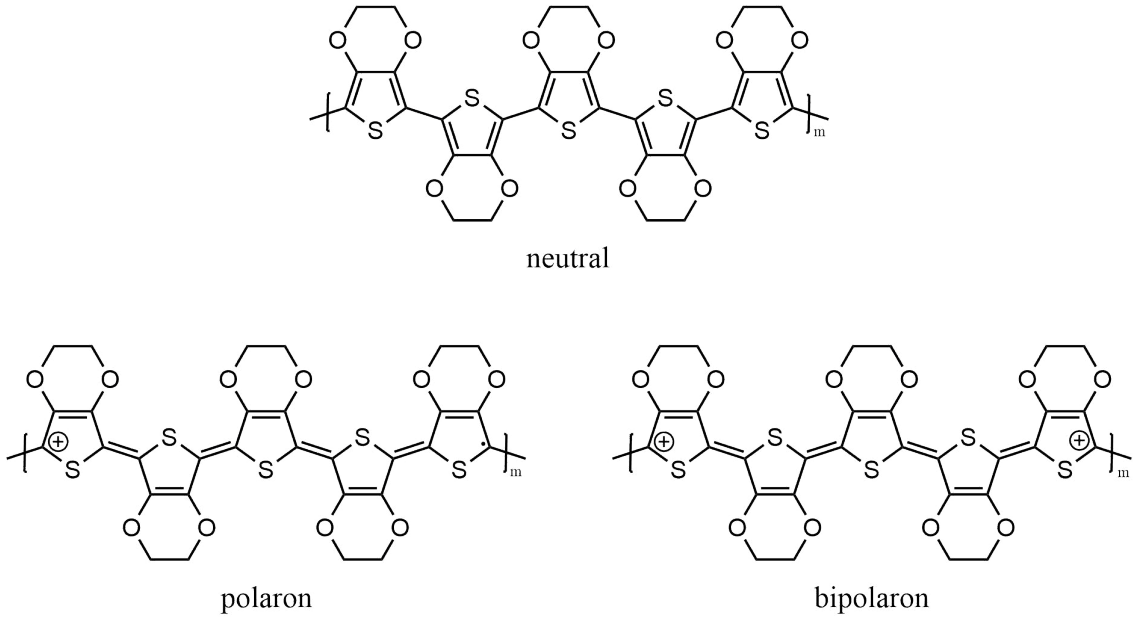

Figure 2.8: Representation of the neutral, polaron and bipolaron structures of PEDOT. The positive charges migrate in an electric field along the conjugated polymer backbone.

Because polymers are organic molecules, there are several ways to add charge to the polymer. By so-called chemical doping, charge can be introduced into the polymer using an oxidizing or reducing agent. The use of an electron acceptor (oxidizing agent) creates a p-type semiconductor. The use of an electron donor (reducing agent) results in an n-type semiconductor. Furthermore, the doping can be carried out electrochemically, where the polymer is oxidized or reduced by an external potential or an external current and where a counterion is taken up from the environment (electrolyte). Electrochemical doping is the source of electrochromism in conjugated polymers.[175, 179, 181, 185]

The most important representatives of the conjugated polymers include polyacetylene, polyphenylene, polyaniline, polypyrrole, polyfuran or polythiophene. Conjugated polymers are used both as permanently doped and thus permanently conductive materials or as organic semiconductors. Applications arise basically in the field of sensor technology, as transistors, supercapacitors or solar cells, as transparent conductive layers or in the form of polymer batteries or electrochromic devices. Compared to inorganic conductors and semiconductors, conjugated polymers offer advantages such as cost-effective processability and mechanical flexibility. As a result, they enable novel and more versatile applications than their inorganic counterparts.[182, 183, 185, 186] Polythiophenes are the most widely investigated conjugated polymers because they differentiate themselves from other conjugated polymers by their higher stability to environmental conditions, their ease of synthesis and processability, as well as their enormous structural diversity and electronic properties.

The most viable conjugated electrochromic polymers (ECPs) are based on electron-rich conjugated five-membered ring polyheterocycles like thiophenes, pyrrols or furans, since they have a lower oxidation potential and better solubility as compared to polyacetylene, poly(p-phenylen) or poly(p-phenylene vinylene) and their derivatives. Basically, the band gap between the valence band (HOMO) and conduction band (LUMO) determines the optical properties of the polymer. The electrochromic effect is explained with the help of the energy diagram in Fig. 2.9 using the example of a p-type semiconducting ECP.[59, 175, 185]

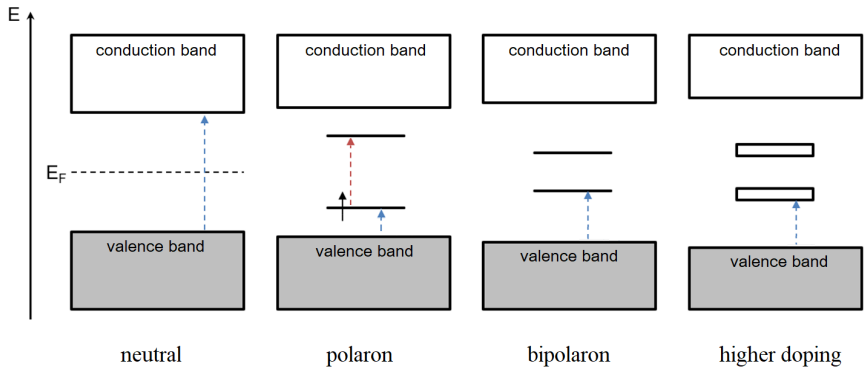

Figure 2.9: Energy diagram of conjugated electrochromic polymers (ECPs). Dashed lines intend allowed electron transition by light absorption.

In the neutral state, the polymer is undoped. Polymers with small band gaps (1.5 eV to 2.0 eV) show π-π^* transitions.[59, 175] Electrons can be lifted from the valence band into the conduction band by light absorption. Because of the energy required for this, an absorption band is therefore evolved in the visible region of the light spectrum. The ECP strongly absorbs in the visible region in its neutral state. If polaron and bipolaron states exist upon doping, electrons can also be lifted within the intermediate states or from the valence band into the intermediate states within the band gap by light absorption. The excitation of the p-doped ECP in the oxidized state requires considerably less energy than in the

neutral, undoped state. The absorption band is then located in the infrared (IR) region of the light spectrum and the material appears therefore colorless in the visible range of the electromagnetic spectrum.[59, 175, 185] The discussed ECP is a cathodically-coloring electrochromic material. Anodically-coloring polymers are higher bandgap materials (>3.0 eV), their neutral-state absorption is located in the UV. Upon oxidation, the polaron and bipolaron states evolve in the visible region and the thin film becomes colored.[17, 167]

ECP systems are highly synthetically flexible allowing for the realization of customizable electrochromic properties. One approach to alter oxidation potential, bandgap and color properties is the substitution of the heteroatom of the heterocycle. For example, poly(3,4-ethylenedioxythiophene) (PEDOT) switches from dark blue to almost colorless and comprises a bandgap energy of 1.6 eV, whereas poly(3,4-ethylendioxypyrrole) (PEDOP) has a red to almost colorless transition and shows a band gap energy of 2.0 eV.[17, 167]

Another approach for optoelectronic property control is the so-called donor-acceptor approach. This method is based on the copolymerization of electron-rich building-blocks (electron donors), such as thiophenes or pyrrols, and electron-poor building-blocks (electron acceptors), like cyanovinylene or benzothiadiazole. Upon incorporation of alternating electron donors and acceptors, a smaller bandgap (red shift of the optical absorption), due to a lowering of the conduction band by the acceptor units, and a double-peak absorption profile, due to the formation of low-lying unoccupied energy bands within the bandgap of the ECP in its neutral state, are achieved. The low-lying unoccupied energy bands allow electron transitions from the top of the valence band to this mid-gap bands besides the transition from the valence to the conduction band.[187–195] Absorption band location, number, width and separation can be controlled through systematic selection of the donor and acceptor units and their relative concentrations, as impressively demonstrated by the *Reynolds Research Group (Georgia Tech)*, who developed black or brown to colorless switching polymers and realized a family of dioxythiophene-based polymers spanning the whole color palette in the neutral state.[163, 164, 167, 182, 195–197]

Heterocycles, such as thiophenes, are further tunable at the 3- and 4-position. Through electron-withdrawing substituents the HOMO level is lowered and through electron-donating substituents the HOMO level is raised, which has an influence on the absorption band position and the oxidation potential. Additionally, the substitution at the 3- and 4-position inhibits polymerization and cross-linking at these positions, prevents conjugation breaks and improves processability. While the acyclic 3,4-substitution is also used to improve the polymer solubility through the incorporation of alkyl chains, cyclic 3,4-substitution, using bridging ethylene, propylene or butylene units, has a major influence on the optical contrast, which is increased with increasing ring size. The alkyl bridges can be further substituted with alkyl chains for solubilizing reasons. An additional substitution option is is the *N*-functionalization in the case of pyrrole heterocycles, which has a subsequent influence on the optoelectronic properties.[198–202]

Optoelectronic properties in conjugated polymers are additionally adjustable by careful tailoring of the steric interactions within the polymer chains. By substitution at the 3- and 4-position of the heterocycle or at the additionally incorporated alkyl bridge, torsional strain or twisting of the polymer backbone can be increased or reduced. Bulky substituents force adjacent units to twist out of plane from one another and reduce the extent of conjugation, resulting in a blue shift of the neutral state absorption. On the other hand, substitution can induce planarisation of the backbone via reduced inter- and intramolecular interactions. If this does not interact with the internal resonance structures of the conjugated backbone, a red shift can be expected as a result of this planarity. Planarity and conjugation length is further affected by sulfur-oxygen interactions, as it is the case for dioxythiophene derivatives, or by hydrogen bonding, for example existent in dioxypyrrole derivatives, regioregularity or the use of unsubstituted conjugated spacer units.[203–207]

The strategies presented in literature to tune ECPs via structural modification enables a high level of control over various material attributes such as the redox behavior, a neutral colored dark state, different color shades as well as optical contrast, processability and switching behavior. However, the major drawback of most ECPs is not yet targeted. The lack of a highly transmissive and fully colorless bright state. The residual coloration in the oxidized state is the result of a common feature of most ECPs, namely an extended tailing of the polaronic and bipolaronic absorption bands into the visible region of the electromagnetic spectrum.[171, 208] This residual coloration is acceptable in the case of very thin films, but this comes at the expense of sufficient darkening in the colored state.[59] A lot of literature is dedicated to the development of ECPs providing a neutrally colored dark state.[162, 209] Although there are a few examples of ECPs fulfilling the demanding color requirements, these materials do not have a completely colorless bright state and are mostly incompatible with high-throughput deposition techniques.[17, 31, 33, 195, 197, 210] Other materials, such as multichromophoric polymers, can actually offer suitable bright and colored states, but require elaborate synthesis routes and have an electrochemical operating window, which poses serious stability problems.[171] To date, the best ECP in terms of synthetic simplicity, color neutrality in the bright state, light transmittance change, and compatibility with high-throughput deposition techniques remains a poly(3,4-propylenedioxythiophene) (ProDOT) derivative. However, this functionalized ProDOT is still distinctively bluish in the oxidized state.[21, 197, 211, 212]

The optical and electrochemical properties of ECPs can be changed according to the strategies discussed above. In order to make these methods more comprehensible, the practical strategy for developing an ECP with a highly transmissive and colorless oxidized state is explained in more detail below. The basic principle for an ECP with such properties is a reduction of the absorption in the visible region of the electromagnetic spectrum, i.e. a bathochromic shift (red shift) of the polaronic and bipolaronic absorption bands, that can be achieved through a reduction of the band gap energy.[197, 211, 212]

A bathochromic shift in ECPs is obtained by the following considerations: Taking the 5-membered ring of thiophene with cyclic 3,4-disubstitution, the conjugation length is increased due to impossible α-β coupling and improved regioregularity. The electron donating effect of alkoxy groups, which increases the HOMO level and lowers the band gap energy also results in a bathochromic shift of the polaronic and bipolaronic absorption bands. This leads to the well-known building blocks of PEDOT and ProDOT. ProDOT derivatives generally have superior properties as compared to PEDOT derivatives as the optical contrast improves as the ring size increases. However, a polymer with a seven-membered ring, i.e. ProDOT, is sterically bulkier than the 6-membered ring of PEDOT. This disturbes interchain interactions, which reduces the planarity and resulting conjugation of ProDOT.[59, 197, 198, 211–213]

The introduction of bulky lateral alkylchains at the ethylene bridge of PEDOT increases the van-der-Waals volume of the polymer and might lead to larger band gaps due to the weakening of interchain interactions resulting from the increase of the distance between the polymer chains caused by the alkylchains. However, the introduction of a terminal double bond at the end of the lateral hexyl side chain promotes a more pronounced π-stacking between neighboring conjugated polymer chains, which leads to a narrowing of the band gap. Furthermore, the literature demonstrates that the terminal double bond of the lateral hexenyl side chain improves the planarity of the conjugated system and favors intramolecular interactions.[21, 59, 198, 213–215]

All these synthetic modifications towards a sidechain-modified 3,4-ethylendioxythiophene (EDOT) derivative result in a bathochromic shift of the polaronic and bipolaronic absorption band, upon which the blue hue, that unsubstituted PEDOT thin films show in their bright state, is removed.[59] Based on this knowledge, a series of sidechain-modified 3,4-ethylenedioxythiophene (EDOT) derivatives with a terminal double bond in the lateral sidechain, produced via straightforward synthetic modifications of the EDOT-MeOH precursor, was developed by *Fraunhofer ISC* and the *University of Milano-Bicocca* and is shown in Fig. 2.10.[21]

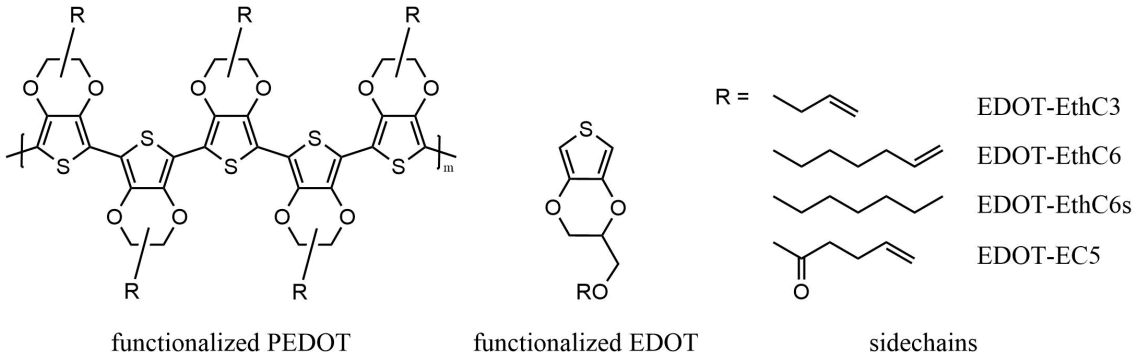

Figure 2.10: Sidechain functionalization of PEDOT (l.) and EDOT derivatives bearing a terminal double bond in the lateral solubilizing chain (r.).

2.3 Prussian Blue

Anodically-coloring Prussian Blue (PB) thin films are introduced in the present work as counter electrodes for cathodically-coloring PEDOT-EthC6 in flexible ECDs. PB, also known as iron(III)-hexacyanoferrate(II), is a mixed-valent complex compound with the molecular formula $Fe_4^{III}[Fe^{II}(CN)_6]_3 \cdot x\ H_2O$ (with $x = 14 - 16$). The face-centered cubic lattice shown in Fig. 2.11 is alternatingly occupied of Fe^{2+} and Fe^{3+}, resulting in a lattice parameter of 10.2 Å. The iron atoms are connected by bidentate cyanide ions (CN^-), whereas the nitrogen coordinates to the Fe^{3+} and the carbon to the Fe^{2+} center. The iron atoms are therefore octahedrally surrounded by six CN ligands. In the so-called insoluble PB, the lattice is occupied of Fe^{2+} and Fe^{3+} in a ratio of 3:4. 25% of the $[Fe^{2+}(CN)_6]_4$ lattice sites remain unoccupied for charge neutrality. The resulting octahedral gap is filled with water molecules, coordinated with the oxygen atom to the Fe^{3+} atom. Additional water molecules or metal cations (M^+) can be stored zeolitically on interstitial sites, as it is the case in the so-called "soluble" PB.[17, 61, 216–218]

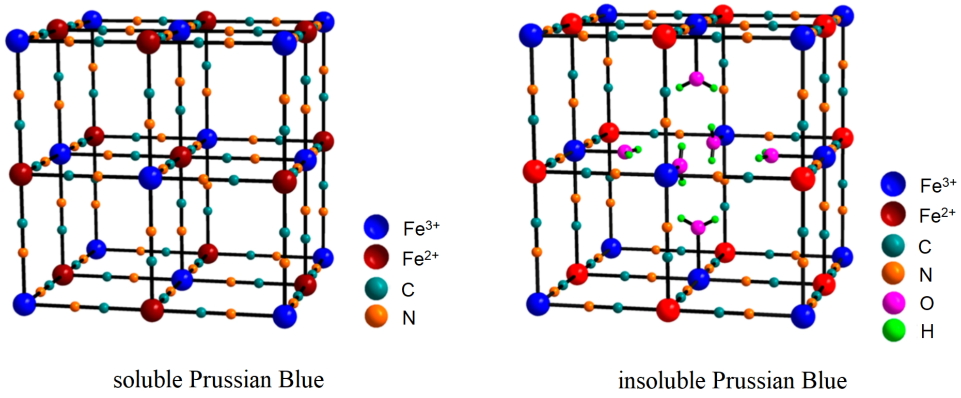

Figure 2.11: Face-centered cubic lattice of soluble and insoluble Prussian Blue (PB). Reprinted (adapted) with permission from the *American Chemical Society* according to reference [219]. Copyright (2020) American Chemical Society.

PB can be produced using precipitation reaction methods. An aqueous solution of a hexacyanoferrate(II) salt is mixed with an aqueous solution containing Fe^{3+}, resulting in a blue precipitate. With an excess of iron(III) salt, e.g. iron(III)-chloride, “insoluble” PB without metal cations is formed as shown below.[17, 130, 217, 220]

$$4\ Fe^{III}Cl_3\ (aq) + 3M_4[Fe^{II}(CN)_6]\ (aq) \longrightarrow Fe^{III}_4[Fe^{II}(CN)_6]_3 \cdot x\ H_2O\ (s) + 12\ MCl\ (aq)$$

On the other hand, “soluble” PB arises from an excess of hexacyanoferrate(II) salt or a stoichiometric mixture of Fe^{2+} and Fe^{3+} compounds during the precipitation reaction. Metal ions and water molecules are stored on the interstitial sites.[17, 130, 217, 220]

$$Fe^{III}Cl_3\ (aq) + M_4[Fe^{II}(CN)_6]\ (aq) \longrightarrow MFe^{III}[Fe^{II}(CN)_6] \cdot x\ H_2O\ (s) + 3\ MCl\ (aq)$$

"Soluble" PB is referred to as "soluble" due to its property of forming colloidal solutions. In this form, the occupation of the lattice varies from the "insoluble" PB, since no

$[Fe^{II}(CN)_6]^{4-}$ lattice sites remain vacant and, thus, only uncoordinated water molecules and alkali metal cations are stored in the lattice.[17, 130, 217] By surface modification with potassium hexacyanidoferrate(II) trihydrate ($K_4[Fe(CN)_6] \cdot 3H_2O$), the water solubility of PB nanoparticles is increased and can be used to produce PB thin films. In addition to precipitation methods, PB can be deposited in thin film form by electrochemical deposition. For this, an aqueous solution of a Fe^{3+} salt and a hexacyanoferrate(III) compound is used. The ions are in equilibrium with the soluble brown-yellow complex $[Fe^{III}Fe^{III}(CN)_6] \cdot 3H_2O$ (Prussian Yellow (PY)), which is reduced electrochemically to Prussian Blue (PB).[95, 220, 221]

$$Fe^{III}\,(aq) + 3[Fe^{III}Fe^{III}(CN)_6] + x\,H_2O + 3e^- \longrightarrow Fe^{III}[Fe^{III}Fe^{II}(CN)_6]_3 \cdot x\,H_2O\,(s)$$

The characteristic blue color of PB, which comes from light absorption with a maximum at around 680 nm, is due to an intervalence charge transfer from the Fe^{2+} via the CN ligand to the Fe^{3+}. The interaction of the stored metal cations and the octahedral coordinated CN ligands leads to a ligand field splitting of the $3d$ orbitals of both iron atoms. Due to the strong ligand field of the carbon, the Fe^{2+} assumes a diamagnetic low-spin d^6 configuration with a spin of $s = 0$, while the Fe^{3+} is in a paramagnetic high-spin d^5 state with $s = \frac{5}{2}$. The charge transfer thus takes place between these two states, as shown in Fig. 2.12. Depending on the exact composition, the properties of PB change slightly, e.g. the maximum absorption can be shifted between 650 nm and 720 nm.[17, 132, 156, 222–224]

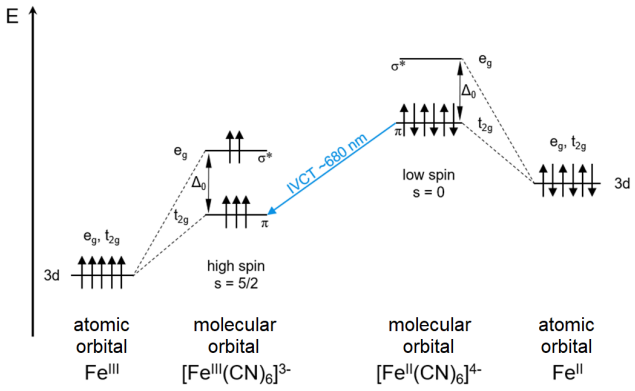

Figure 2.12: Molecular orbital scheme of Prussian Blue (PB), illustrating the intervalence charge transfer from the Fe^{2+} via the CN ligand to the Fe^{3+}.

PB can exhibit different color states. First, Prussian Blue (PB) can be reduced to Prussian White (PW), so that only Fe^{2+} cations are present. As a result, there is no energy difference between the $3d$ orbitals and no coloring charge transfer is possible. By partial oxidation of PB, the mixed-valent and greenish complex Berlin Green (BG) is formed. The iron atoms are mainly present as Fe^{3+} and partly as Fe^{2+}. Further oxidation leads to the completely oxidized yellow-brownish Prussian Yellow (PY), in which only Fe^{3+} cations are present. All redox states are shown below.[17, 61, 131, 221, 222, 225, 226]

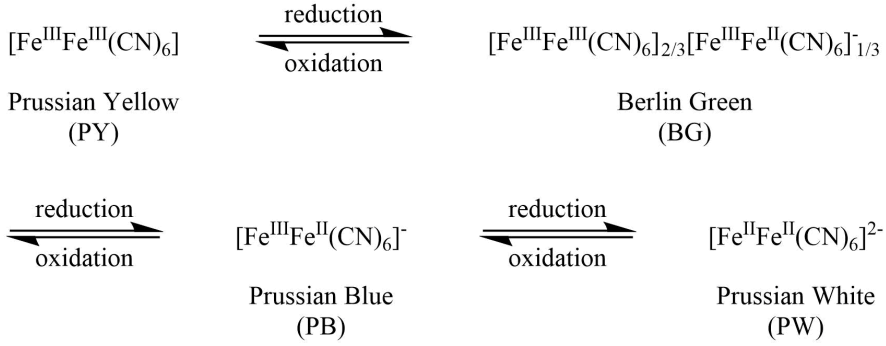

All redox states can be specifically controlled in an electrochemical cell by applying a certain potential. The characteristic absorption spectra and a cyclic voltammogram of the redox processes are shown in Fig. 2.13. The blue state of Prussian Blue (PB) with an absorption maximum at approx. 680 nm is reduced to Prussian White (PW) by applying a potential of −0.2 V vs. saturated calomel electrode (SCE), whereby the absorption band almost completely disappears. By increasing the potential, Berlin Green (BG) forms at 1.1 V vs. SCE and then Prussian Yellow (PY) forms at 1.4 V. vs SCE. The absorption band is shifted from a maximum of 680 nm to around 790 nm. Additionally, a further absorption band gradually emerges at approx. 425 nm, corresponding to the absorption maximum of $[Fe^{III}(CN)_6]^{3-}$.[17, 61, 131, 220, 222, 226–228]

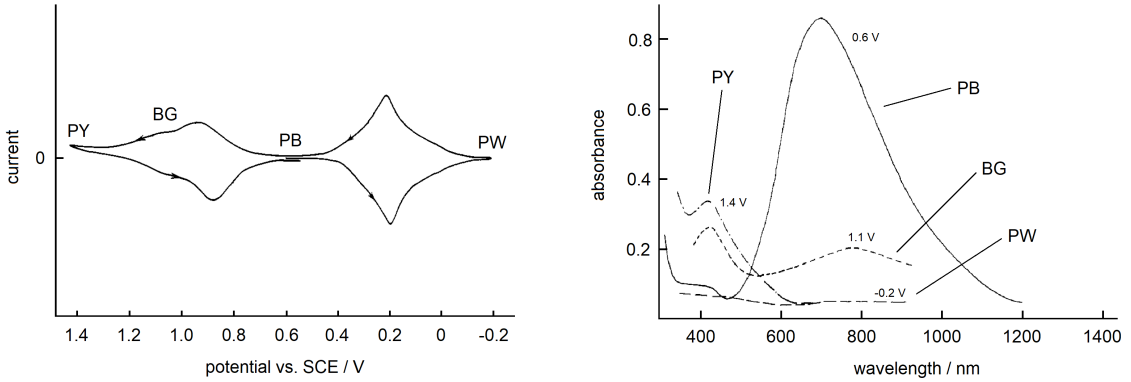

Figure 2.13: Cyclic voltammogram with a scan rate of 20 mV s^{-1} (l.) and absorption spectra at different electrode potentials vs. saturated calomel electrode (SCE) (r.) of a PB thin film in 1 M *KCl* (pH 4.0). Reprinted (adapted) with permission from the *American Chemical Society* according to reference [129]. Copyright (2020) American Chemical Society.

The stability of the redox states of PB differs. The redox reaction between PB and PY leads to changes in the lattice structure, which is why film delamination occurs after a few cycles.[229] In addition, Prussian yellow is reduced in an aqueous environment due to the oxidation of water at higher potentials and is therefore not stable.[217, 228] Since the redox reaction between PB and PW is completely reversible and has a very high cycle stability, this transition is interesting for electrochromic applications.[218, 230].

2.4 Characterization of Electrochromic Materials and Devices

The absorption or transmittance of a transparent electrochromic film or device as a function of the wavelength can be measured by UV-Vis-NIR spectroscopy. The relationship between transmitted light I_{trans} and incident light I_0 results from the Lambert-Beer law. A measure of the strength of the absorption is the optical density OD, which can be calculated from the transmittance T:[39, 95, 184]

$$OD = -\log T = -\log \frac{I_{trans}}{I_0}. \tag{2.1}$$

The intensity of the color change of an electrochromic film or device is expressed by the optical density change ΔOD, corresponding to the difference between the optical density in the bright state OD_{bright} and the optical density in the colored state $OD_{colored}$ of the sample at a specific wavelength. The contrast ratio CR, which represents the ratio of the transmittance in the bright state to the transmittance in the dark state, also characterizes the intensity of the color change. The logarithm of the contrast ratio corresponds to the change in the optical density ΔOD:

$$\Delta OD = \log CR = \log \frac{T_{bright}}{T_{colored}}. \tag{2.2}$$

The ratio of the change in the optical density ΔOD and the charge density q is called the coloration efficiency η:

$$\eta = \frac{\Delta OD}{q} = \frac{\log \frac{T_{brighted}}{T_{colored}}}{q}. \tag{2.3}$$

The coloration efficiency is positive for cathodically-coloring and negative for anodically-coloring materials or devices. It is usually calculated at a certain wavelength.[95]

The light transmittance in the visible range of the spectrum τ_v and the total energy transmittance g are particularly relevant for building and vehicle glazing. The calculation is carried out according to DIN EN 410, as shown in the following equations:

$$\tau_v = \frac{\sum_{380\,\mathrm{nm}}^{780\,\mathrm{nm}} D_\lambda \cdot \tau(\lambda) \cdot V(\lambda) \cdot \Delta\lambda}{\sum_{380\,\mathrm{nm}}^{780\,\mathrm{nm}} D_\lambda \cdot V(\lambda) \cdot \Delta\lambda}, \tag{2.4}$$

$$g = \tau_e + q_i = \frac{\sum_{300\,\mathrm{nm}}^{2500\,\mathrm{nm}} S_\lambda \cdot \tau(\lambda) \cdot \Delta\lambda}{\sum_{300\,\mathrm{nm}}^{2500\,\mathrm{nm}} S_\lambda \cdot \Delta\lambda} + q_i, \tag{2.5}$$

where D_λ is the relative spectral distribution of the standard illuminant D65 (solar radiation on a summer day in Northern and Central Europe), S_λ the relative spectral distribution of solar radiation, $\tau(\lambda)$ the spectral transmittance, $V(\lambda)$ the spectral sensitivity of the human eye (maximum at approx. 550 nm) and $\Delta\lambda$ the corresponding wavelength interval. q_i is the secondary degree of heat dissipation of the glazing to the interior. The difference in visible light transmittance and total energy transmittance between bright and colored state $\Delta\tau_v$ and Δg are important parameters of electrochromic films and devices.[231]

The color of an electrochromic film or device is determined by a colorimetric measurement according to DIN 5033 as a part of the CIELAB system shown in Fig. 2.14. The $L^*a^*b^*$ color space describes all perceptible colors by using a three-dimensional color space, in which the brightness value L^* is perpendicular to the a^*-b^*color plane. The L^* value denotes the brightness of the film or device and ranges from $L^* = 0$ (black) to $L^* = 100$ (white). The a^* values identify the green-red axis. The smallest value is $a^* = -100$ (green) and the largest value is $a^* = 100$ (red). Accordingly, the b^* value denotes the blue-yellow axis with the limit values $b^* = -100$ (blue) and $b^* = 100$ (yellow). At the origin of the a^*-b^* plane the color gray is located, while the bright colors are at the edge of the plane.

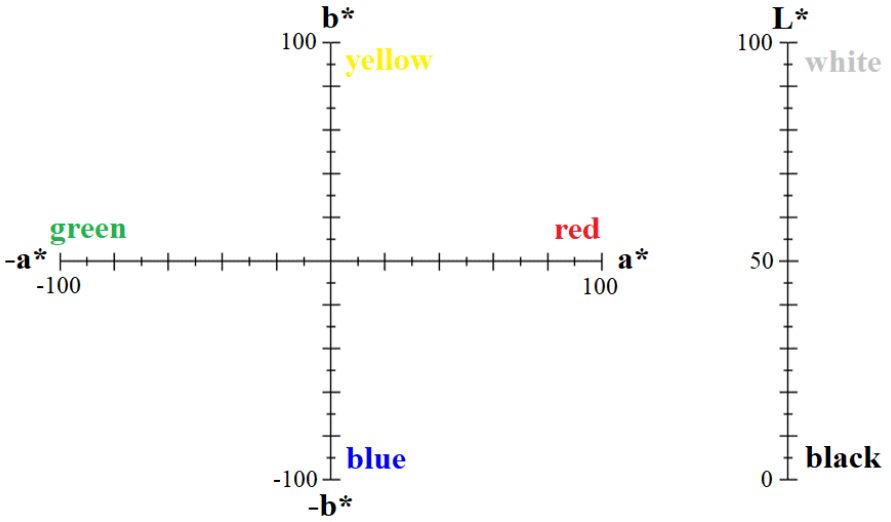

Figure 2.14: The CIELAB color space is three-dimensional with the brightness axis L^* (r.) perpendicular to the a^*-b^* color plane (l.). The L^* value denotes the brightness, whereas the a^* value identifies the green-red axis and the b^* value the blue-yellow axis.

The most important feature of the $L^*a^*b^*$ color space is perceptual relevance, which means that colors are defined regardless of how they are generated or reproduced in the way a normal observer perceives them under standard lighting conditions. The $L^*a^*b^*$ color space therefore describes the color perception better than the CIE-XYZ color space due to uniform equidistancing. Upon the inclusion of the normal observer, it is advantageous compared to RGB, CMYK or other common mathematical color systems.

A measure of the homogeneity of the color is the so-called color difference ΔE. A color location can be assigned in a three-dimensional space to every color that actually occurs (Graßmann's law). The value of ΔE between the color location 1 and 2 is calculated according to EN ISO 11664-4 as Euclidean distance and is defined as

$$\Delta E = \sqrt{(L_1^* - L_2^*)^2 + (a_1^* - a_2^*)^2 + (b_1^* - b_2^*)^2}. \tag{2.6}$$

If ΔE is between 0 and 1, a color difference cannot be recognized by the human eye. An irregularity in the color can only be recognized from values greater than 1. ΔE values greater than 10 indicate different colors.[95, 232]

The quantification of the relative haze of an electrochromic film or device must be taken into account especially for transparent see-through systems. The cloudiness of a film or device results from the layer structure, material or surface defects or from film roughness. Materials based on nanoparticles often form agglomerates during coating, on which the incident light is scattered and the layer thus becomes cloudy. The haze is determined by measuring the diffuse light scattering in accordance to DIN 52 347. The ratio of scattered light to transmitted light is taken as a percentage of haze and is referred to as the haze value. To do this, a directed white light beam penetrates the sample and crosses a subsequent hollow sphere. Non-scattered light passes through the hollow sphere and is not picked up by the detector. Haze values below 2% indicate transparent layers with no apparent cloudiness.[233]

The response time t_s is an important variable for the application of an electrochromic film or device and specifies the time in which an electrochromic film or device is colored or decolored. The response time depends, among other things, on the ion conductivity of the electrolyte, the operating voltage, the film thickness and structure, and the ion diffusion at the interface of the film and into the film. The response time is adjusted according to the respective application. Displays, sunglasses or automotive glazing should have the shortest possible response times, whereas in architectural glazing longer response times are perceived as more pleasant. In this work, the response time is determined in a potentiostatic experiment and accordingly assigned to the time after which the current has dropped to 10% of the starting value (maximum value) during the switching process.[40]

Long-term durability is mainly determined by the electrochemical resistance of the electrodes and the electrolyte of the electrochromic film or device. Degradation is usually reflected in longer response times as well as in a loss of charge density and electrochromic contrast. Long-term durability is usually expressed in terms of cycle stability. The cycle stability can be quantified by specifying the charge density or optical contrast retention as a function of the number of switching cycles. For example, the charge retention QR corresponds to the ratio of the charge density of the last cycle q_n and the charge density of the first cycle q_1:

$$QR = \frac{q_n}{q_1}. \tag{2.7}$$

In addition to the electrochemical influence and cycling stress, humidity, oxygen, UV radiation and temperature also play a role with regard to the switching behavior and stability of the electrochromic film or device.[20, 38]

2.5 Durability of Electrochromic Materials and Devices

ECD lifetime in general includes device production, stocking, transport, installation and operation until the planned demolition. Cycling durability covers the ability of an ECD to be cycled between the bright and darkened state without significant degradation of the device or it's components. Elapsed time durability includes the durability performance of an ECD with regard to elapsed time independent of any cycling, external environmental or operational stress. Elapsed time durability is often referred to as "shelf-life".[17]

Long-term performance and durability are major obstructions on the way to a successful commercialization of ECDs.[31] The requirements of the device lifetime, measured in years and number of cycles, is rather high reaching up to 25 years or 10^5 cycles under harsh conditions for architectural or automotive applications. The durability of ECPs is affected by various environmental factors such as solar radiation (mainly UV), humidity, elevated or very low temperatures or mechanical stress as well as operational factors such as switching method or the magnitude of operating voltage and current. All these factors are strongly dependent on intrinsic device properties, its individual components and the actual application. Especially for automotive application stability requirements regarding environmental and operational factors are particularly severe.[17, 31–33]

According to Harlan Byker, founder and CEO of *Pleotint* and inventor of the chemistry of the first commercially successful ECD, the automatic dimming rear-view mirror, commercialized by *Gentex*, the development of a novel set of materials takes only a fraction of time necessary for the development of an environmental and operational stable ECD.[234] Although, major advances in the development of novel organic electrochromic materials were made in the past decades, long-term performance and stability and degradation mechanism in organic ECDs are still to the greatest possible extent untapped research fields and literature is accordingly scarce.

A look at the state-of-the-art reveals that ECDs based on inorganic materials partly have sufficient long-term durability for commercialization. EC systems based on organic EC materials, with exception of the viologen-based *Gentex* night-vision system NVS®, generally do not have sufficient long-term durability for a quick market launch. Table 2.1 shows the properties concerning EC performance and device durability for two purely inorganic EC systems based on tungsten oxide and PB, as well as for the combination of organic ECP, namely PEDOT or PEDOT derivatives and PB. The listed *SageGlass* product passed ASTM E-2141-06, the standard American test method for assessing the durability of ECDs laminated between insulating glass units. The durability is estimated to 100 000 cycles and 30 years. In addition, *SageGlass Inc.*, as one of the first companies offering electrochromic systems for exterior building glazing, offers a 10 years warranty on its windows.[7, 17, 31] The tungsten oxide-based product from *EControl-Glas GmbH* passed EN ISO 12543-4, the European standard test method. *EControl-Glas* offers a 10 years guarantee on their windows as well.[7]

Table 2.1: Properties concerning electrochromic perfomance and durability of ECDs based on tungsten oxide (WO_x) or (modified) PEDOT and Prussian Blue (PB) half-cells.

ECD configuration	max. absorption wavelength λ_{max} / nm	transmission at λ_{max} T_{dark} | T_{bright} / %	contrast ratio at λ_{max} CR	coloration efficiency at λ_{max} η / $cm^2\,C^{-1}$	ref.
SageGlass®	550	3 | 71	23.7	—	[7]
WO_x/PB	550	3 | 55	18.3	75	[235]
PEDOT/PB	590	15 | 63	4.2	338	[236]
PEDOT/PB	630	22 | 52	2.4	296	[237]
PEDOT/PB	640	—	11.3	270	[166]
PEDOT-EthC6/PB	630	0.5 | 46.7	93.4	563	[238]

	operating voltage V_{dark} | V_{bright} / V	number of cycles n	contrast ratio before cycling at λ_{max} CR_1	contrast ratio after cycling at λ_{max} CR_n	ref.
SageGlass®	—	100 000	23.7	—	[7]
WO_x/PB	-0.6 | 1.2	20 000	18.3	—	[235]
PEDOT/PB	-2.1 | 0.6	50 000	4.2	1.8	[236]
PEDOT/PB	-1.5 | 1.0	2 500	2.4	1.5	[237]
PEDOT/PB	-1.0 | 1.0	21 000	11.3	2.3	[166]
PEDOT-EthC6/PB	-1.4 | 1.8	10 000	93.4	116.5	[238]

The listed examples of ECDs based on PEDOT or PEDOT derivatives are pre-commercial systems and, due to their earlier stage of development, are only partially comparable with the properties of commercial products. At least the optical properties of the shown examples are remarkable. However, their long-term stability seems yet to be the Achilles' heel of these systems on the way to a successful commercialization. Other examples of ECP-systems showing enhanced long-term durability could not be found in the literature. This points out that immense research is still necessary to understand possible degradation phenomena and to enable a wide range of applications of EC systems.[166, 235–237]

In the following, a survey on degradation phenomena and possible counteractions focusing on ECP-based electrochromic devices is given. As operational degradation factors, the method of switching and the magnitude of operational voltage and current are important to mention.[32, 239] ECDs are very similar to rechargeable lithium-ion batteries when considered as an electrochemical system. Lithium-ion batteries have been investigated extensively with regard to their durability and it has been found in particular, that the lifetime of batteries is inversely proportional to the operational current.[240, 241] Application driven high electrode potentials, for example to obtain short response times, high optical contrasts or uniform coloration, bear the risk of parasitic side reactions and accelerated aging of the components and materials of an ECD.[32, 239, 242, 243] The lifetime may be increased by altering the operating voltage or current as well as the operating algorithm, e.g. by reducing the current density or choosing between potentiostatic or galvanostatic device operation. However, this is expected to have an impact on the overall device performance.[32, 244]

Regarding degradation upon solar radiation as an environmental factor, it is known that the combination of oxygen, moisture and light is the reason for photochemical breakdown of conjugated electrochromic polymers (ECPs), which becomes apparent by a linear decrease in optical density over time.[33, 245–251] Further, the absorbance maximum is slightly shifted to smaller wavelength, which is a sign of decreased average conjugation length. The observed photobleaching and photolytic chain scission are amplified with decreasing irradiation wavelength and occur upon two separate degradation mechanism.[251–254] Photobleaching is assigned to an oxidation of the alkyl sidechains, while chain scisson is attributed to an oxidation of the thiophene backbone which are attacked mainly at the terminal thiophene units and at positions in the polymer chain where the conjugated system is interrupted. This results in a loss of conjugation.[253–259] In general, besides alkyl side chains, quaternary sites, *C-N* and *C-O* bonds are believed to photochemically destabilize ECPs, while aromatic polycyclic units stabilize the polymers.[260] To put things right and prevent ECPs from light induced degradation, ECDs are equipped with oxygen and UV barrier foils that considerably prolong the lifetime of the devices.[31, 33, 246, 247]

ECDs based on ECPs further show a high loss of performance in terms of their long-term stability upon the involvement of humidity.[17, 31] While appropriate sealing methods can be used to suppress the diffusion of water inside an ECD, residual diffusion of water can never be ruled out completely. In addition, water is displaced into an ECD during device assembly by adsorption of residual amounts of water on the electrodes or within the electrolyte.[261–264] Therefore, water is still available for parasitic side reactions when an ECD is operated.[239, 261, 263, 264] The electrochemical stability window, in which water undergoes no redox reactions is rather narrow with 1.23 V under thermodynamic equilibrium. At a pH value of 7.0 the cathodic and anodic potential limits are located at 2.62 V and 3.85 V vs. Li/Li^+.[262, 263] As shown below, above the anodic stability limit, water is oxidized to form protons and oxygen gas, while below the cathodic stability limit, water is reduced to form hydroxide and hydrogen gas.[261]

$$2\,H_2O \longrightarrow 4\,H^+ + 4\,e^- + O_2 \qquad 3.85\ \text{V vs. Li/Li}^+$$

$$2\,H_2O + 2\,e^- \longrightarrow 2\,OH^- + H_2 \qquad 2.62\ \text{V vs. Li/Li}^+$$

These potential limits are often exceeded when operating an ECP-based ECD leading to undesirable redox reactions of water, which causes the electrochemical properties of the ECD to deteriorate over a high number of operating cycles. Further, water has an influence on the ion mobility of the charge carriers in the electrolyte of an ECD. Most commonly, lithium ion-based electrolytes are applied to ECDs. Alkali metal cations, in particular lithium cations, are highly hydrated resulting in massively enlarged ion radi.[265–269] For example, the ion radius of Li^+ increases from 76 pm to 340 pm upon hydration.[270–272] This leads to hindered ion intercalation from the electrolyte into the active EC layers and decreases the ion mobility resulting in less optical contrast and higher response time.[273, 274]

To overcome water induced degradation of ECP-based ECDs, a constriction of the operating potentials is possible to prevent parasitic side reactions of water during device operation. However, this comes along with a reduced device performance in terms of optical contrast or response time.[32, 244] To influence decreased ion mobility and hindered ion intercalation, it is conceivable to substitute commonly applied lithium salts with sodium or potassium analogs, since the larger the size of the alkali metal ion, the smaller is the degree of hydration.[267, 268, 275–277] Besides appropriate sealing, electrochemically inert water scavenger can be applied to ECDs in order to intercept water molecules.

Degradation upon thermal exposure and thermal shock or cycling has to be considered as well. The typical air temperature in various climates ranges from −40 °C to 50 °C. Depending on the device construction and actual location in a building or vehicle for example, much lower or higher temperatures could be reached. In addition, heating rates of up to $3\,\mathrm{K\,min^{-1}}$ are expected, which is equal to a temperature rise of 45 °C within 15 min.[17, 31, 32] Stresses due to thermal expansion and phase transitions are immense and damages to each layer of an ECD upon different thermal expansion coefficients is possible. Apart from that, any parasitic side reaction is accelerated with increasing temperature according to van 't Hoff's rule. Furthermore, the electronic conductivity of the electrolyte increases with increasing temperature, leading to faster self-discharge of the ECD.[278] Additional mechanical stress besides thermal exposure occurs mainly upon intercalation and deintercalation of ions into and out of the active layers, inducing a swelling of the EC films, but also improper handling, transport or installation, excessive bending and deforming of flexible devices, or other physical strains such as snow loads, wind or erosion in the case of architectural glazing.[17, 31]

Environmental and operational factors as well as combinations thereof are known to cause degradation of ECP-based ECDs. As the degradation mechanism of organic ECDs is poorly understood or not published yet, the most practical approach is to use appropriate substrates and sealing materials to suppress the diffusion of moisture, oxygen or pollution gases and particles into the interior of the ECDs. However, a residual diffusion of degradation causing substances can not be ruled out completely, especially in the case of flexible polymer substrates. Similarily, due to processing conditions, undesired substances such as water are likely adsorbed or dissolved in the components and electrolyte of an ECD. Ultimately, parasitic substances present in an ECD can not completely avoided. In addition, the costs for processing and production increase with increasing requirements for a clean production.[17, 31, 32] In the automotive sector in particular, there is an extreme cost pressure, so that production under clean or dry room conditions or under a protective gas atmosphere is a particular obstacle to the commercialization of ECP-based ECDs. It is therefore of eminent importance to understand the degradation mechanisms and to avoid them in ways other than through expensive sealing methods or sophisticeted processing, for example through appropriate selection and combination of materials as well as through appropriate operational control.

3 Materials and Methods

3.1 Materials and Subtrates

Electrochromic thin films were deposited on commercially available PET-ITO substrates (OC50) from *Eastman Chemical Company*. The PET-ITO substrates used had a thickness of 127 µm (5*mil*) and an average sheet resistance of 50 Ω □ according to specification. The chemicals used for ECD preparation are listed in Tab. 3.1.

Table 3.1: List of chemicals used for electrochromic device preparation including CAS-No., molecular formula, molecular weight, supplier and purity. All chemicals were used as received.

Substance	CAS-No.	Formula	MW / g mol^{-1}	Supplier	Purity / %
PEDOT-EthC6 Preparation					
EDOT-EthC6[a]	n.a.	$C_{13}H_{18}O_3S$	254.36	COC	98.0
Acetonitrile	75-05-8	C_2H_3N	41.05	Sigma-Aldrich	99.8
Ethanol	64-17-5	C_2H_6O	46.07	Sigma-Aldrich	99.8
n-Butanol	71-36-3	$C_4H_{10}O$	74.12	Sigma-Aldrich	99.4
n-Heptanol	111-70-6	$C_7H_{16}O$	116.20	Sigma-Aldrich	98.0
Propylene amine	107-10-8	C_3H_9N	59.11	Sigma-Aldrich	98.0
Ethylene diamine	107-15-3	C_2H_8N	60.10	Sigma-Aldrich	99.5
Clevios™ C-B 40 V2[b]	n.a.	n.a.	n.a.	Heraeus	n.a.
Clevios™ C-E 60[c]	n.a.	n.a.	n.a.	Heraeus	n.a.
Prussian Blue Preparation					
aq. n-PB dispersion	n.a.	n.a.	n.a.	COC	n.a.
Borchi® Gen1253[d]	n.a.	n.a.	n.a.	OMG Borchers	n.a.
Potassium ferricyanide	13746-66-2	$K_3[Fe(CN)_6]$	329.26	Sigma-Aldrich	99.0
Iron trichloride hexahydrate	10025-77-1	$FeCl_3 \cdot 6H_2O$	270.30	Sigma-Aldrich	n.a.
Hydrochloric acid 1 M	7647-01-0	HCl	36.46	Applichem	n.a.
Polymer Electrolyte Preparation					
HQ674[e]	n.a.	n.a.	n.a.	Hydro-Québec	n.a.
Propylene carbonate	108-32-7	$C_4H_6O_3$	102.09	Sigma-Aldrich	99.7
LiTFSI[f]	90076-65-6	$LiC_2F_6NO_4S_2$	287.10	SOLVIONIC	99.9
$LiClO_4$[g]	7791-03-9	$LiClO_4S_2$	106.39	Sigma-Aldrich	99.9
Irgacure® 651[h]	24650-42-8	$C_{16}H_{16}O_3$	256.30	BASF SE	n.a.

[a] 3,4-(1-(6-Hexenyloxymethyl)etylene) dioxythiophene
[b] Iron(III) p-toluene sulfonate ($Fe(C_7H_7SO_3)_3$) solution in n-butanol
[c] Iron(III) p-toluene sulfonate ($Fe(C_7H_7SO_3)_3$) solution in ethanol
[d] Acrylic ester copolymer solution in water
[e] Polyethylene oxide-based polymer for UV-curable polymer electrolyte
[f] Lithium bis(trifluoromethanesulfonyl)imide
[g] Lithium perchlorate
[h] Photoinitiator based on 2,2-dimethoxy-1,2-diphenylethan-1-one

3.2 Manufacturing of Electrochromic Devices

ECDs with an active area of 5 x 5 cm^2 were assembled in a vertical, sandwich-like configuration with R2R-produced sidechain-modified PEDOT-EthC6 thin films on PET-ITO as working electrode (charge density: approx. 3.5 $mC\,cm^{-2}$) and PB thin films on PET-ITO as counter electrode (charge density: approx. 4.5 $mC\,cm^{-2}$). A solid polymer electrolyte (HQ674), based on polyethylene oxide, developed by *Hydro-Québec*, with LiTFSI as salt, was used as electrolyte and separator in the devices. For first proof-of-concept devices, a methyl acrylate/ethyl methacrylate-copolymer electrolyte, swollen with a solvent mixture of propylene carbonate and diethyl carbonate containing 1 M $LiClO_4$ was used.

3.2.1 PEDOT-EthC6-Based Working Electrode

PEDOT-EthC6 thin films on PET-ITO were prepared by a chemical *in-situ* polymerization process. In previous works (EU-project *EELICON*), a modular R2R coating machine, shown in Fig. 3.1, was developed and customized to suit the unique *in-situ* polymerization of EDOT-EthC6. The polymerization of EDOT-EthC6 occurs after deposition of a polymerization mixture - *in-situ* - on the PET-ITO substrate. The polymerization mixture contains the EDOT-EthC6 monomer, dissolved in n-butanol, iron (III)-tosylate as the oxidizing agent and n-propyl amine as the moderator. The PET-ITO substrate was coated using a slot die with a maximum coating width of 500 mm. The polymerization of EDOT-EthC6 takes place in a 6 m polymerization section. After a drying step (5 m oven section at 120 °C), the PEDOT-EthC6 films were rewound and stored. In a second R2R process, the PEDOT-EthC6 thin films were rinsed in reservoirs successively filled with n-butanol, n-butanol-water mixtures and ethanol and were subsequently dried in a 1 m oven module at 100 °C. The web speed was set to 0.2 $m\,min^{-1}$. The rinsed PEDOT-EthC6 thin films are partly oxidized ("as obtained"). The thin films were further treated with ethylene diamine resulting in dark blue, but transparent thin films.

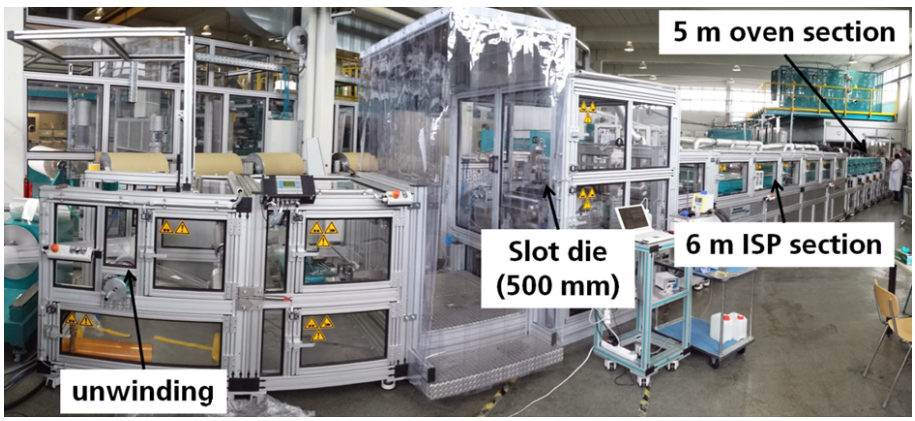

Figure 3.1: Modular R2R coating machine from *Coatema Coating Machinery GmbH* for the pilot-scale deposition of *in-situ* polymerized PEDOT-EthC6 thin films on PET-ITO. The coating machine comprises a 6 m long *in-situ* polymerization (ISP) section as a special feature. Reprinted (adapted) with permission from *Fraunhofer ISC*. Copyright (2020) Fraunhofer ISC.

For the preparation of smaller PEDOT-EthC6 electrodes, e.g. for proof-of-concept experiments on the laboratory scale, the deposition method was changed to spin coating. The polymerization mixture was not modified compared to the slot die (R2R) deposition process explained above. Within a time interval of 20 min after the addition of the oxidizing agent to the remaining polymerization mixture, the polymerization mixture was applied onto the PET-ITO substrates. Spin coating was performed by means of a *KSM Karl-Süss* spin coater model *RC8*. After manual application of the polymerization mixture onto the substrate by a pipette it was spun off subsequently at 600 rpm for 30 s and at 1200 rpm for 10 s. The resulting wet films were left for 60 min at 120 °C in a circulating air oven.

3.2.2 Prussian Blue-Based Counter Electrode

Prussian Blue on PET-ITO was obtained from a further R2R process. For the slot die coating, a PB dispersion with a solid content of 2.4 wt.% was used. For this, modified PB nanoparticles purchased from *Centre for Organic Chemistry* were dispersed in deionized water and 0.5 wt.% of the wetting and dispersing additive *Borchi® Gen1253* were added. In order to remove agglomerates from the aqueous PB dispersion, the dispersion was filtered with a syringe filter (pore size: 5 µm) before coating. The PET-ITO substrates were subjected to a corona pretreatment (0.5 kW, *Arcotec GmbH*, model *CG 061*) and coated using a slot die with a maximum coating width of 500 mm. After drying (2 m oven section at 100 °C), the sky blue, but transparent n-PB thin films were rewound and stored.

For proof-of-concept experiments on the laboratory scale, the deposition method was carried out to either a spin coating (n-PB) or a galvanostatic deposition process (ed-PB). For the spin coating, the same PB dispersion as for the slot die (R2R) deposition process was used. The PET-ITO substrates were subjected to a corona pretreatment (0.5 kW, *Arcotec GmbH*, model *CG 061*). Spin coating was performed by means of a *KSM Karl-Süss* spin coater model *RC8*. After manual application of the n-PB dispersion onto the substrate by a pipette, it was spun off subsequently at 300 rpm for 30 s. The resulting wet films were left for 60 min at 60 °C in a circulating air oven. Additionally, ed-PB thin films were produced using a galvanostatic deposition method. For this purpose, potassium(III) hexacyanidoferrate ($K_3[Fe(CN)_6]$) and iron(III) chloride hexahydrate ($FeCl_3 \cdot 6H_2O$) were dissolved in a mixture of deionized water and hydrochloric acid. The deposition was carried out in a beaker with a potentiostat/galvanostat from *IPS Elektroniklabor GmbH Co. KG* model *PGU 20V-10A*. The PET-ITO substrate exhibited the working electrode and a carbon fiber net (*Goodfellow GmbH*) represented the counter electrode. After immersing the PET-ITO substrates into the aqueous iron salt solution, a current density of 0.275 A cm^{-2} was applied for 200 s. After that, the samples were rinsed with deionized water and dryed in a circulating air oven for 30 min at 100 °C and then for 20 min at 120 °C.

3.2.3 Polymer Electrolyte

A UV-curable polymer electrolyte (HQ674), based on polyethylene oxide, developed by *Hydro-Québec* was used as electrolyte and separator in the devices. Typically, lithium bis (trifluoromethanesulfonyl) imide (LiTFSI) was used as salt.

3.2.4 Other Components

Further components for ECD assembly were a double-sided adhesive tape with a thickness of approx. 50 µm from *3M*, which was used as a spacer between the two electrodes, and a conductive and adhesive copper tape from *3M*, which was used as bus bars. The devices were eventually sealed with a modified polyisobutylene based sealing material *HelioSeal® PVS 101* from *Kömmerling Chemische Fabrik GmbH* or sealing adhesives from *DELO Industrie Klebstoffe GmbH* and *SAES Getters S.p.A.* to protect the hygroscopic polymer electrolyte from moisture that may diffuse into the device.

3.2.5 Electrochromic Device Assembly

Vertically stacked ECDs were assembled by laminating the working electrode, consisting of a PEDOT-EthC6 thin film deposited on PET-ITO, and a counter electrode, consisting of a Prussian Blue thin film deposited on PET-ITO, by means of a polymer electrolyte (HQ674). The device assembly was carried out with pre-reduced PEDOT-EthC6 working electrodes and a PB counter electrodes in it's mixed valence state, so that both films were simultaneously in their absorbing (darkened) states. The device assembly is schematically shown in Fig. 3.2. Typical laboratory-scale devices had a total size of 6 x 7 cm^2 comprising an active area of 5 x 5 cm^2. Therefore, pieces for the working and counter electrode were cut out of the appropriate PEDOT-EthC6 and PB rolls and redundant EC material was cleaned off the PET-ITO substrate (1). All around the square electrochromic area, the double-sided adhesive spacer was placed onto the PET-ITO substrate (2). In an argon-filled glovebox, the pasty polymer electrolyte was deposited onto the PEDOT-EthC6 electrode with a wet film thickness of 60 µm via the doctor blade technique (3). For particular measurements with reference electrode, a strip of lithium was laminated into the electrolyte layer through a gap in the spacer. Subsequently, the PB counter electrode was applied on top of the polymer electrolyte in such a way that on the opposite edges of the device a small off-set (1 cm) was formed (4). Then, the pasty polymer electrolyte was UV-cured by means of a LED-UV-emitter from *Dr. Hönle AG* (365 nm, 200 mW cm^{-2}) for 5 s (5). In a last step, pieces of an adhesive copper tape (bus bars) were applied onto the off-set areas for contacting (6). Afterwards, the devices were eventually sealed before operation. At each step of the device assembly, strict atmosphere control with boundary values of 5 ppm for oxygen and water was established.

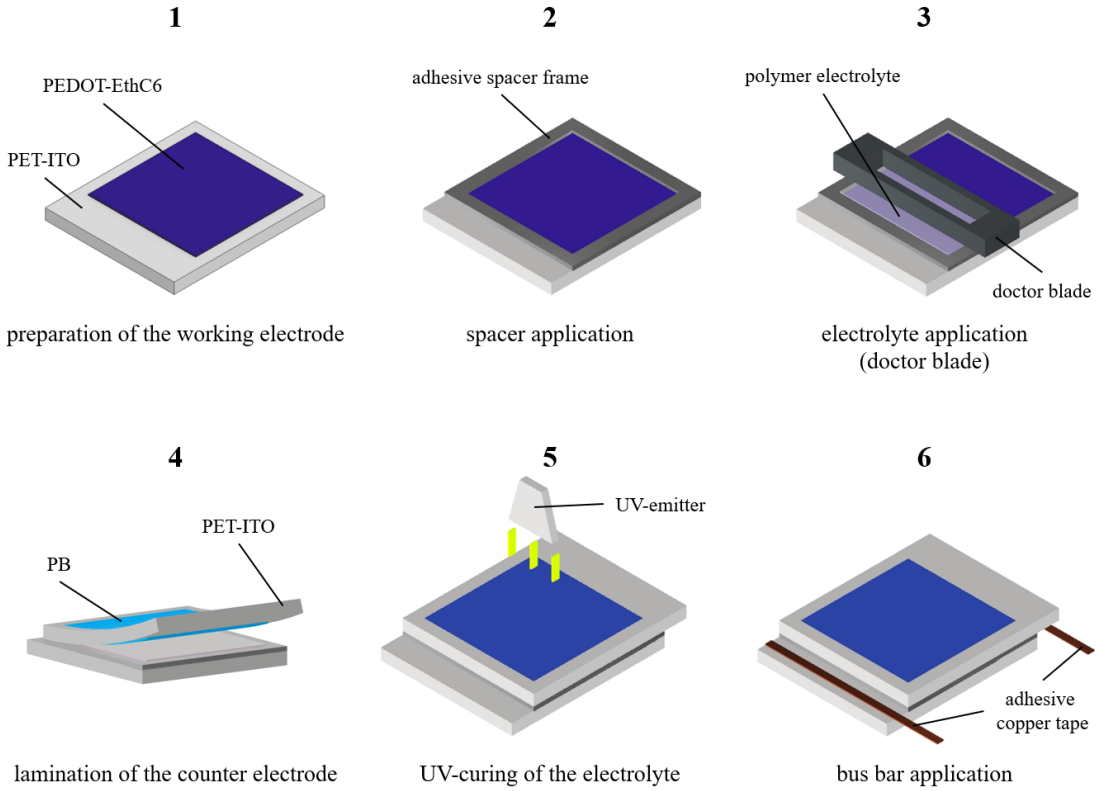

Figure 3.2: Stepwise assembly of electrochromic devices, based on a PEDOT-EthC6 working electrode, a Prussian Blue counter electrode and a UV-curable polymer electrolyte.

The assemled ECDs were eventually sealed with a modified polyisobutylene-based sealing tape *HelioSeal® PVS 101* from *Kömmerling Chemische Fabrik GmbH* or sealing adhesives from *DELO Industrie Klebstoffe GmbH* and *SAES Getters S.p.A.*. The sealing materials were manually applied around the edges of the device. The *HelioSeal® PVS 101* tape was heat-cured on a heating plate at 120 °C for 5 min from each side. The devices were weighed with a 5 kg balance weight. The sealing adhesives from *DELO Industrie Klebstoffe GmbH* and *SAES Getters S.p.A.* were UV-cured by means of a LED-UV-emitter from *Dr. Hönle AG* (365 nm, 200 mW cm^{-2}) for 60 s.

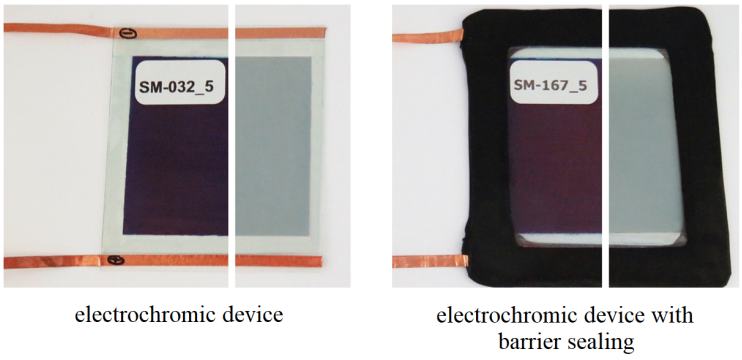

Figure 3.3: Vertically stacked electrochromic devices, based on a PEDOT-EthC6 working electrode, a Prussian Blue counter electrode and a UV-curable polymer electrolyte.

3.3 Characterization

3.3.1 Optical Characterization

The electrodes surface structures were investigated by means of a field emission scanning electron microscope SEM Ultra 55 from Carl Zeiss, equipped with an electron dispersive X-ray spectroscopy (EDX) detector system from *EDAX*. The appropriate parameters are given with the corresponding images. Prior to analysis, thin platinum or carbon layers were deposited on the sample surfaces by sputtering with an *Oerlikon Balzers* device, model *MED010*. For cross-section analysis, a cross section polishing (CSP) preparation was performed. Therefore, the sample was treated with an argon ion beam in order to obtain clean and polished surfaces.

The diffuse light scattering of the EC layers and devices was determined using a *Hazegard XL-211* device from *Pacific Scientific*. The measurements were performed versus air as reference. The EC layers were faced to the incident light source. All samples were tested at five different positions and the average haze value was calculated. The contribution of the substrate is included in all denoted haze values.

3.3.2 UV-Vis-NIR Spectroscopy and Colorimetry

Color changes as a result of redox processes of the EC layers and devices were quantitatively studied by means of UV-Vis-NIR spectroscopy and colorimetry. UV-Vis-NIR spectra and color coordinates (CIELAB color space, with L* (lightness from black to white (0-100)), a* (negative values indicate green, positive values indicate magenta), and b* (negative values indicate blue, positive values indicate yellow)), were recorded using a *Ava-Spec-2048* standard fiber optic spectrometer from *Avantes*, combined with a balanced deuterium-halogen light source (wavelength range from 200 nm to 2500 nm). All measurements were performed under an argon atmosphere at room temperature.

3.3.3 Electrochemical and Spectroelectrochemical Characterization

A *Solartron Multistat 1470E* multi-channel potentiostat/galvanostat and an *Ava-Spec-2048* standard fiber optic spectrometer from *Avantes*, combined with a balanced deuterium-halogen light source (wavelength range from 200 nm to 2500 nm), were used for all electrochemical and spectroelectrochemical characterization of EC layers and devices. Preparation and characterization of the EC layers and devices were performed at room temperature in an argon-filled glove box (<5 ppm oxygen and water).

For electrochemical measurements, EC layers on PET-ITO (active area: 1.7 x 3.0 cm^2) were contacted with adhesive copper tape from *3M* and placed into a 4-neck flask with the help of an electrode pin. Counter and reference electrodes were cut from lithium foil and placed into the flask with electrode pins as well. 1*M* LiTFSI in propylene carbonate was used as the electrolyte.

Spectroelectrochemical characterizations of EC layers on PET-ITO were conducted *in-situ*. Therefore, UV-Vis spectra and color coordinates (CIELAB color space) were recorded *in-situ* during potentiostatic switching. The switching voltage was generated using a *Voltcraft PS 302-A* laboratory power supply. The samples were cut to an active area of 1.7 x 3.0 cm^2, contacted with adhesive copper tape from *3M* and placed together with a lithium strip as counter and reference electrode into a quartz cuvette filled with $1M$ LiTFSI in propylene carbonate as the electrolyte.

The electrochemical and spectroelectrochemical characterization of the ECDs (active area: $5\,cm^2 \times 5\,cm^2$) was performed under identical conditions to that of the EC layers. The PEDOT-EthC6 and PB thin films represent the working and counter electrodes accordingly. The ECDs were contacted with the copper bus bars to the poteniostat/galvanostat and were likewise placed into the spectrometer sample stage for characterization.

After the spectroelectrochemical characterization, EC layers and devices were potentiostatically cycled for five cycles to determine the response time. Then, CVs with several scan rates (five cycles each) as well as charging and discharging experiments at several current densities were performed. Finally, the EC layers and devices were cycled for up to $10,000$ cycles under inert glove box conditions (dry argon atmosphere). In addition, the cycling of the ECDs took place either under ambient conditions (laboratory atmosphere), in a dry air laminar flow box or under a humid argon atmosphere (90% rH) in a glove bag.

3.3.4 Karl Fischer Titration

The Karl Fischer titration is a direct method to determine the water content of a sample. The method is especially useful for low moisture levels (<1%), as it is the case for the components of an ECD. Coulometric Karl Fischer measurements were performed in a single-electrode Coulometer type *KF-Coulometer 831* equipped with an oven, model *KF-Thermoprep 832* and a stirring unit type *728 Stirrer* from *Metrohm*. *Hydranal Coulomat AK*, a solution of sulfur dioxide, 1H-imidazole monohydriodide and imidazol hydrobromide in a mixture of ethylene glycol monomethyl ether, chloroform and 2,2,2-trifluoroethanol.

For electrolyte analysis 5 g benzoic acid per 100 mL test solution were added, as carbonates react with the *Hydranal Coulomat AK* and release water. After adding a sample of the electrolyte with a syringe, the solution was stirred at the highest stirring setting for 60 s before the measurement was started in order to ensure a complete dissolving of the polymer electrolyte and to avoid an excessive side reaction with the generator electrode. Karl Fischer titrations itself were carried out for 120 s and stopped after a device drift of $<10\,\mu g\,min^{-1}$ was reached.

For electrode analysis the samples were put into the device oven and were heated to 200 °C. The solution was stirred at a medium stirring setting. Via a dry air carrier gas stream, the expelled moisture from the heated sample flows directly into the titration cell, in which the Karl Fischer water determination takes place. Karl Fischer titrations were carried out for 150 s and stopped after a device drift of $<20\,\mu g\,min^{-1}$ was reached.

3.3.5 Post-Mortem Characterization

Post-mortem analysis of operated ECDs was typically performed after 10,000 switching cycles, whereby the devices were stepwise disassembled. The solid polymer electrolyte and the EC layers were removed with water or ethanol to finally reveal the bare PET-ITO substrates. Post-mortem characterization covers spectroelectrochemical analysis of the operated device, detailed characterization of the electrodes (including scanning electron microscopy (SEM), haze and adhesion analyis, UV-Vis-NIR spectroscopy and colorimetry as well as electrochemical and spectroelectrochemical analysis) and SEM and X-ray diffractometry (XRD) analysis of the bare PET-ITO substrates.

3.3.6 Others

The crystallographic properties of the PET-ITO substrates were analyzed by XRD. A *Malvern Panalytical Empyren* XRD diffractometer with copper K_α wavelength and grazing incidence geometry was used. The diffraction patterns were recorded from 25° to 55° 2Θ, with a 0.02° step size, 30 s step time and an incidence angle of 0.50°.

GC/MS measurements of the PEDOT-EthC6 dispersion were performed with a gas chromatograph type *Clarus 500* from *Perkin Elmer*, equipped with an auto sampler and a mass spectrometer. Samples were prepared by solvent extraction with n-heptanol and distilled water, oxidized with sodium thiosulfate and diluted with ethanol.

Hydrodynamic diameters and zeta potential of the PEDOT-EthC6 nanoparticles were analyzed by dynamic light scattering (DLS, *Malvern Instruments Zeta Sizer*).

Kinematic viscosity of the PEDOT-EthC6 dispersion was measured with a *Schott AVS 400* capillary viscometer.

4 Results and Discussion

This section of work is predominately made up of excerpts from published materials from internationally recognized peer-reviewed journals ("kumulative Dissertation"). The publications build on one another and are summarized and discussed individually first. This is followed by a joint discussion and evaluation of all results achieved.

This work will begin by addressing an aforementioned drawback of most ECPs: the lack of highly transmissive and fully colorless bright states. This is accomplished by the evaluation of a series of EDOT derivatives with a terminal double bond in the lateral sidechain to potentially achieve a fully colorless bright state. All of the EDOT derivatives are electrochemically polymerized on the laboratory scale and are characterized by means of (*in-situ*) (spectro-)electrochemistry in order to identify the influence of the terminal double bond on transmittance and color neutrality of the sidechain-modified polymers bright states. Based on this detailed evaluation and comparison, the best performing compound is intended to be chosen for up-scaling towards a continuous and large-area R2R-process in an industrially relevant environment.[21]

Regarding the R2R-produced sidechain-modified ECPs, the results obtained from a single electrode have a limited significance for the practical usability in ECDs. The novel polymer has to be combined with a suitable counter electrode and electrolyte to form a functional ECD. As a secondary aim, the sheet-to-sheet (S2S) laminated devices are optically and (spectro-)electrochemically characterized to verifiy the functionality of the novel ECP in the set-up of an ECD. Beyond that, not only the initial performance of laboratory-scale ECDs are important, but also the results obtained from prolonged cycling tests and the scalability of the manufacturing process. Regarding these challenges, prolonged cycling tests are performed under laboratory conditions and the manufacturing process is examined with regard to the implementation of large-area ECDs by customized and high-throughput S2S and R2R lamination processes.[238]

Common practice in scientific literature is to perform cycle testing under strict laboratory conditions or in inert, highly controlled atmospheres. This does not represent the standard conditions, in which an ECD operates, i.e. in the presence of UV-light, oxygen and air moisture. It is therefore crucial to demonstrate the cycle performance of the S2S laminated ECDs in demanding environmental conditions. As such, the following portion of this work is dedicated to the results of conscious environmental aging tests applied to the devices based on the sidechain-modified polymer.

As it is indicated by the title of this work, the emphasis of the research presented here is concentrated on the influence of air moisture and the subsequent failure mechanisms regarding the sidechain-modified polymer-based ECDs. In this context, serious stability problems may arise, if the presence of water is combined with high operating voltages of an ECD. If the operating voltage of ECDs are adjusted to maximize the light transmittance change and to minimize the response time, poor stability may result due to side reactions of the active layers. Additionaly, the diffusion of water into the ECDs can hardly be completely suppressed during operation. For ECDs, these considerations imply a possible degradation of the single components if the appropriate potential and moisture are present. ECDs are aged in the third portion of this work by means of accelerated aging tests at humid atmospheres (90 % rH). After the aging, the ECDs are intended to be subjected to a post-mortem characterization in order to assign possible degradation to the corresponding layers or components.[279]

In addition to the understanding of the degradation mechanisms, it is also important to investigate measures to avoid the degradation of ECDs. This is primarily associated with the avoidance of appropriate electrode potentials necessary for side reactions in humid atmospheres. As an intrinsic action point, the electrode potentials are investigated via a three-electrode set-up of an all-solid-state ECD. Extensive knowledge on the electrode potentials allows to eventually avoid the voltage- and moisture-induced degradation in the flexible ECDs. The implementation of an unbalanced electrode configuration (charge density ratio between working and counter electrode) enables smaller potential windows and thus limits the range for potential side reactions. This is usually associated with a deterioration of the device properties, such as lower optical contrast or longer switching times, as the potentials are no longer sufficient for maximum device performance. This trade-off between actual device performance and cycling stability during operation in humid atmospheres must be taken into account and adapted to the requirements of the corresponding applications.[279]

The avoidance of the mentioned moisture-related degradation phenomena is further associated with appropriate sealing methods and materials as well as appropriate electrode and device fabrication processes. Since a variety of sealing materials is commercially available, due to the commercial launch of organic photovoltaic (OPV) and organic light emitting diodes (OLEDs), the focus in the present work is put to water-free electrode fabrication. As an extrinsic action point, a novel preparation method of a nanoscale ECP dispersion based on organic solvents is presented here in a final step. The water-free processing method gives further access to straightforward printing and coating processes on flexible substrates and thus represents a promising alternative to the established, but water-based $PEDOT{:}PSS$.[280]

4.1 PEDOT-Based Polymer with Colorless Bright State for Flexible Electrochromic Devices

The content of this section is published in Macher, S., Schott, M., Sassi, M., Facchinetti, I., Ruffo, R., Patriarca, G., Beverina, L., Posset, U., Giffin, G. A., Löbmann, P., New Roll-to-Roll Processable PEDOT-Based Polymer with Colorless Bleached State for Flexible Electrochromic Devices, *Advanced Functional Materials* **2020**, 30, 1906254. Text and figures are reprinted (adapted) with permission from *WILEY-VCH Verlag GmbH & Co. KGaA* according to reference [21].

As described above, a common drawback of most ECPs is the lack of a highly transmissive and fully colorless bright state. This is the result of the extended tailing of the polaronic and bipolaronic absorption bands into the visible region of the electromagnetic spectrum.[171, 208] A reduction of the absorption in the visible region of the electromagnetic spectrum can be achieved through a bathochromic shift of the polaronic and bipolaronic bands.[197, 211, 212] A bathochromic shift in PEDOT- and ProDOT-like structures is obtained by the introduction of bulky lateral sidechains that increase the van-der-Waals volume of the polymer and improve the planarity of the conjugated system.[187, 188] The introduction of a terminal double bond at the end of the lateral hexyl side chain in the case of poly(3-hexylthiophene) (P3HT) promotes a more pronounced π-stacking between neighboring conjugated polymer chains, which leads to a narrowing of the band gap. Furthermore, it is demonstrated that the terminal double bond of the lateral hexenyl sidechain improves the planarity of the conjugated system and favors intramolecular interactions.[214, 215]

In this work, a series of EDOT derivatives with a terminal double bond in the lateral sidechain is described. The results highlight the influence of the terminal double bond on the improved light transmittance change and the color neutrality in the bright state. The monomers reported in Fig. 4.1 can be prepared in a straightforward, one-step synthesis starting from the 9:1 mixture of the EDOT-MeOH and ProDOT-OH monomers.

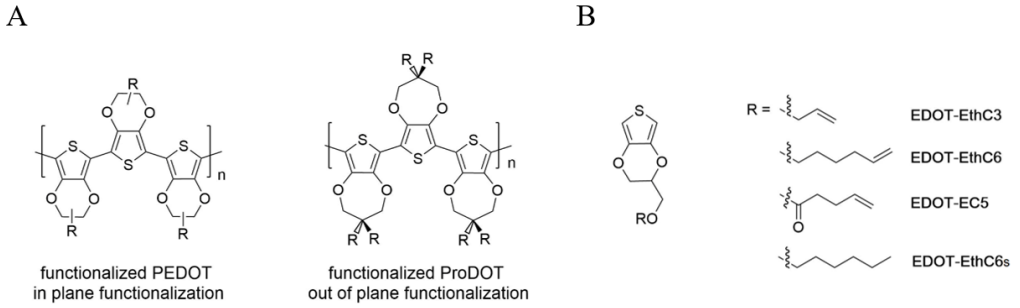

Figure 4.1: Sidechain functionalization of the PEDOT and ProDOT monomers. Depicted are the substitution patterns of PEDOT and ProDOT highlighting the in-plane and out-of-plane geometries (A) and sidechain functionalized EDOT derivatives bearing a terminal double bond in the lateral solubilizing chain, along with the control derivative EDOT-EthC6s (B).

All functionalized monomers were electrochemically polymerized to EC polymer thin films with comparable film thickness in order to compare the EC properties of the corresponding polymers on a laboratory scale under standard conditions (Fig. 4.2).

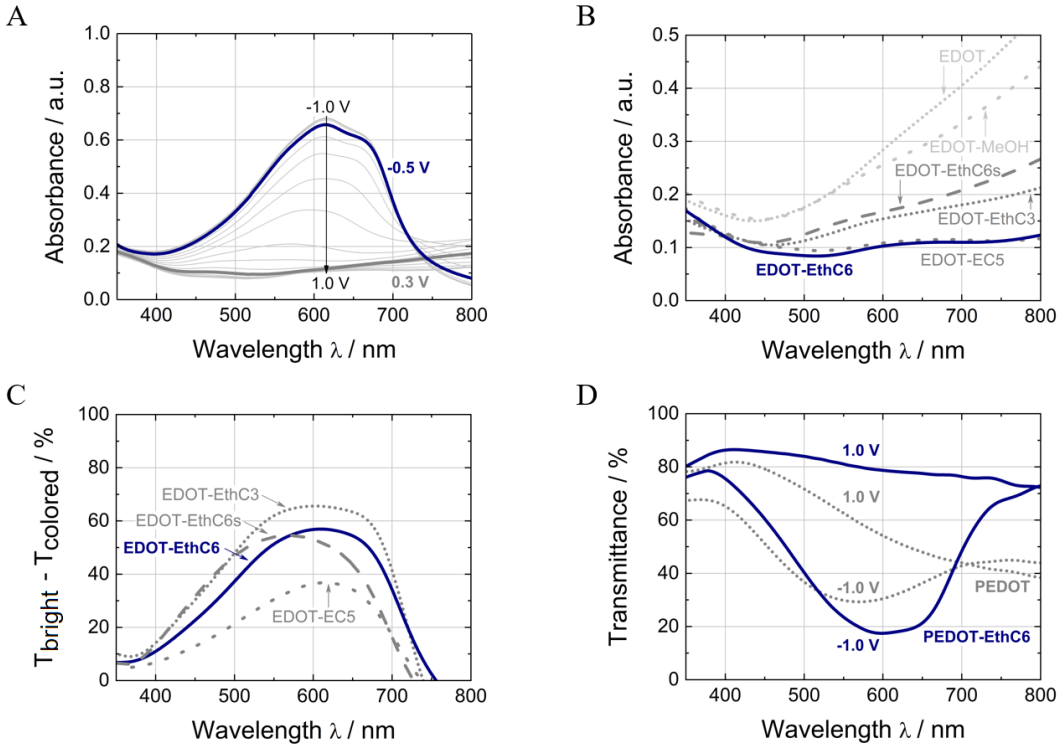

Figure 4.2: Electropolymerized PEDOT-based thin films. Shown are the absorption spectra at different potentials (1.0 V $\leftrightarrow$ −1.0 V vs. $Ag/AgCl$, 0.1 V steps) of a PEDOT-EthC6 thin film (A), absorption spectra of all polymer thin films in their bright (charged/oxidized) states (B), transmittance change ($\Delta\, T$) of all polymer thin films (C) and transmittance spectra of chemically (*in-situ*) polymerized PEDOT and PEDOT-EthC6 thin films in their bright (charged/oxidized at 1.0 V vs. $Ag/AgCl$) and colored (uncharged/reduced at −1.0 V vs. $Ag/AgCl$) states (D).

Figure 4.2A shows the (*in-situ*) spectroelectrochemical characterization of PEDOT-EthC6. The absorption spectra illustrate that the PEDOT-EthC6 thin film is in its highly transmissive (bright) state at a potential above 1.0 V vs. $Ag/AgCl$, where the PEDOT-derived backbone is charged/oxidized and has a very weak absorption. At a potential of −1.0 V vs. $Ag/AgCl$, the polymer thin film is in the uncharged/reduced state and the layer turns deep blue due to a strong and broad absorption with a maximum at around 620 nm. Figure 4.2B shows the comparison between the absorption spectra of all polymers in the bright state and the corresponding absorptions of PEDOT-MeOH – the common precursor – and the unsubstituted PEDOT. The shift of the polaronic/bipolaronic band towards the NIR region is particularly evident for PEDOT-EthC6 and PEDOT-EC5, the monomers containing longer alkyl side chains with a terminal double bond. Figure 4.2C shows that PEDOT-EthC3 and PEDOT-EthC6 have the highest light transmittance change ($\Delta\, T$) of the series . However, while PEDOT-EthC3 is not colorless in its bright state, PEDOT-EthC6 has a virtually colorless bright state and a high light transmittance change, which made it the polymer of choice for upscaling.

A technique more suitable for upscaling - compared to electropolymerization - is a chemical *in-situ* polymerization process, since it is compatible with high-throughput and large-area R2R deposition methods. Therefore, all monomers were also chemically polymerized according to literature protocols.[281] Only the EDOT-EthC6 derivative gave results comparable with those obtained by electrochemical polymerization. Figure 4.2D shows a direct comparison between the limiting states in the (*in-situ*) spectroelectrochemistry analysis of chemically (*in-situ*) polymerized PEDOT and PEDOT-EthC6. Both the increase in the bright state transmittance and the light transmittance change are evident for PEDOT-EthC6. For upscaling, a modular R2R coating machine was developed and customized to suit the unique *in-situ* polymerization process. The polymerization of the EDOT-EthC6 occurs after deposition of a polymerization mixture directly on the PET-ITO film.

In Fig. 4.3A, a SEM image of a PEDOT-EthC6 thin film is depicted. The topography of the PEDOT-EthC6 layer appears as a characteristic three-dimensional, periodical honeycomb pattern. The honeycomb structure is ascribed to a rinsing process of the solid PEDOT-EthC6 thin films performed after the *in-situ* polymerization process, in which the remaining oxidizing agent is removed from the polymer film with alcoholic and water solvent mixtures. The cross-section image in Fig. 4.3B demonstrates a film thickness of around 400 nm and a smooth interface between the PEDOT-EthC6 and ITO layer, thus indicating good interlayer adhesion and a highly transparent film stack. The high transparency is reflected in the haze measurement with values below 1%, which means that only very little light is wide angle scattered or diffused due to irregularities or rough interfaces in the thin film.

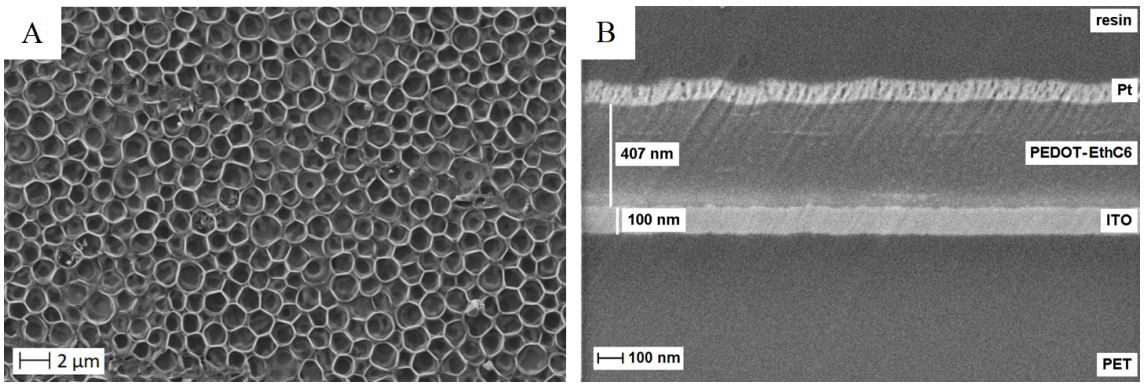

Figure 4.3: Characteristic SEM images of a PEDOT-EthC6 thin film. Depicted are the surface morphology, showing a characteristic three-dimensional, periodical honeycomb pattern (A) and a cross-section image indicating a film thickness of approx. 400 nm (B).

The spectroelectrochemical characterization of *in-situ* polymerized PEDOT-EthC6 is depicted in Fig. 4.4A. The absorption spectra illustrate that the color neutral (bright) state is reached at a potential of 3.7 V vs. Li/Li^+. The PEDOT-derived backbone is charged/oxidized and shows a very weak absorption. The visible light transmittance τ_v is 63%. At a potential of 2.1 V vs. Li/Li^+ a strong and broad absorption with a maximum at around 620 nm ($\tau_v = 4\%$) is responsible for the deep blue color (darkened) that occurs when the backbone is in its uncharged/reduced state.

The analysis of the L*a*b* values (CIELAB color space), L* = 83.8, a* = 4.3, b* = −4.1 and L* = 29.7, a* = 17.0, b* = −58.2, further confirms the neutral color of the bright state and the deep blue color of the darkened state, respectively. The visible contrast ratio can be estimated as CR = 15.8 (ΔL* = 54.1). The coloration efficiency at the absorption maximum of 620 nm is calculated to be approx. 530 $cm^2\,C^{-1}$, which substantially exceeds most commonly-used inorganic EC materials.[114, 171] The *in-situ* polymerized PEDOT-EthC6 films are significantly thicker than the electrochemically polymerized PEDOT-EthC6 thin films, which leads to a higher contrast ratio. The appropriate film thickness depends on the application and can be adjusted by the web speed and the delivery volume of the polymerization mixture during the *in-situ* polymerization process.

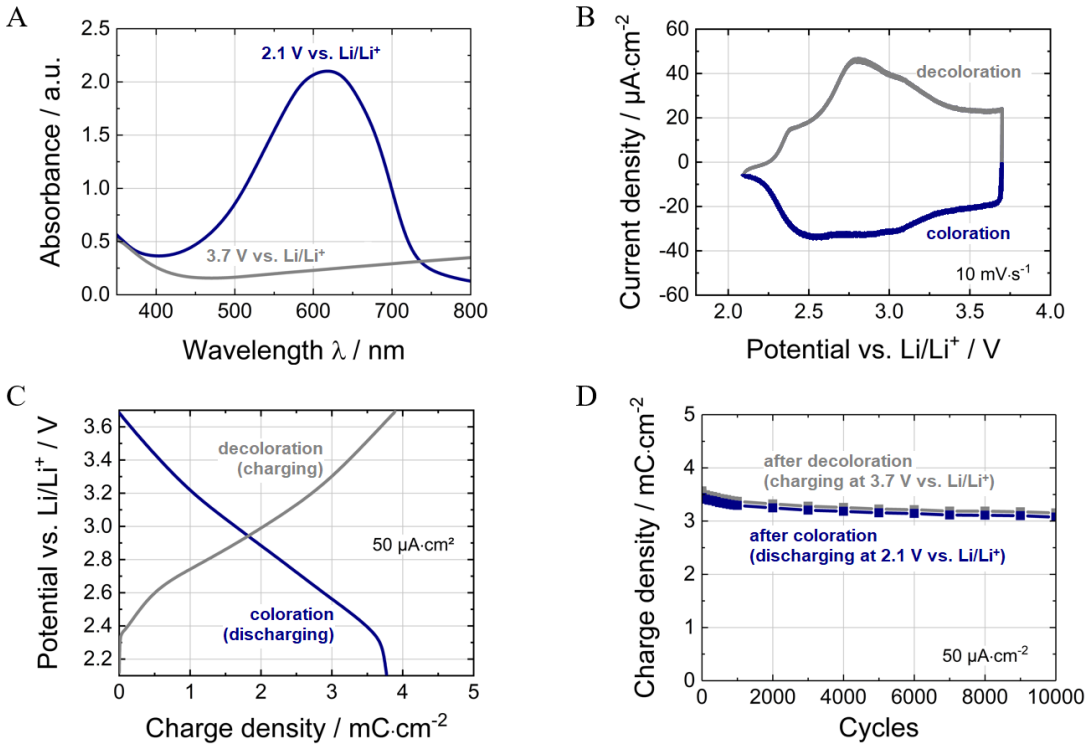

Figure 4.4: (Spectro-)electrochemical characterization of the PEDOT-EthC6 thin films on PET-ITO in 1 *M* $LiClO_4/PC$ including absorption spectra of the PEDOT-EthC6 thin film in its charged/oxidized (3.7 V vs. Li/Li^+) and uncharged/reduced (2.1 V vs. Li/Li^+) state (A), a cyclic voltammogram at a scan rate of 10 mV s^{-1} (B), the charging/discharging behavior at a current densities of 50 µA cm^{-2} (C) and cycle stability measurements over 10 000 switching cycles (2.1 V ↔ 3.7 V vs. Li/Li^+) at a current density of 50 µA cm^{-2} (D).

The electrochemical properties of the *in-situ* polymerized PEDOT-EthC6 thin films were initially investigated by cyclic voltammetry (CV). Figure 4.4B shows the CVs at a scan rate of 10 mV s^{-1}. The *in-situ* polymerized film exhibits reversible redox peaks at a potential of 2.8 V (anodic scan) and 2.5 V (cathodic scan) vs. Li/Li^+ (ΔE_p = 300 mV) corresponding to the oxidation (decoloration) and reduction (coloration) process, respectively, of the conjugated backbone.

The substantially broadened cathodic and anodic half-waves are an unavoidable consequence of hindered diffusion and insertion of the perchlorate counter anions and molecular inhomogeneities in the polymer matrix (e.g. different chain length, different sizes of crystalline domains, polymer particle dimensions, pore dimensions). The mentioned inhomogeneities are assigned to the molecular level and affect therefore the redox potentials but do not cause haze. The coulombic efficiency is approximately 1, indicating a reversible redox process. The results from the CV measurements are in agreement with previously published data of similar PEDOT and PEDOT-like species.[165, 281, 282] The PEDOT-EthC6 films were further characterized in galvanostatic charging/discharging experiments with current densities between $1\,\mu A\,cm^{-2}$ and $1000\,\mu A\,cm^{-2}$. The charge and discharge curves are depicted in Fig. 4.4C. They also show a reversible oxidation and reduction behavior, while the coulombic efficiency is around 0.98 at a current density of $50\,\mu A\,cm^{-2}$. The maximum charge density is determined after the discharging (reduction) process at 2.1 V vs. Li/Li^+ and depends on the applied current density. The PEDOT-EthC6 film exhibits a maximum charge density of $4.1\,mC\,cm^{-2}$ at a current density of $1\,\mu A\,cm^{-2}$.

The results from the cycle stability measurements are shown in Fig. 4.4D. The measurement was performed by charging and discharging the PEDOT-EthC6 thin film on PET-ITO in a 1 M $LiClO_4/PC$ electrolyte with a current density of $50\,\mu A\,cm^{-2}$. The results indicate a reversible redox switching behavior with only a small drop of charge density in the first 1 000 cycles ($0.1\,mC\,cm^{-2}$), which can be attributed to formation processes and further electrochemical polymerization of the polymer chain. Additional loss of charge density can be explained by hindered diffusion and insertion of the perchlorate counter anions during the accelerated cycling experiment. After 10 000 switching cycles, the PEDOT-EthC6 thin film on PET-ITO shows a total charge retention of more than 91%, the charge density decreases from $3.5\,mC\,cm^{-2}$ to $3.2\,mC\,cm^{-2}$.

The performance of the PEDOT-EthC6 thin films were tested under inert conditions in a typical sandwich-like ECD with an active area of 5 x $5\,cm^2$. The cathodically-coloring PEDOT-EthC6 functions as the working electrode, while a PB thin film on PET-ITO was used as the anodically-coloring, and therefore complementarily-switching, counter electrode.[61, 283, 284] The colored state of the ECD (−1.4 V) shows an intense deep blue color (L* = 24.4, a* = 10.4, b* = −47.2), whereas the bright state (1.8 V) is distinguished by a highly transmissive neutral coloration (L* = 76.3, a* = −5.7, b* = 2.5). The high transparency of the ECD is reflected in the haze measurement with values below 2% for the colored and decolored state. It should be noted that the optical properties of the PET-ITO substrate are included as the measurements were conducted versus air. The corresponding absorption spectra of the colored and bright state are presented in Fig. 4.5A. In the dark state, a strong and broad absorption peak with a maximum at 635 nm is visible, which is attributed to the signal of the PEDOT-EthC6 film superimposed with that of the PB thin film. The shoulder at around 690 nm is associated with the PB layer, which on its own exhibits an absorption maximum at 690 nm.

The visible contrast ratio is estimated to be 16.7, a result which clearly outperforms the properties of commonly-used PEDOT-based ECD.[285] Furthermore, the response time, which is considered to be the time corresponding to a current drop to 10% of the starting (maximum) value, was analyzed in a potentiostatic experiment (Fig 4.5B). For the decoloration and coloration processes, a response time of around 8 s and 10 s, respectively, was measured. The response time of the full device (PEDOT-EthC6/PB) is limited by the sheet resistance of the PET-ITO (approx. 50 Ω □) and the insulating PB layer. The cycling stability tests of the ECD (100 cycles) show enhanced durability with a total charge retention of more than 97%.

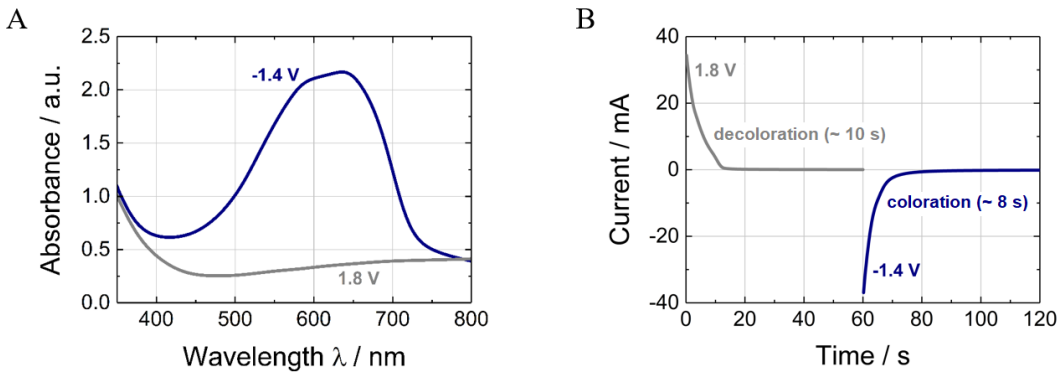

Figure 4.5: Characterization of the proof-of-concept ECD with PEDOT-EthC6 as the working electrode and PB as the counter electrode and a $LiClO_4$-containing polymer electrolyte. Absorption spectra of the ECD with (A) and the response time measurement during potentiostatic cycling (60 s at 1.8 V ↔ 60 s at −1.4 V) (B) are shown.

In conclusion, PEDOT-EthC6 thin films, obtained from the customized R2R process, have enhanced EC properties in terms of coloration efficiency, transmittance and color neutrality in the bright state, cycle stability and reversibility. The PEDOT-EthC6 films were further successfully incorporated into a proof-of-concept electrochromic device using a Prussian Blue (PB) counter electrode. The following investigations are focused on a closer examination of the PEDOT-EthC6/Prussian Blue ECDs with respect to optical and (spectro-)electrochemical properties as well as long-term durability as a particularly important parameter in the present work.

4.2 Flexible Electrochromic Devices with Enhanced Cycling Stability

The content of this section is published in Macher, S., Schott, M., Dontigny, M., Guerfi, A., Zaghib, K., Posset, U., Löbmann, P., Large-area Electrochromic Devices on Flexible Polymer Substrates with High Optical Contrast and Enhanced Cycling Stability, *Advanced Materials Technologies* **2021**, 6, 2000836. Text and figures are reprinted (adapted) with permission from *WILEY-VCH Verlag GmbH & Co. KGaA* according to reference [238]. In the context of the present dissertation, results from reference [21] and section 4.1, respectively, serve as the fundamental basis of this section. An explicit multiple use of results is only given for the spectroelectrochemical characterization of the PEDOT-EthC6 thin films (see Fig. 4.4A and Fig. 4.8C).

The performance of the PEDOT-EthC6 thin films were tested in a proof-of-concept ECD with an active area of 5 x 5 cm^2 before. PEDOT-EthC6 was combined with a PB counter electrode. The above-mentioned PEDOT-EthC6 exhibits a deep blue color in its reduced state. In contrast to that, PB is blue in its partly oxidized mixed-valence state and turns completely colorless upon reduction to PW.[20, 286, 287] At best, the joint properties of such "half-cells" lead to improved optical properties, e.g. a higher visible light transmittance change. However, the interplay of switching characteristics and charge balance of the EC half cells, increase the complexity of the system and has to be considered as well. Many academic research groups are primarily concerned with the fundamental feasibility of innovative new material concepts.[167] Aspects regarding device assembly, electrolyte and counter electrode choice as well as the full device processing remain mostly unconsidered.

For large area manufacturing of ECDs, cost-effective and scalable processing and assembly techniques are required. If liquid stable precursors for the electrochromic materials are at hand, large-area and high throughput R2R fabrication by means of slot-die coating on flexible substrates may be the method of choice. For example, commercially available tin-doped indium oxide-coated polyethylene terephthalate (PET-ITO) films can be used as substrate. After application of the two complementary switching EC films on two single conductive sheets, they must be laminated by a jellylike or pasty electrolyte material. The lamination step is possibly followed by electrolyte curing, bus bar application, edge sealing and eventually device packaging. Ideally, the whole device processing can be done continuously on large areas under a dry air atmosphere.

In Fig. 4.6A the schematic representation of the PEDOT-EthC6/PB ECDs under study is given. The active EC materials are sandwiched between two commercially available ITO-coated (100 nm) PET films (127 µm) that serve as transparent conductive electrodes. The upper EC layer is an approx. 400 nm thick PEDOT-EthC6 polymer coating (half cell 1), while the lower electrochromic EC-layer is a PB thin film of approx. 100 nm thickness (half cell 2). These two half cells are separated by an UV-cured polymer electrolyte with a thickness of approx. 80 µm.

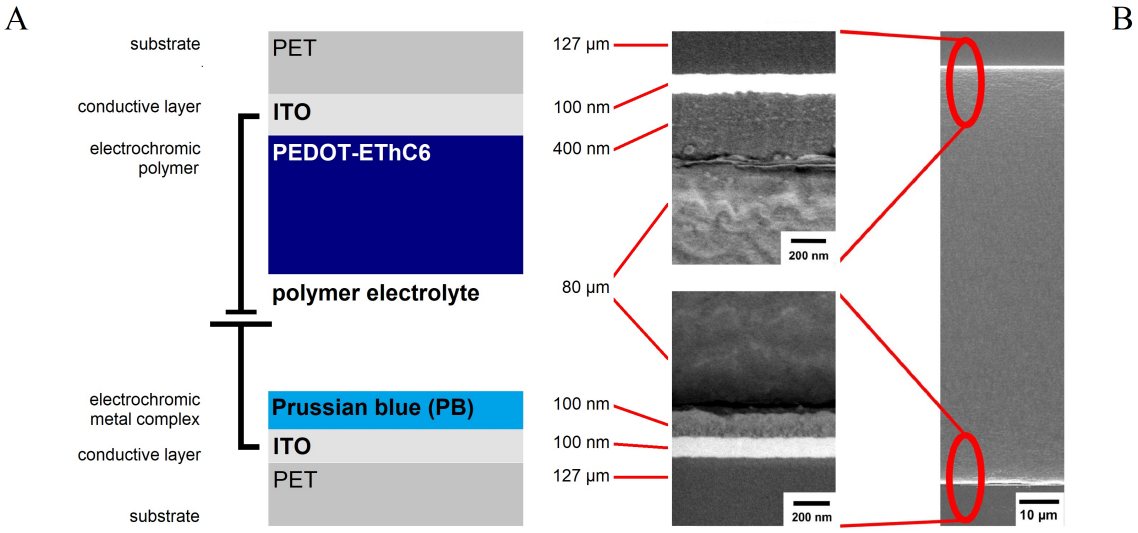

Figure 4.6: Schematic representation (A) and cross-sectional SEM images (B) of the flexible electrochromic devices.

As the vertical dimensions of the substrate films and the polymer electrolyte considerably differ from those of the electrochromic films and the ITO layers, in Fig. 4.6B a SEM overview cross-section image is shown for clarification with two cutouts taken at higher magnification. The ITO layers on the PET substrates appear highly uniform with a well-defined interface. The PEDOT-EthC6 layer has a granular substructure and its boundary surface to the subjacent polymer electrolyte has a more irregular shape. This profile is ascribed to the honeycomb structure of the PEDOT-EthC6 film reported above.[21] The nanoparticular PB layer at the bottom exhibits comparable structural features. The apparent gap between the EC layers and the electrolyte layer is presumably due to SEM sample preparation and thereby arising locally increased temperatures and shear forces. However, in wide-ranging SEM investigations, the multilayer assembly appears homogeneous and free of defects. In Addition, the high uniformity is supported by the low haze values of the large-area ECDs (below 2%) in both the bright and colored state. This means that only very little light is scattered at a wide angle or diffused due to macroscopic irregularities or rough interfaces in between the ECD layers.

Another important component of an ECD, in addition to the half cells from which it is composed, is the electrolyte that has to be tailored and optimized in terms of mechanical, chemical and electrochemical properties for each EC system. In the present work, an UV-cuarable polymer electrolyte (HQ674) based on polyethylene oxide with LiTFSI as salt was used as electrolyte and separator. The molecular weight of the HQ674 polymer is in the range of 8 000 to 10 000 $g\,mol^{-1}$. Acrylate groups are introduced to the main chain in order to maintain a better mechanical strength of the polymer electrolyte after coating and UV-curing. LiTFSI was used as the conducting salt to complex with the networked polymer.

The ionic conductivity of the electrolyte polymer generally depends on the temperature resulting from macro- and micro-relaxations of the segmental movement of the polymer chains. Fig. 4.7A shows the temperature dependence of the ionic conductivity for the HQ674 polymer electrolyte containing LiTFSI in an amount corresponding to an oxygen/lithium ratio of 30. The correlation of the ionic conductivity and temperature is almost linear, indicating the absence of crystalline domains in the electrolyte matrix. The ionic conductivity was found to be approx. $5.5 \times 10^{-5}\,\mathrm{S\,cm^{-1}}$ and $4.2 \times 10^{-4}\,\mathrm{S\,cm^{-1}}$ at temperatures of 30 °C and 70 °C, respectively. Fig. 4.7B shows the thermogravimetry curve of the HQ674 polymer electrolyte. A thermal stability of up to approx. 280 °C was measured, making this electrolyte suitable for use in safe (no electrolyte leakage) all-solid-state ECDs.

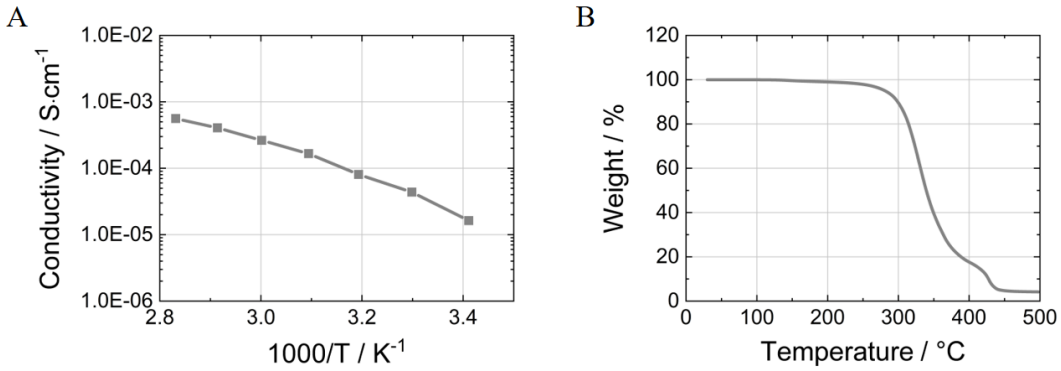

Figure 4.7: Arrhenius plot of the ionic conductivity (A) and thermogravimetry curve (B) of the HQ674 solid polymer electrolyte for flexible electrochromic devices.

The electrochemical properties of the ECDs were initially investigated by cyclic voltammetry (CV) at overall operation voltages between −1.4 V and 1.8 V with a scan rate of $10\,\mathrm{mV\,s^{-1}}$. The cyclic voltammogram is shown in Fig. 4.8A. During the anodic scan at voltages between −0.5 V and 1.2 V the course of the current suggests the superposition of two processes, namely the oxidation of PEDOT-EthC6 and the reduction of PB. The representative device is switched to the bright state. Upon reversal of the voltage (cathodic scan), the respective back reactions set in at 1.1 V and are completed at −1.4 V. During this process, the device turns blue. The respective redox peaks are located at 0.3 V (anodic scan) and 0.2 V (cathodic scan).

The substantial broadening of the redox peaks is a consequence of hindered diffusion in the electrolyte and insertion of the electrolyte ions from the polymer electrolyte into the EC layers[288, 289] as well as the superposition of the two signals of the two EC half cells. The coulombic efficiency is close to 1, indicating completely reversible redox processes to occur. The CV results are in accordance with previously published data obtained from similar ECDs building on PEDOT and PEDOT derivatives.[21, 165, 236]

The switching processes of the ECDs were further characterized in potentiostatic switching experiments between −1.4 V and 1.8 V as displayed in Fig. 4.8B. The areal charge density is calculated to be approx. 4.5 mC cm^{-2}. The response time that is considered the time corresponding to a current drop to 10% of the starting (maximum) value amounts to 7 s for decoloration and 6 s for coloration. The response time of the ECDs is mainly limited by the sheet resistance of the ITO employed (approx. 50 Ω □).[166] The insulating properties of the PB layer have a certain, but comparably small effect.[287, 290, 291] For similar PEDOT/PB devices (5 x 4 cm^2, approx. 50 Ω □) Duluard et al. reported response times of more than 15 s for coloration. These systems, however, had a lower areal charge density of 1.2 mC cm^{-2}, indicating faster kinetics for the PEDOT-EthC6/PB devices.[166]

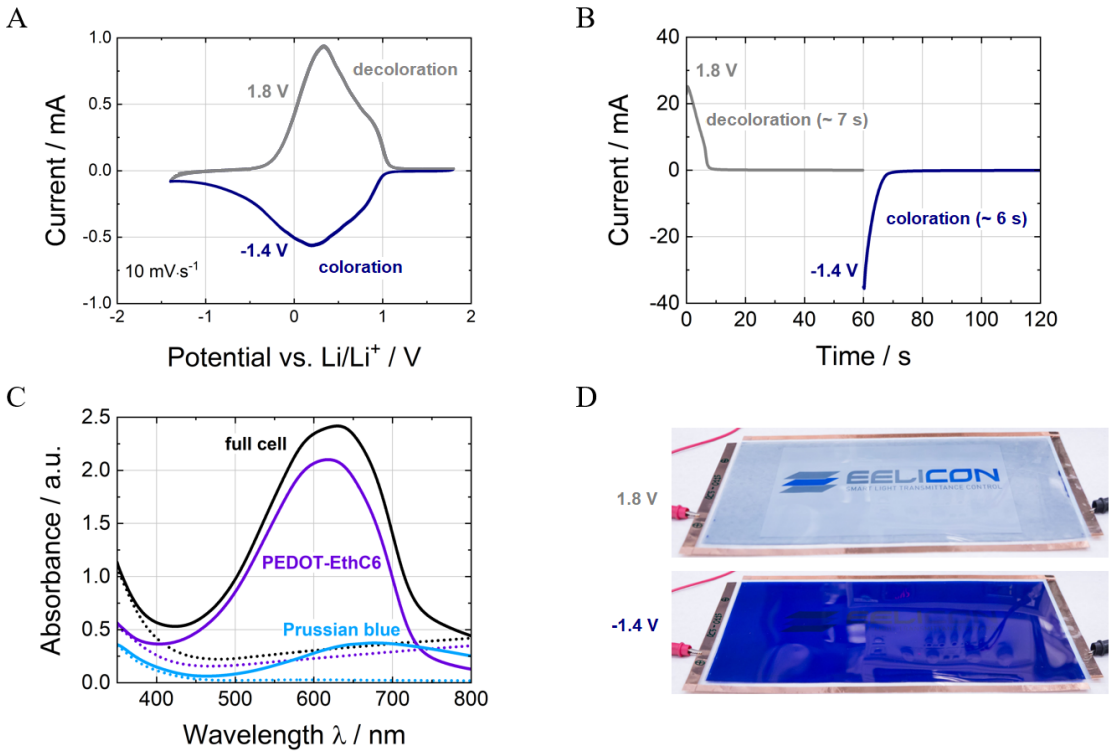

Figure 4.8: Cyclic voltammogram (A), response time analysis (B), absorbance spectra (C, results already shown in reference [21] and section 4.1, respectively (see Fig. 4.4A)) and photographs (D) of the electrochromic devices. The respective colored states (−1.4 V) are given in solid lines, the bright states (1.8 V) in dotted lines.

Fig. 4.8C displays the absorption spectra of the full PEDOT-EtC6/PB device in the dark and bright state. The dark state (−1.4 V) shows an intense deep blue color (L* = 26.8, a* = 12.8, b* = -52.9; τ_v = 4%), whereas the bright state (1.8 V) is distinguished by a highly transmissive almost neutral tint (L* = 77.9, a* = -5.9, b* = -0.6, τ_v = 53%). In the spectral range from 380 nm to 780 nm an overall change of the lightness value ΔL* of 51.1 takes place. The colored state is characterized by a strong and broad absorption band with a maximum at 630 nm. The transmittance at the max. absorbance wavelength is 46.7%. This signal is attributed to the individual absorption of the PEDOT-EthC6 film superposed with that of the PB thin film (shoulder at around approx. 690 nm).

In the bright state the transmittance at the max. absorbance wavelength is 0.5%, resulting in a contrast ratio CR of 93.4 and a (theoretical) coloration efficiency of $563\,\mathrm{cm^2\,C^{-1}}$ (assuming that the available charge density of the full cell is equal to the charge density of the half cell with the lower charge density (PEDOT-EthC6: $3.5\,\mathrm{mC\,cm^{-2}}$)). Additionally, the individual contributions of the respective PEDOT-EthC6 (results already shown in reference [21] and section 4.1, respectively (see Fig. 4.4A)) and PB half-cells are given.[21] The latter material only has a minor impact on the overall light transmittance change of the device, however, in contrast to other commonly used counter electrodes, PB stands out due to its highly transmissive and colorless bright state. The color impression of sole PEDOT-EthC6-based electrochromic films tends to be of a characteristic violet-blue hue, which is perfectly complemented by the rather turquoise hue of the PB dark state. Consequently, the presented PEDOT-EthC6/PB pairing results in a full device with an aesthetically appealing royal blue dark state and a highly transmissive and color neutral bright state as can be seen in Fig. 4.8D. The complementary material system therefore has a distinct contribution to the aesthetic appearance of the final device.

The results from the optical and *in-situ* spectroelectrochemical characterization clearly outperform the properties of previously published data of a proof-of-concept PEDOT-EthC6/PB devices.[21] The improvement of the device performance is due to the use of an accordingly adjusted solid polymer electrolyte (HQ674) that comprises widely extended amorphous domains as well as excellent ionic dissociation and lithium ion transport properties. The ion transport is coupled to the movement of the polyethylene oxide chains within the amorphous domains of the polymer electrolyte, which are maintained by the introduction of asymmetric units such as propylene oxide moieties to the main chain of the electrolyte polymer. The excellent ionic dissociation is due to the low lattice energy and the therefore highly dissociative character of the LiTFSI salt. Further advantages are the high transparency, the low molecular weight, leading to improved interfacing with the electrodes (low interfacial resistance), and the ability of cross-linking (UV-curing) of the electrolyte polymer after device lamination, thus establishing good electrode/electrolyte interfaces.

For practical applications, it is crucial that the ECDs show a performance constant in time over many cycles of operation. Unfortunately, there are not many scientific publications focusing on long-term cycling stability and EC materials are sometimes described as stable, although parameters such as light transmittance change or charge capacity show a drop over the course of several thousand cycles. Barbosa et al. gave account of 180 switching cycles for a PEDOT/PB-based electrochromic system. They observed an exponential decay in the absorbance change by 65%.[237] Other ECDs based on PEDOT and PB were operated more than 50 000 times by Tung et al. resulting in a decrease of the light transmittance change from 50% to 27%.[236]

In contrast to the above cases, electrochromic devices based on PEDOT-EthC6 and PB (active area: 5 x 5 cm^2) were potentiostatically switched between −1.4 V to 1.8 V (overall operational voltage). Both voltage steps were held for 60 s. This process was repeated 10 000 times, which resulted in a measurement time of approximately 14 days. The results indicate a reversible redox switching behavior with a drop of charge density in the first 1 000 cycles of approximately 1.3 mC cm^2, which can be attributed to formation processes of the device and further electrochemical polymerization of the polymer chain. The additional loss in charge density can be explained by hindered diffusion in the electrolyte and insertion of the electrolyte ions from the polymer electrolyte into the active layers during the fast performed cycling experiment.[21] Within the period from cycle 1 000 to 10 000 the charge density remains remarkably stable. The maximum current during decoloration and coloration decreased from 22 mA (1 000^{th} cycle) to 17 mA (10 000^{th} cycle) and from 29 mA (1 000^{th} cycle) to 22 mA (10 000^{th} cycle), respectively as shown in Fig. 4.9A. The response time remains constant with 7 s for decoloration and 6 s for coloration. The same is valid for the charge density which decreases only from 3.2 mC cm^{-2} to 3.0 mC cm^{-2} for the decoloration process and from 3.1 mC cm^{-2} to 3.0 mC cm^{-2} for the coloration process between cycle 1 000 and cycle 10 000. This corresponds to a respective charge retention of 94% and 97% as it is illustrated by Fig. 4.9B).

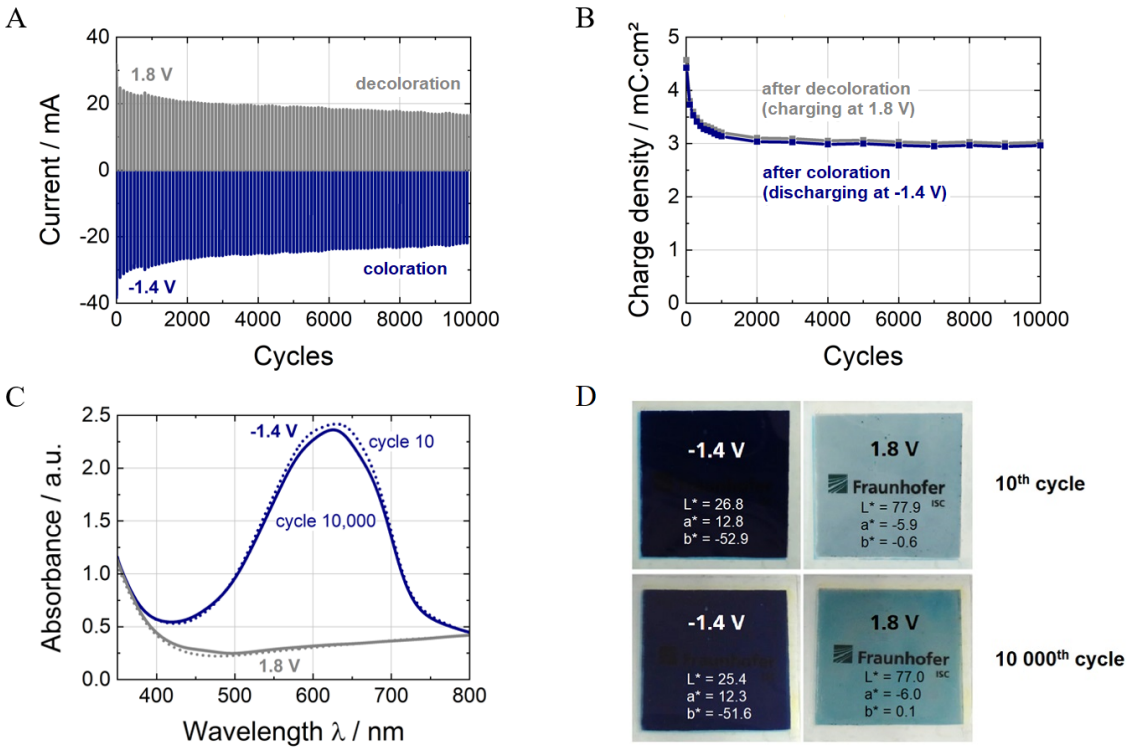

Figure 4.9: Current (A), charge density (B), absorbance spectra (C) and photographs of the electrochromic device after 10 and 10 000 switching cycles.

From the practical point of view, changes in the optical performance of the devices are more important than their electrochemical aging behavior. In 4.9C, the absorbance spectra of an ECD after 10 000 operations is compared to its pristine performance. The visible light transmittance changes from 3%/50% to 2%/50% (dark/bright state). The results from the electrochemical durability investigation over the course of 10 000 switching cycles show a drop in areal charge density. However, both response time and visible light transmittance change remain roughly constant during the test.

Consequently, the observed drop in charge density does not correspond to a degradation of the EC films themselves. In fact, the areal charge density of the PEDOT-EthC6 half-cell is approx. 3.5 mC cm^{-2}. The capacity of the full device should not exceed the capacity of the PEDOT-EthC6 half-cell, provided no side reactions occur. Therefore, during the formation (approx. 1 000 cycles), the device levels off to its actual charge density. The fact that the optical properties, i.e. the visible light transmittance and colors remain almost constant over the course of 10 000 cycles underlines this argument. The visible light transmittance changes go in hand with a small loss in areal charge density. Duluard et al. reported a similar PEDOT/PB device showing a formation period over the first 200 cycles and losses in areal charge density and absorbance change of 3% and 15%, respectively, between cycle 200 and cycle 1 000.[166]

Going beyond this academic level, it is highly challenging to transfer results from the lab to pilot or even industrial production. The ECDs described here were scaled-up to a size of 45 x 65 cm^2 (active area) by means of a customized S2S lamination process established in a dry room (100 ppm H_2O) on PET-ITO substrates. In an initial step PEDOT-EthC6 (half cell 1) and PB (half cell 2) were separately deposited on PET-ITO roll material by means of slot-die coating and drying at 120 °C and 100 °C, respectively.[21] In a second R2R process, the PEDOT-EthC6 films (half cell 1) were rinsed in reservoirs successively filled with water and alcoholic solvent mixtures and subsequently dried at 100 °C.[21]

In a last step, the two half cells were S2S laminated by means of the HQ674 polymer electrolyte to obtain the final ECDs. Therefore, the viscous polymer electrolyte resin was deposited onto half-cell 1 by doctor blade coating (coating width: 45 cm) under a dry air atmosphere (dry room, 100 ppm H_2O). Subsequently, the second half-cell was laminated under slight pressure (calendaring roller) on top of the wet polymer electrolyte layer that underwent curing by UV irradiation afterwards. The ECDs were fitted with bus bars (copper tape), packed and sealed. Fig. 4.10 shows a schematic drawing of the device processing along with photographs of the single sections.

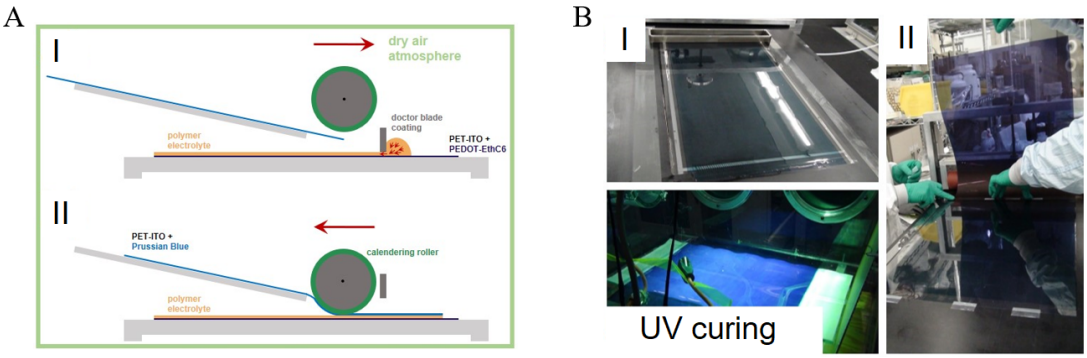

Figure 4.10: Schematic representation (A) and photographic images (B) of large-area processing of flexible electrochromic devices.

With regard to the manufacturing process (S2S or R2R), possibly on an industrial scale, the consideration of environmental aspects and green chemistry metrics is also important. For the production of the EC materials, ethanol and butanol (for PEDOT-EthC6) as well as water (for Prussian Blue) are required. For the lamination of the ECDs no further solvents are needed besides the negligible small amounts of solvents (mainly propylene carbonate) used in the electrolyte. The exclusive use of water and alcohols provides a good starting point for the large-scale production of the ECDs, especially with regard to the processing of other ECPs, which are commonly processed with much more harmful solvents like chloroform or methanol.[164, 171, 197, 208, 292]

The ECDs resulting from the up-scaled manufacturing process correspond in material selection and device lamination exactly to the small-format laboratory test devices. For this reason, a detailed characterization of the S2S laminated large-area ECDs (45 x 65 cm^2) was omitted and instead the basic functionality and homogeneity analyzed. Figure 4.11 shows the in-situ spectroelectrochemical characterization of the large devices (45 x 65 cm^2). The dark state (−1.4 V) shows the intense deep blue color (L* = 33.8, a* = 2.6, b* = -48.1) and a visible light transmission of 6 %, whereas the bright state (1.8 V) is distinguished by the highly transmissive, almost neutral tint (L* = 78.2, a* = -5.2, b* = -2.7) and a visible light transmission of 53 % again. In the spectral range from 380 nm to 780 nm an overall change of the lightness value ΔL* of 44.4 takes place. The results from the large-area device differ only slightly from the results of the small devices (5 x 5 cm^2, visible light transmission: 4 % ↔ 53 %) .

For examination of device homogeneity, the in-situ spectroelectrochemical characterization was performed at 5 different measuring points along the longitudinal axis. The spectra in Figure 4.11 overlap in both the dark and bright state almost perfectly. The color difference value ΔE is in the range from 0.9 to 2.5 with one exception in the bright state at position 5. This can be attributed to a local defect or contamination in one of the seven layers of the device. Overall, the color difference can be classified as very small. The response time for the large ECDs (45 x 65 cm^2) is approx. 45 s for coloration and decoloration.

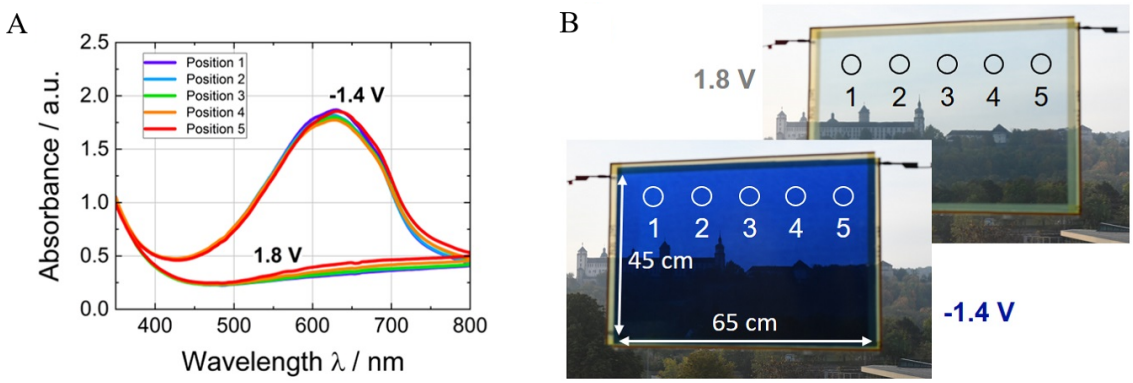

Figure 4.11: Absorption spectra (A) and photographs (B) of the ECDs with an active (switchable) area of 45 x 65 cm^2. The photographs include the measuring positions (1 – 5) of the colored (−1.4 V, bottom) and decolored (1.8 V, top) device.

In anticipation of further scaling and going to pilot production, it was eventually elaborated on transferring the S2S device assembly batch process to a continuous R2R lamination process. First attempts to fabricate complete R2R processed continuous ECDs as a proof-of-concept experiment were successful. Half cell 1 and 2 with a coating width of 50 cm were laminated and then cut into sheets of 100 cm length.

In conclusion, the flexible ECDs under investigation, based on PEDOT-EthC6 and Prussian Blue, show enhanced EC properties in terms of coloration efficiency, optical contrast, cycling stability (10 000 switching cycles) as well as transmittance and color neutrality in the bright state. The ECD fabrication was scaled-up to a maximum size of 45 x 65 cm^2 (active area) via a customized large-area S2S lamination process. The final device assembly was transferred to a continuous large-area R2R lamination process. As it is common practice in the scientific literature, the cycling tests performed so far were executed under an inert argon atmosphere. As in reality electrochromic systems are operated under ambient conditions, the influence of e.g. air moisture has to be considered. The following section is targeted at this factor and possible failure mechanism.

4.3 Water- and Voltage-Induced Degradation in Flexible Electrochromic Devices

The content of this section is published in Macher, S., Rumpel, M., Schott, M., Posset, U., Giffin, G. A., Löbmann, P., Avoiding Voltage-Induced Degradation in PET-ITO-Based Flexible Electrochromic Devices, *ACS Applied Materials & Interfaces*, **2020**, 12, 32, 36695-36705. Text and figures are reprinted (adapted) with permission from the *American Chemical Society* according to reference [279]. In the context of the present dissertation, results from reference [238] and section 4.2, respectively, serve as the fundamental basis of this section. Explicit multiple use of results is given only for the cycling and spectroelectrochemical characterization of the ECDs based on PEDOT-EthC6 and PB under dry argon atmosphere (see Fig. 4.9B, C and Fig. 4.12A, C).

If the driving voltage of ECDs is adjusted to maximize the light transmittance change and to minimize the response time, poor stability may result due to side reactions of the active layers and potentially the conductive layers as well. During operation, the diffusion of water into the ECDs can hardly be completely suppressed. Together with elevated electrode potentials, this is a daring combination with regard to parasitic side reactions and subsequent ECD degradation.

For the conducting layer of flexible ECDs, indium tin oxide, deposited on poly(ethylene terephthalate) (PET-ITO) is the most widely used material to date.[7, 18, 56] However, it is well known that the application of ITO as transparent conducting layer is limited by its potential window. Outside of its potential limits, ITO degrades under extreme anodic or cathodic polarization and may lose conductivity and transparency.[293–301] In the absence of alternatives to PET-ITO, it is important to understand the electrochemical behavior and reduction mechanism of PET-ITO in the setting of an ECD. It is generally accepted that ITO is reduced at very low potentials upon intercalation of H^+ and Li^+ cations. Reduced ITO films turn brown in color and are much less conductive.[293, 295, 302] Depending on the anodic potential (3.9 V vs. Li/Li^+), water is split into H^+ and O_2 and provides the required proton for the reduction of ITO.[297, 302–304] Further proton or water sources could be the electrolyte or the electrodes themselves by introducing adsorbed water into the electrochemical cell. For ECDs, these considerations imply a possible degradation of the ITO layers if the appropriate potential and water or protons are present.

In the following, a conscious aging of the ECDs based on PEDOT-EthC6 and PB was conducted in both a dry and a humid argon atmosphere. An intense brown coloration was only observed in the humid atmosphere and is related to significant ITO reduction. The cycling stability of the ECDs is given in Fig. 4.12. The devices were potentiostatically cycled between −1.4 V (60 s) and 1.8 V (60 s) for 10 000 cycles in total. One set of ECDs was cycled in a dry argon atmosphere (glovebox) with a water content of less than 2 ppm H_2O (Fig. 4.12A and 4.12C, results already shown in reference [238] and section 4.2, respectively (see Fig. 4.9B, C)), while the second set was subjected to the same cycling procedure, but in an argon atmosphere with a relative humidity of more than 90% rH (Fig. 4.12B and 4.12D).

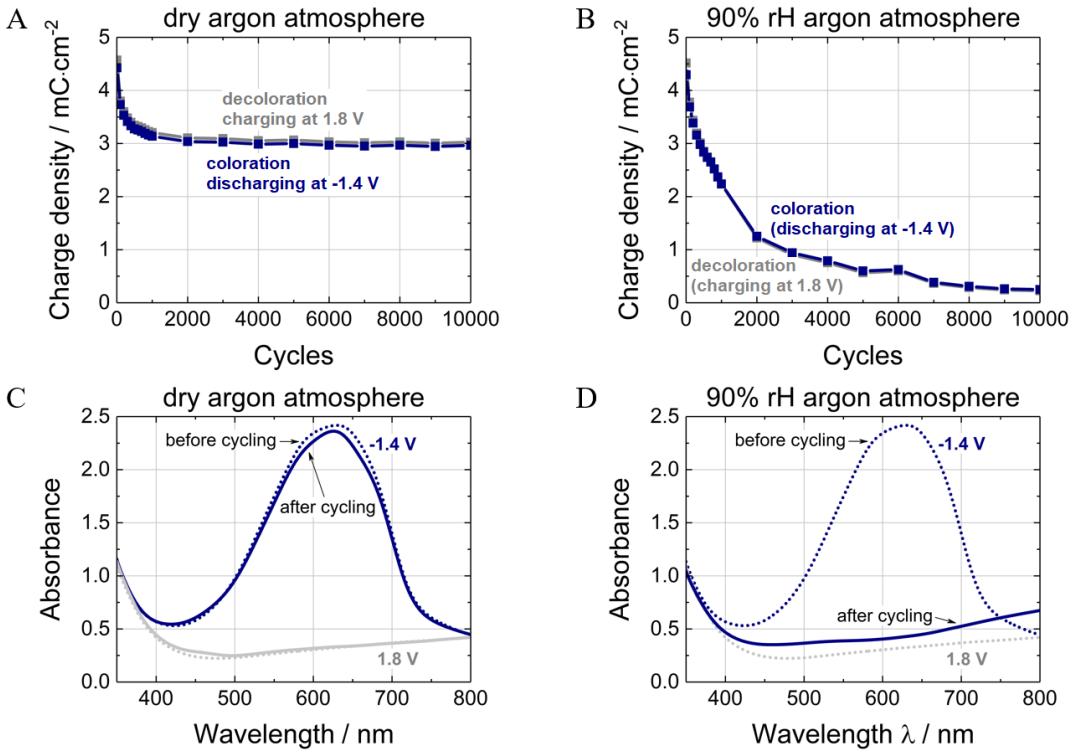

Figure 4.12: Charge density retention and absorbance spectra before/after 10 000 switching cycles of PEDOT-EthC6/PB based ECDs in a dry (A and C, results already shown in reference [238] and section 4.2, respectively (see Fig. 4.9B, C)) and wet (B and D) argon atmosphere.

In a dry argon atmosphere (Fig. 4.12A, results already shown in reference [238] and section 4.2, respectively (see Fig. 4.9B, C)), the ECD maintains a total charge retention of almost 80% over the course of 10 000 switching cycles (3.8 mC cm^{-2} to 3.0 mC cm^{-2}). The most dramatic decrease in charge density, from 3.8 mC cm^{-2} to 3.2 mC cm^{-2}, occurs during the first 1 000 cycles. This drop is attributed to formation processes in the ECD. In comparison, the results from the following 9 000 cycles indicate a reversible switching behavior with a charge retention of more than 93% (3.2 mC cm^{-2} to 3.0 mC cm^{-2}). The *in-situ* spectroelectrochemical characterization before and after cycling in a dry argon atmosphere is depicted in Fig. 4.12C (results already shown in reference [238] and section 4.2, respectively (see Fig. 4.9B, C)). The visible light transmittance τ_v can be calculated as 4%/53% ($\Delta L^* = 51.1$) before and as 3%/51% ($\Delta L^* = 51.6$) after cycling. The very small loss underscores the excellent cycling stability of the ECD. In stark contrast to the results in dry conditions, a substantial loss of charge density with cycling is observed in a humid argon atmosphere, as shown in Fig. 4.12B. The ECD has a total charge retention of less than 7% over the course of 10 000 switching cycles (4.6 mC cm^{-2} to 0.3 mC cm^{-2}). The *in-situ* spectroelectrochemical characterization before and after cycling (Fig. 4.12D) shows no optical switching of the ECD after 10 000 switching cycles (τ_v = 21%/21%, $\Delta L^* = 0$). This performance loss is attributed to water ingress into the device occurring in the 90% rH atmosphere. Whereas disastrous failure of the ECD occurs in the humid atmosphere, the functionality of the ECD is retained over 10 000 cycles in the dry atmosphere.

A post-mortem analysis performed after 10 000 switching cycles in humid argon atmosphere revealed that the electrodes had developed a brownish hue and metallic gloss. Upon closer examination, whereby the devices were disassembled and the solid polymer electrolyte and the electrochromic layers were removed to expose the bare PET-ITO substrates, the discoloration could be clearly attributed to a significant degradation of the ITO layers. Fig. 4.13 shows the SEM images of the bare PET-ITO substrates from both electrodes (PEDOT-EthC6 and PB) and a pristine PET-ITO sheet as a reference. The pristine ITO-layer (Fig. 4.13A) has a more homogeneous surface morphology with closely and regularly attached grains. By contrast, a grainy surface structure with loosly bound particles on top of the layer is visible for the samples recovered from the aging experiments (Fig. 4.13B and 4.13C), which may indicate a partial dissolution of the layers, most probably due to the irreversible reduction of the ITO.[297] The ball-shaped particles were identified to be metallic In and Sn, i.e. the final reduction products of ITO.[298] The size of the particles is significantly larger for the samples recovered from the PB electrodes.

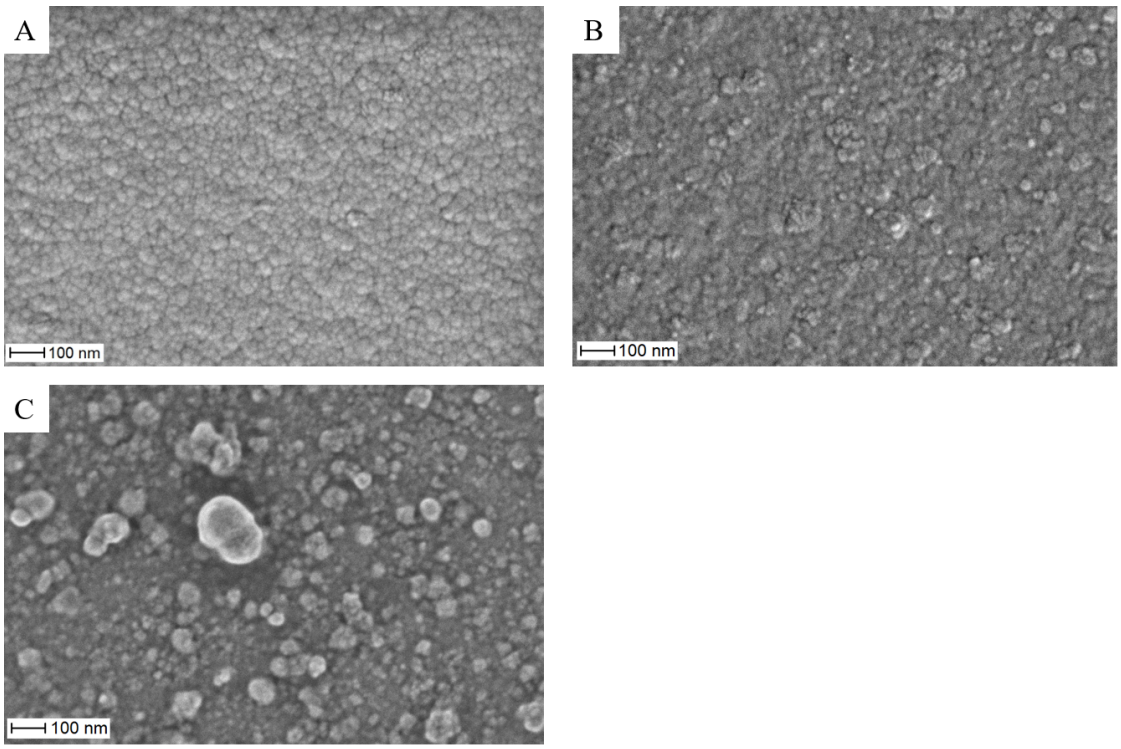

Figure 4.13: SEM images of a pristine PET-ITO sheet (A) and PET-ITO samples recovered from the PEDOT-EthC6 (B) and PB (C) electrode of the ECD cycled in a 90% rH argon atmosphere.

The recovered PET-ITO samples were further characterized by means of XRD, as shown in Fig. 4.14. The diffractograms of pristine PET and PET-ITO are shown as references. The reflections of ITO can be identified at 30.5°, 35.4° and 50.9° 2Θ, corresponding to the main phase of ITO, $In_{1.88}Sn_{0.12}O_3$.[297, 305] In addition to these patterns, reflections of metallic indium at 33.0°, 39.2° and 54.5° 2Θ can be seen in the diffraction patterns of both PET-ITO samples taken from the ECD operated under a humid argon atmosphere.[299]

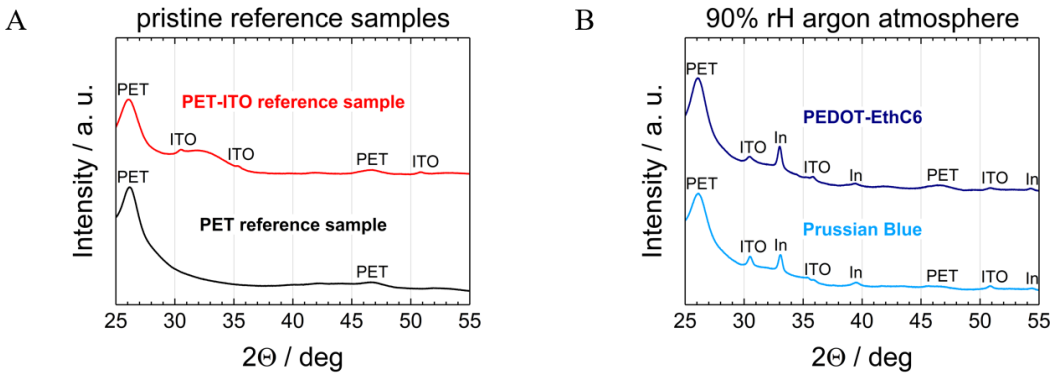

Figure 4.14: XRD analysis of pristine PET and PET-ITO sheets (A) and the PET-ITO samples recovered from the electrodes of an ECD operated in a 90% rH argon atmosphere (B).

CV measurements were carried out to explore the reduction and oxidation potentials of ITO. In Fig. 4.15A, a maximum of the anodic peak is seen at 1.9 V vs. Li/Li^+, while the first cathodic peak is at 1.5 V vs. Li/Li^+. The anodic peak is related to the oxidation of metallic indium,[294] and its intensity evolves upon cycling. The several reduction peaks, which also increase upon cycling, are attributed to the electrochemical reduction of ITO to metallic indium.[297] The onset potential of the ITO reduction is located between 1.9 V and 2.0 V vs. Li/Li^+.

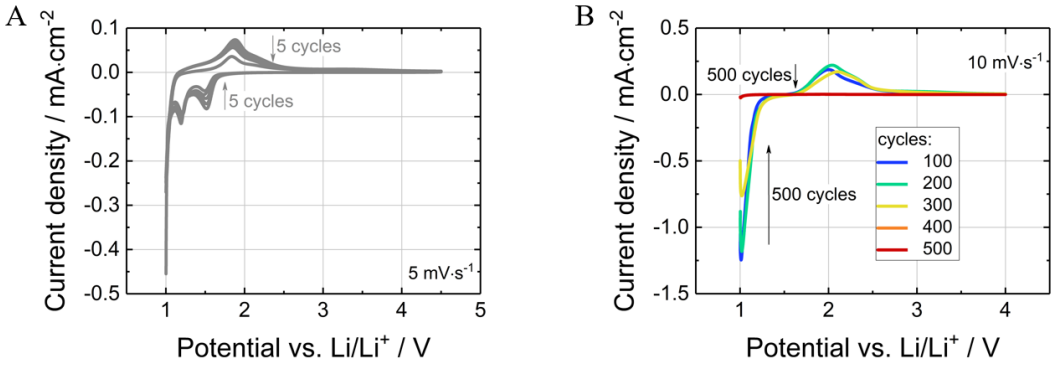

Figure 4.15: CV data at a scan rate of 5 mV s^{-1} (A) and cycling at a scan rate of 10 mV s^{-1} (B) of a pristine PET-ITO sheet.

As the ITO reduction correlates with a visible brown discoloration of the substrates, UV-Vis measurements were performed in dry and ambient conditions. Pristine PET-ITO samples were initially reduced under a dry argon atmosphere (Fig. 4.16A) and under ambient conditions (Fig. 4.16B). Under dry conditions (< 2 ppm H_2O, argon atmosphere), the transmittance of the PET-ITO dropped in the range of 350 nm to 600 nm after 1 h and over the course of 24 h further transmittance losses between 350 nm to 800 nm occurred that are attributed to the brown discoloration of the ITO layer. Under ambient conditions (40% rH, air), the brown discoloration became evident in much shorter times. The discoloration noted after 3 h was comparable with those after 24 h in the dry argon atmosphere. Further losses were evident until the visible light transmittance had almost reached 0% after 24 h.

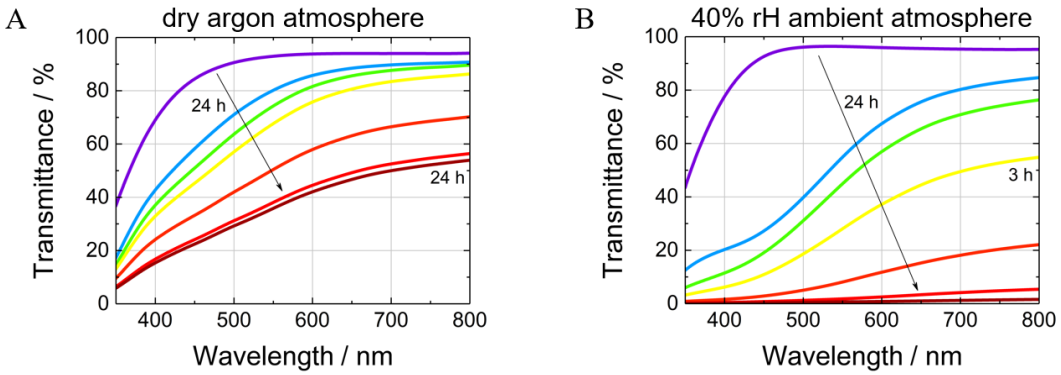

Figure 4.16: UV-Vis spectra recorded *in-situ* during the reduction of pristine PET-ITO samples at -3.0 V vs. platinum under dry (A) and ambient conditions (B).

The combined SEM, XRD, CV and UV-Vis results demonstrate that the ITO degradation is occurring during cycling of the ECDs. Irreversible ITO reduction occurs at voltages below 2.0 V vs. Li/Li^+ and is accelerated in humid atmospheres as protons catalyzing the ITO reduction are formed upon water oxidation during cycling in humid atmospheres.

The diffusion of water into the ECDs can never completely be suppressed, not even through the use of appropriate sealing materials. Therefore, another strategy is needed to prevent ITO degradation in ECDs. In the following, an adjustment of the driving voltage is explored to minimize ECD degradation while minimizing the initial performance loss in terms of visible light transmittance change, response time and cycling stability.

In order to understand the potential behavior of the individual electrodes in the full ECD (i.e. PEDOT-EthC6 on PET-ITO vs. PB on PET-ITO), a three-electrode set-up with a lithium reference electrode was implemented. The results from such a set-up are shown in Fig. 4.17. The integration of the lithium reference electrode has little effect on the cycling stability as it is evident from the minimal change in charge density over the course of 10 000 switching cycles in Fig. 4.17A and the almost perfect overlap of the CVs measured after each 1 000^{th} cycle (Fig. 4.17B).

The separated electrode potentials over the course of 10 000 switching cycles are depicted in Fig. 4.17C and Fig. 4.17D for PEDOT-EthC6 on PET-ITO and PB on PET-ITO, respectively. During coloration (−1.4 V), the potential range of the cathodically-coloring PEDOT-EthC6 electrode is between 1.7 V and 2.6 V vs. Li/Li^+, while the potential ranges from 3.5 V to 4.2 V vs. Li/Li^+ during decoloration (1.8 V). The anodically-coloring PB operates in the potential range from 3.1 V to 4.0 V vs. Li/Li^+ and from 1.8 V to 2.4 V vs. Li/Li^+ during coloration and decoloration, respectively. Hence, ITO degradation is possible in the ECD since the electrode potentials fall below 2.0 V vs. Li/Li^+ which is the onset potential for ITO reduction.

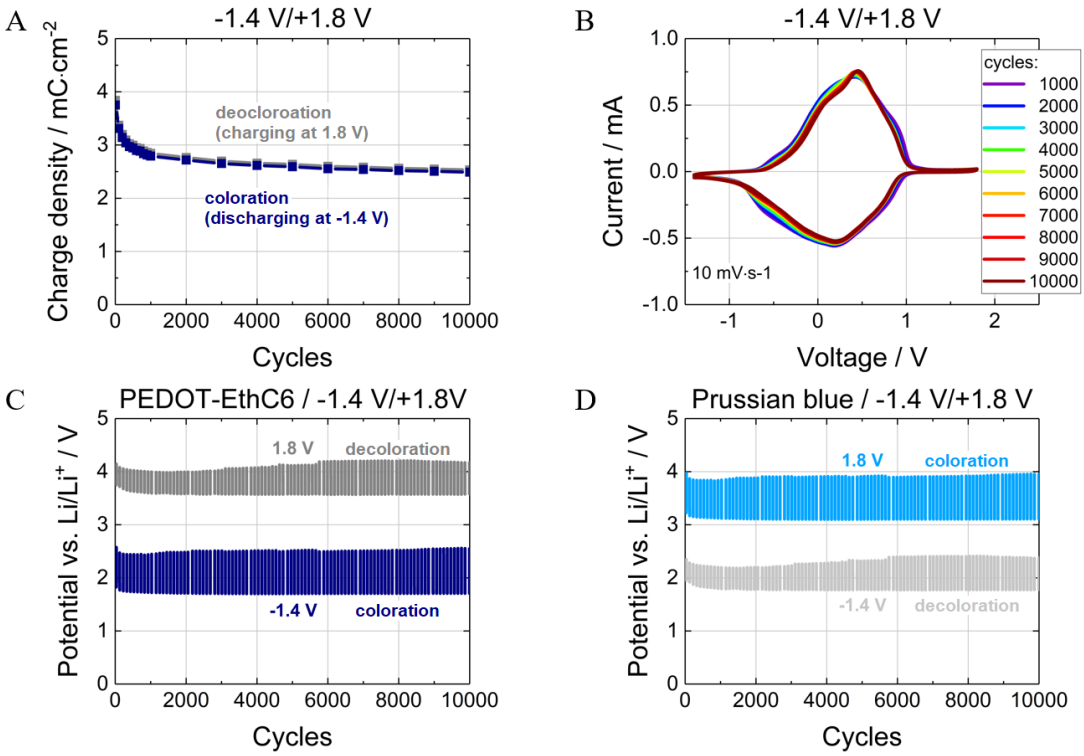

Figure 4.17: Electrochemical measurements of the PEDOT-EthC6/PB ECD with an additional lithium reference, operated within the cell voltage range of −1.4 V/1.8 V. Cycling stability analysis including evolution of the charge density (A), CVs of every 1 000th switching cycle (B) and the potential course over 10 000 switching cycles of the PEDOT-EthC6 (C) and PB (D) electrode.

To prevent a drop of the potential below 2.0 V vs. Li/Li^+, the electrode configuration was adjusted as described by Hassab et al.[210] in order to shift the electrode potentials above 2.0 V vs. Li/Li^+. Hassab and co-workers showed that the redox behavior of an ECD is highly dependent on the charge density ratio between working and counter electrode.[210] In a cell configuration with a charge density ratio = 1 ("balanced configuration"), both electrodes are switched in their maximum potential window. In cell configurations with a charge density ratio ≠ 1 ("unbalanced configuration"), the electrode with the lower charge density is fully switched, while the electrode with the higher charge density is only partially switched, since the charge consumed at each electrode is always the same. Therefore, smaller potential windows are sufficient to utilize the required amount of charge. As a result, the overall driving voltage for unbalanced configurations is always lower than in balanced configurations. In the case of an oversized counter electrode, the overall cell voltage is shifted up from the lower potential limit. The inherent decrease of the cell voltage by appropriate electrode dimensioning, therefore, has the potential to minimize the observed ITO reduction and contributes to enhanced device durability. In order to shift the cell voltage window from the lower limit, a PEDOT-EthC6 electrode with a charge density of approx. 3.5 mC cm^{-2} (working electrode) was paired with a PB electrode with a charge density of approx. 4.5 mC cm^{-2} (counter electrode) in a three electrode cell with a lithium reference and an appropriate driving voltage of −1.1 V/0.9 V.

The resulting ECD had an excellent cycling stability as can be seen from the evolution of the charge density in Fig. 4.18A and the almost perfectly overlying CVs at each 1 000th cycle in Fig. 4.18B. The potential profiles over 10 000 cycles of each electrode are shown in Fig. 4.18C (PEDOT-EthC6 on PET-ITO) and Fig. 4.18D (PB on PET-ITO). A splitting of the electrode potentials was still observed during switching, although this splitting is less pronounced. For the unbalanced ECD, the potential of the PEDOT-EthC6 electrode varied from 2.1 V to 2.6 V and from 3.2 V to 3.4 V vs. Li/Li^+ during coloration and decoloration, respectively. The potential of the PB electrode was in the range from 3.1 V to 3.7 V and from 2.3 V to 2.5 V vs. Li/Li^+ during coloration and decoloration, respectively.

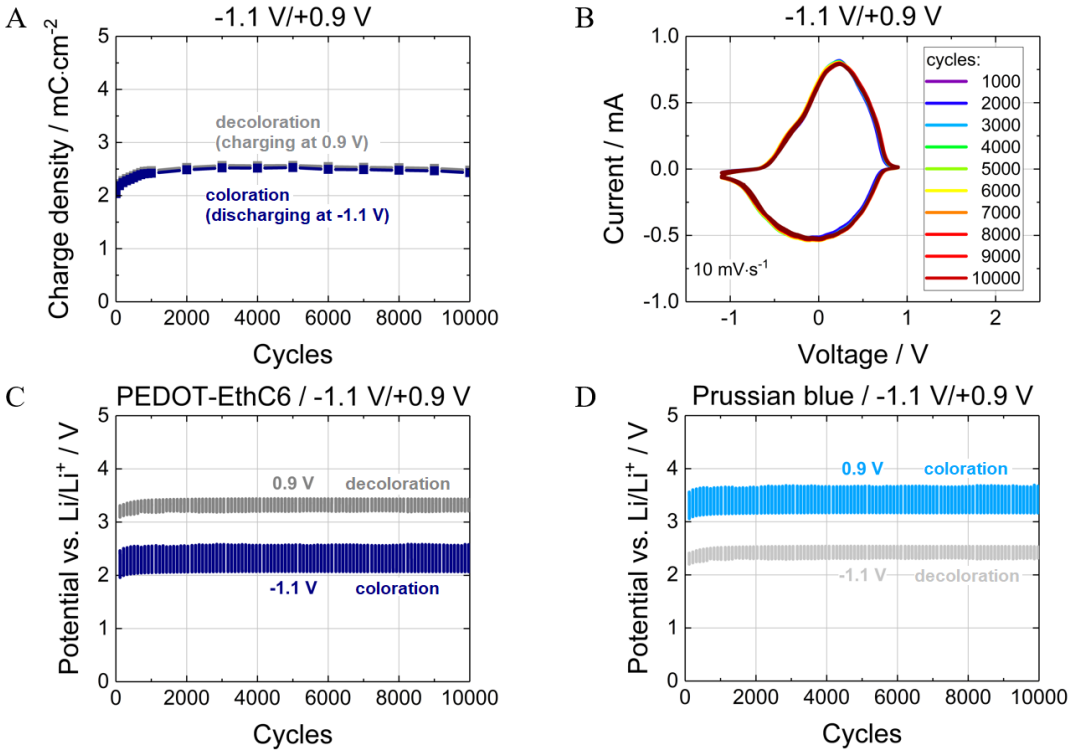

Figure 4.18: Electrochemical measurements of the PEDOT-EthC6/PB ECD with an additional lithium reference, operated within the cell voltage range of −1.1 V/0.9 V. Cycling stability analysis including evolution of the charge density (A), CVs of every 1 000th switching cycle (B) and the potential course over 10 000 switching cycles of the PEDOT-EthC6 (C) and PB (D) electrode.

Shifting the electrode potentials above the ITO reduction onset potential can eliminate ITO degradation. Nevertheless, as both half waves in the CV experiments are fully developed, the ECD shows full switching behavior and the cycling stability is not affected by the narrowed driving voltage. The elevated charge density in the first 1 000 cycles is rather suppressed, although the ECD still seems to need formation. In this case, the charge density increases over the initial cycles rather than decreases as depicted in Fig. 4.12A. The results obtained predict an enhanced device durability due to suppressed ITO degradation without a loss of performance. Therefore, an ECD with the unbalanced electrode configuration was further tested under dry conditions with respect to the optical contrast, response time and cycling stability.

The *in-situ* spectroelectrochemical characterization of the ECD with the unbalanced electrode configuration, operated with the optimized driving voltage (−1.1 V/0.9 V), is depicted in Fig. 4.19A. The visible light transmittance τ_v can be calculated as 6%/53% ($\Delta L^* = 46.2$, contrast ratio CR = 8.8) which is only 2% less than the device operated within the cell voltage of −1.4 V/1.8 V. The small difference is derived from a slightly less-transmissive bright state. Moreover, the response time remains unaffected with 8 s for decoloration and 5 s for coloration (Fig. 4.19B).

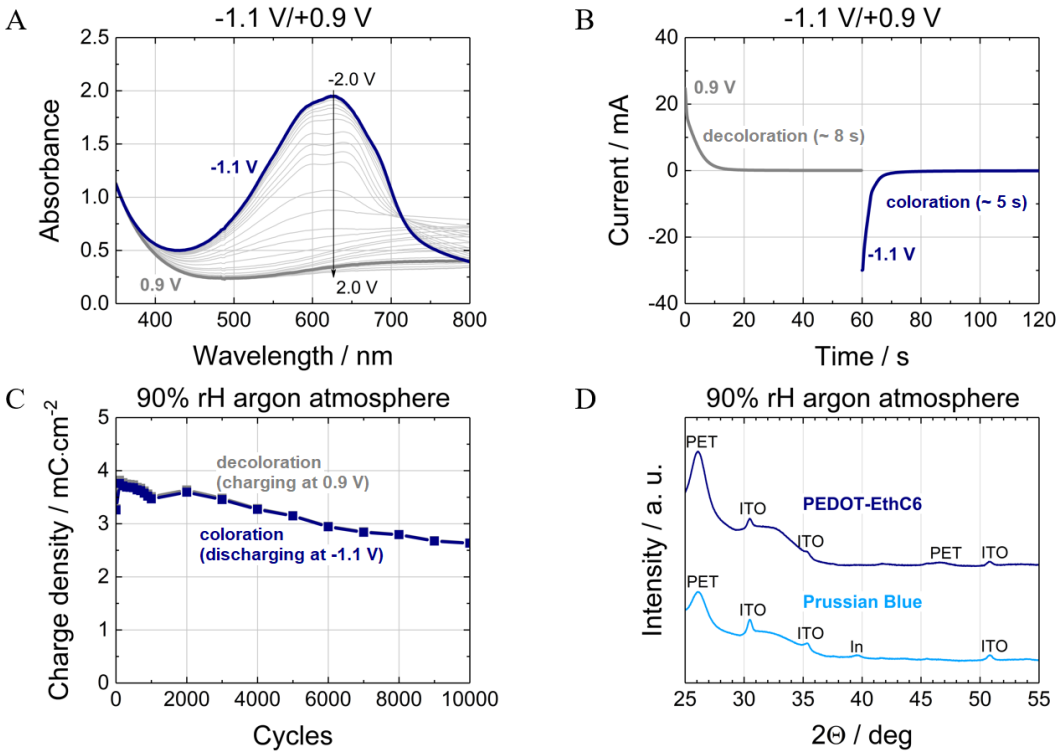

Figure 4.19: PEDOT-EthC6/PB ECD, operated with a cell voltage of −1.1 V/0.9 V. Shown are absorbance spectra (A) and response time analysis (B) as well as cycling stability analysis under a humid argon atmosphere (90% rH) including charge density evolvement (C) and post-mortem XRD characterization of the aged PET-ITO substrates (D).

Based on the results presented above, it seems feasible to limit ITO-induced degradation in a humid environment through the use of an unbalanced electrode configuration. This premise was tested with cycling stability experiments over 10 000 cycles in a wet argon atmosphere (90% rH). The charge retention is 82% (3.2 mC cm^{-2} to 2.6 mC cm^{-2}) after 10 000 switching cycles, which is a very good result considering the harsh conditions (Fig. 4.19A). Fig. 4.19B shows the results from the XRD characterization of PET-ITO samples from both electrodes after cycling. Only one small additional reflection at 39.2° from metallic indium is present in addition to the reflections attributed to PET at 26° and 46° and ITO ($In_{1.88}Sn_{0.12}O_3$) at 30.5°, 35.4°, 50.9°, which supports the conclusion of deminished ITO degradation.[297, 305] The ECD run under a humid argon atmosphere consumed slightly less charge after 10 000 switching cycles (2.6 mC cm^{-2}) in comparison to the ECD cycled under a dry argon atmosphere (3.0 mC cm^{-2}).

Although, the ITO degradation is restrained, many other degradation mechanisms induced by moisture, e.g. hydration of the lithium salt in the electrolyte or debalancing of the ECD due to parasitic side reactions at the electrochromic electrodes still have to be considered.[31, 33, 58, 241, 242, 278]

To draw a final conclusion with regard to moisture-induced degradation of ECD, the performance loss of the ECDs is due to the degradation of the conducting ITO-layers. The irreversible reduction of PET-ITO in flexible electrochromic devices under a humid atmosphere (90% rH) was attributed to the electrode potentials in combination with moisture ingress into the ECDs. The moisture-induced ITO degradation is manifested in the formation of metallic indium particles on the surface of the ITO layers upon dissolution of the ITO thin films.

By incorporation of auxiliary reference electrodes (lithium), knowledge on the actual electrode potentials in the environment of an ECD was obtained. This allowed the driving voltage window to be adjusted in an unbalanced cell configuration (charge density ratio) to an extent in which irreversible ITO reduction no longer occurs. A detailed investigation of ECDs with the optimized cell configuration (charge density ratio < 1) showed that the overall device performance with regard to visible light transmittance change and response time is not hindered and that the cycling stability under humid atmospheres (90% rH) is dramatically improved.

Since other degradation mechanisms also play a role with respect to the influence of moisture, it is considered reasonable to counteract the degradation mechanism not only by intrinsic measures (unbalanced cell configuration) but also by extrinsic measures. Therefore, in the following, measures are investigated to limit the general entry of moisture into ECDs. This can be achieved on the one hand by using suitable sealing methods and materials and on the other hand by water-free manufacturing of the individual components of the ECDs. Since suitable sealing methods are already known, especially from the organic light emitting diodes (OLED) and organic photovoltaics (OPV) sector,[306–308] this work concentrates in the following in particular on the water-free production of the device components.

4.4 Simple and Water-Free Production of a PEDOT-Based Polymer for Flexible Electrochromic Devices

The content of this section is published in Macher, S., Sassi, M., Beverina, L., Posset, U., Schott, M., Giffin, G. A., Löbmann, P., Electrochromic Polymer Ink Derived from a Sidechain Modified EDOT for Electrochromic Devices with Colorless Bright State, *ChemElectroChem* **2021**, 8, 726-734 and granted in Macher, S., Posset, U., Beverina, L., Sassi, M., Schott, M. (2020) Colloidal Coating Dispersion, European Patent EP 3,654,094, 15.11.2018. Text and figures are reprinted (adapted) with permission from *Wiley-VCH Verlag GmbH & Co. KGaA* according to reference [280].

With regard to the knowledge about the influence of moisture on ECDs achieved in the present work, it becomes clear that the processes for manufacturing ECDs must be better performed under dry conditions. As described above, the production of the PEDOT-EthC6 thin films is complex and time-consuming. In particular, the mandatory post-treatment (aqueous polymer film rinsing) executed in a second process step and the collection and recycling of volatile solvents which are evaporated throughout processing are two areas which cause difficulty during dry processing. Due to negligible solubility of most conjugated polymers, caused by the rigidity of conjugated polymer backbones, their lack of conformational freedom in solution and the strong inter-chain interactions,[19, 21, 114, 165, 167, 171, 208, 292] *in-situ* polymerization is - apart from electropolymerization - the deposition method of choice to date to obtain high quality ECP thin films.[14, 21]

An alternative polymerization method for EDOT in general is the so-called BAYTRON P synthesis, developed at *Bayer AG*. The water-soluble EDOT monomer is polymerized in an aqueous solution in the presence of a polyelectrolyte (most commonly polystyrene sulfonate (PSS)), which functions as a counter ion and dispersing agent. The dark blue, aqueous PEDOT:PSS microdispersion is well known under its former trade name BAYTRON P (*Bayer AG*) and its current trade name Clevios^{TM} (*Heraeus Epurio*). Resulting PEDOT:PSS films are highly conducting and transparent, mechanically and environmentally stable as well as insoluble in any common solvent.[114, 177, 282, 285, 309–313] Drawbacks in the context of ECD arise, however, from wettability issues, residual water content and the fact that this process cannot be applied to water-insoluble monomers such as PEDOT-EthC6.[177, 314, 315] To tackle these drawbacks and - particularly important at this stage - to establish a water-free process, a novel preparation method for a nanoscale PEDOT-EthC6 dispersion (nano-PEDOT-EthC6) based on organic solvents is presented. This method enables coating and printing processes on flexible substrates to be implemented in a straightforward manner, which is a simplified and water-free alternative to the established BAYTRON P synthesis and the R2R *in-situ* polymerization of EDOT derivatives. Unlike the BAYTRON P synthesis, the novel preparation method is not limited to water soluble monomers and does not require the use of dispersing agents such as PSS, which is an electro-optically inactive component that compromises the EC performance of the resulting active thin films.

The nanoscale ECP dispersion can be formed from the EDOT-EthC6 derivative, containing a hexenyl sidechain with a terminal double bond. Through the inclusion of a lateral sidechain, the planarity of the conjugated system is improved. Furthermore, intramolecular interactions and high supramolecular order are favored. The consequent narrowing of the band gap results in a bathochromic shift of the polaronic and bipolaronic absorption bands.[21] As reported in Figure 4.20, EDOT-EthC6 is prepared via a Williamson etherification of EDOT-MeOH in anhydrous acetonitrile (ACN) with 6-bromo-1-hexene as the alkylating agent in the presence of sodium hydride (NaH) as the base. The monomer is then oxidatively polymerized in an ACN/H_2O- mixture with iron(III)-tosylate as the oxidizing agent in a double-walled reaction vessel (3 h at −8 °C).

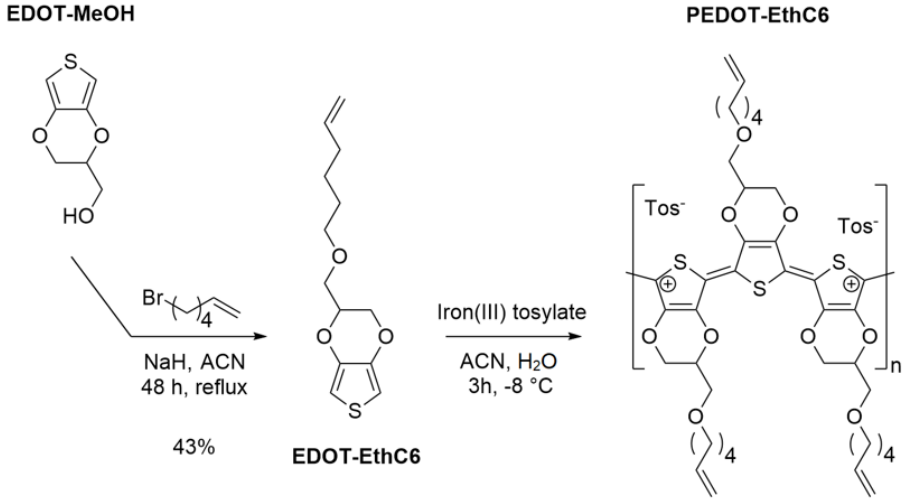

Figure 4.20: Synthesis of the PEDOT-EthC6 polymer via oxidative polymerization of EDOT-EthC6 in solution at −8 °C.

The oxidative polymerization of EDOT and its derivatives in solution is a complex system with numerous influencing factors and intrinsic interactions e.g. between the electron-rich thiophene groups of EDOT-EthC6 and the electron-poor oxidized oligomers, which are easy to oxidize due to their extended chain length. Furthermore, interactions between the aprotic-polar acetonitrile and the radical cations of the monomers, the oxidized oligomers or the oxidizing agent are possible. In order to gain knowledge of these factors, a detailed analysis of the polymerization was performed by in-situ redox potential measurements and GC/MS analysis (Figure 4.21A and B). The redox potential measurement allows the consumption of the oxidizing agent during the polymerization to be followed. The GC/MS measurements provide information about the monomer concentration in the reaction mixture. While the monomers and oligomers are oxidized by iron(III)-tosylate, the Fe^{3+} is reduced to Fe^{2+}. The reduction is associated with a voltage drop, which can be measured in a 3-electrode setup. In the present case, the potential between a platinum electrode and a saturated calomel electrode as refernce was measured. The redox potential measurement in Figure 4.21A shows significant drops after 48 h and 66 h and levels off again after 96 h.Within 100 h, the potential drops to 0.34 V in total.

Figure 4.21B depicts the results of the GC/MS data. The reference compound tetrahydronaphthalene, which is unreactive under the given conditions, is added to the reaction mixture and can be easily identified in the GC/MS data. Samples of the reaction mixture were taken and analyzed by GC/MS. The ratio of the EDOT-EthC6 monomer and the reference allows the monomer consumption to be tracked. The GC/MS data also shows a substantial decrease of the EDOT/reference ratio, i.e. a significant consumption of monomer, which is almost completed after approx. 70 h.[177] The monomer is consumed earlier than the oxidizing agent. This can be explained by an oxidation of the oligomers. The oxidation potential of the oligomers decreases with increasing chain length, so that the oxidizing agent consumption is increased by the oxidation of the oligomers and is preferred in comparison to the oxidation of monomers. This can also be observed from the redox potential, which decreases progressively with increasing polymerization time. The fact that some monomer remains in the reaction mixture even after 100 h can be explained by the under-stoichiometric oxidizing agent concentration.

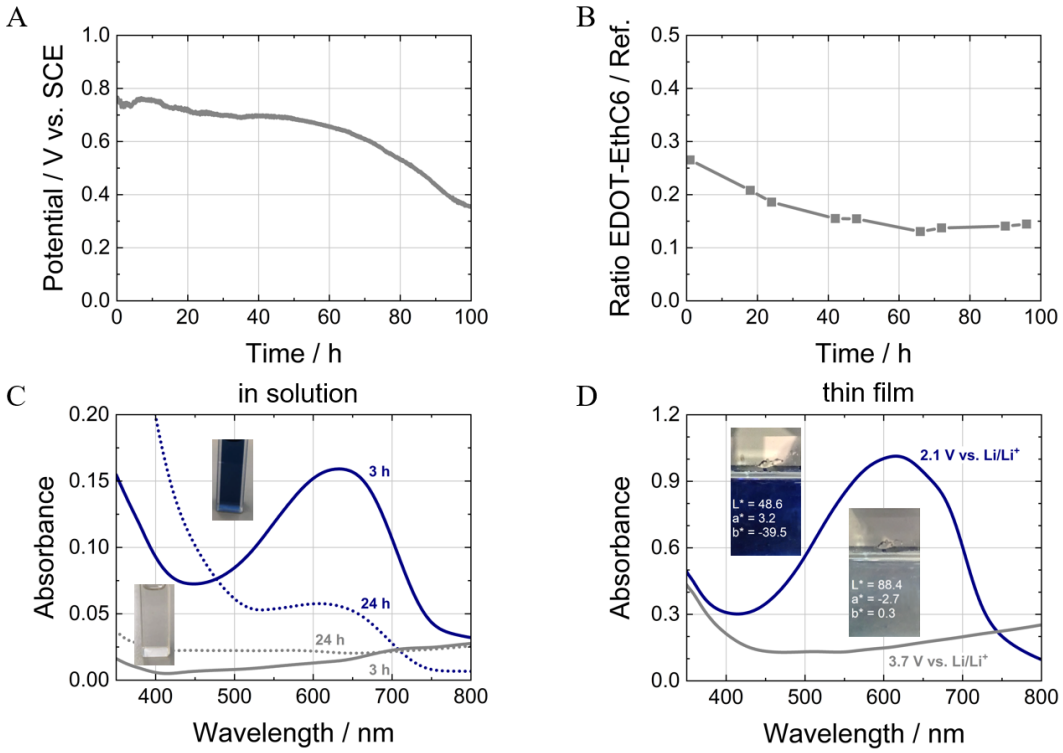

Figure 4.21: *In-situ* redox potential measurements of the reaction mixture (A), GC/MS data illustrating the monomer consumption based on decreasing monomer/refernce compound ratio (B) during polymerization of EDOT-EthC6 over the course of 100 h(B), UV-Vis spectra of the diluted (n-butanol) PEDOT-EthC6 ink (chemical oxidation and reduction) as a function of polymerization time after 3 h and after 24 h (C) and *in-situ* spectroelectrochemical data and L^* a^* b^* color coordinates of the nano-PEDOT-EthC6 thin films (D).

As the oligomer and polymer chains grow during the oxidative polymerization, the different diffusivity of the polymer chains of different molecular weight influences the kinetics of nucleation, so that individual polymer chains of a certain chain length and weight agglomerate in the colloidal environment of the reaction mixture to form nanoparticles.

Large polymer agglomerates result in precipitation of the polymer. The precipitate is filtered off prior to coating. Therefore, the particle size distribution is shifted to smaller values. This precipitation leads to a loss of EC performance as the long chain polymers are either filtered off or arrange themselves into inactive macroscopic material clusters on the film. The conductivity of the polymer is not sufficient enough to switch large particle clusters. Smaller particles that do not remain in the filter (e.g. 5 µm pore size) stay in the coating dispersion and either cause macroscopic clusters on the film or significant light scattering (haze). Agglomerates are difficult to re-disperse. Various re-dispersion methods (intense stirring, ultra sound or shear treatment) can only partially dissolve the agglomerates. As such, there is polymer chain length that depends on the reaction time and represents a trade-off between film quality and EC performance.

The optimal time to stop the polymerization can be further influenced by the reaction temperature. It is expected that the reaction kinetics accelerate with increasing temperature. Information about the ideal polymerization time and temperature was obtained by UV-Vis spectroscopy accompanying the polymerization. Samples were taken from the reaction mixture at certain time intervals, purified and examined with regard to the position of the absorption maximum. Figure 4.21C shows examples of the UV-Vis spectra obtained from the diluted PEDOT-EthC6 coating dispersion after 3 h and 24 h (intermediate data points are not shown). The sample is switched to its bright or dark state by chemical oxidation or reduction. A high absorbance modulation is achieved after 3 h polymerization time. The UV-Vis spectra show that after 24 h reaction time the polymerization has proceeded too far. The intensity of the absorption band is reduced, while the position of the absorption band remains at the same wavelength (approx. 630 nm). Although the polymerization continues according to the *in-situ* redox potential measurement and GC/MS analysis, the long-chain polymeric material precipitates and no longer contributes to the color change.

As indicated above, it was found that the best EC properties and thin film quality are obtained at polymerization temperatures of −8 °C after 3 h (see Figure 4.21D, thin film characterization). The polymerization is terminated by solvent extraction (n-heptanol/water). The organic polymer nanoparticles migrate into the organic phase, while the oxidizing agent accumulates in the aqueous phase. The solid content of the purified deep blue polymer dispersion is adjusted for the specific coating requirements by addition of n-butanol. After addition of n-butanol, the PEDOT-EthC6 dispersion appears homogeneous. Rather large particle aggregates with an average diameter of 266 ± 20 nm and a polydispersity index (PI) of 0.53 ± 0.17 (particle size) were observed by means of dynamic light scattering analysis. The PI indicates an intermediate state between a monodisperse and a polydisperse polymer suspension, which is due to aggregation and explains the rather large particle diameters.[316] However, zeta potential measurements showed very favorable results with an average value of 90.5 ± 10.7 mV. The very large electrostatic repulsion is most probably the reason for the homogeneous appearance of the PEDOT-EthC6 dispersion. The kinematic viscosity is 7.2 $mm^2\,s^{-1}$, making it applicable in R2R slot-die coating and ink-jet printing.

In summary, this novel polymerization approach enables water-free, wet-chemical coating and printing processes on flexible substrates to be implemented in a straightforward way, which makes it a simplified and viable alternative to the *in-situ* polymerization of EDOT derivatives and a more flexible method adapted to the needs of ECPs when compared to the established BAYTRON P synthesis. Unlike the BAYTRON P synthesis. The novel preparation method is not limited to water soluble monomers and does not require the use of dispersing agents such as PSS, which is an electro-optically inactive component that compromises the EC performance of the resulting active thin films.

Compared to conventional oxidative polymerization routes in solution, the novel method does not require a complex re-dispersion step and therefore offers advantages in terms of optical film quality. In contrast to R2R *in-situ* polymerization, the dispersion route proposed requires neither a reactive coating step, nor a aqueous rinsing step, resulting in an overall process simplification for further cost reduction of ECP thin film production. The deposition is therefore easier to control during coating and is applicable to a variety of wet-chemical deposition methods. Furthermore, the nanoscale dispersion stands out in terms of atom economy and other green chemistry metrics. In the R2R *in-situ* polymerization process, considerable losses of monomer have to be tolerated during rinsing. In comparison, less monomer is presumably lost in the present dispersion route and recovery is conceivable.[21] The dispersion step is water-free and is therefore suitable for processing under dry conditions.

For thin film deposition, the PEDOT-EthC6 coating dispersion was spin-coated on flexible PET-ITO substrates at 200 rpm for 30 s and subsequently annealed in a circulating air oven at 100 °C for 90 min. The spectroelectrochemical characterization of the nano-PEDOT-EthC6 thin films on PET-ITO is depicted in Figure 4.21D. The absorption spectra illustrate that the color neutral bright state is reached at potentials of 3.7 V versus Li/Li^+. The bright state transmittance is 70 % (620 nm). At potentials of 2.1 V versus Li/Li^+, a strong and broad absorption with a maximum at approx. 620 nm is responsible for the deep blue color that occurs when the PEDOT backbone is reduced from its oxidized bipolaron state (bright) to its neutral state (dark). The dark state transmittance is 10 % (620 nm), resulting in a contrast ratio of 7.0. The coloration efficiency at the absorption maximum of 620 nm is calculated to be 245 $cm^2\,C^{-1}$.

The analysis of the optical properties (CIELAB color space and visible light transmittance τ_v) further confirms the neutral tint of the bright state and the large optical contrast. The color coordinates in the bright state are L* = 88.4, a* = -2.7, b* = -0.3, while the visible light transmittance τ_v is 73 %. The dark state shows a visible light transmittance τ_v of 16 % and the color coordinates are L* = 48.6, a* = 3.2, b* = -39.5. Nano-PEDOT-EthC6 thin films prepared according to the novel route exhibit similar properties in terms of color neutrality and transmissivity in the bright state as well as optical contrast when compared to the *in-situ* polymerized material.[21]

In Figure 4.22, SEM images of a nano-PEDOT-EthC6 thin film are depicted. The thin film shows a grainy, but smooth surface. In comparison, the *in-situ* polymerized PEDOT-EthC6 thin films appear as a characteristic three-dimensional, periodical honeycomb pattern. The honeycomb structure is ascribed to the rinsing process of the solid PEDOT-EthC6 thin films, in which the remaining oxidizing agent is removed from the polymer film.[21] The novel approach does not require any rinsing of the thin films, since the excess oxidizing agent is removed before coating. As can be taken from the SEM images, this leads to significantly less surface roughness, which can also cause light scattering (reflection haze). In addition, the high uniformity is supported by low haze values of the nano-PEDOT-EthC6 thin films of approx. 2 %. For the nano-PEDOT-EthC6 thin films, this means that only very little light is scattered at wide angles or diffused due to macroscopic irregularities.

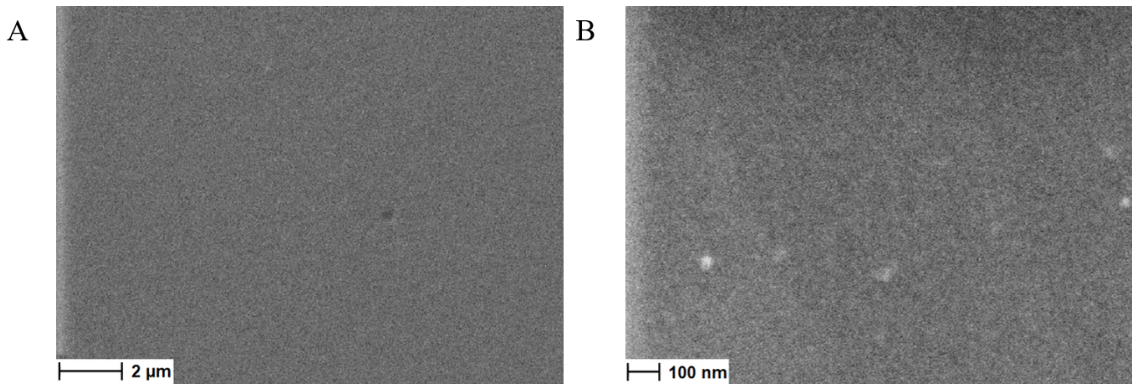

Figure 4.22: Characteristic SEM images of a nano-PEDOT-EthC6 thin film as an overview image (A) and at higher magnification (B). The thin film shows a grainy, but smooth surface.

The electrochemical properties of the nano-PEDOT-EthC6 thin films were initially investigated by cyclic voltammetry (CV). Figure 4.23A shows the CVs at a scan rate of $10\,\mathrm{mV\,s^{-1}}$ (red line). The thin films exhibits reversible redox peaks at potentials of 2.7 V (anodic scan) and 3.0 V versus Li/Li^+ (cathodic scan) corresponding to the oxidation (decoloration) and reduction (coloration) process, respectively, of the conjugated backbone. The substantially broadened cathodic and anodic half-waves are an unavoidable consequence of hindered diffusion and insertion of the counter anions and molecular in-homogeneities in the polymer matrix (e.g. different chain length, different sizes of crystalline domains, polymer particle dimensions, and pore dimensions). The in-homogeneities affect the redox potentials, but are not expected to compromise cycling stability. The coulombic efficiency is approximately 1, indicating a reversible redox process. The results from the CV measurements are in agreement with previously published data of the *in-situ* polymerized PEDOT-EthC6 thin films.[21] Furthermore, the results from the CV analysis are comparable with previously published data of similar PEDOT and PEDOT-like species.[165, 282] Figure 4.23B shows the CVs of nano-PEDOT-EthC6 thin films at various scan rates from $5\,\mathrm{mV\,s^{-1}}$ to $100\,\mathrm{mV\,s^{-1}}$. The redox peaks are shifted by approx. 200 mV when scan rates between $5\,\mathrm{mV\,s^{-1}}$ and $100\,\mathrm{mV\,s^{-1}}$ are applied. The small shifts indicate fast reaction kinetics and promise a prompt response in prospective ECDs.

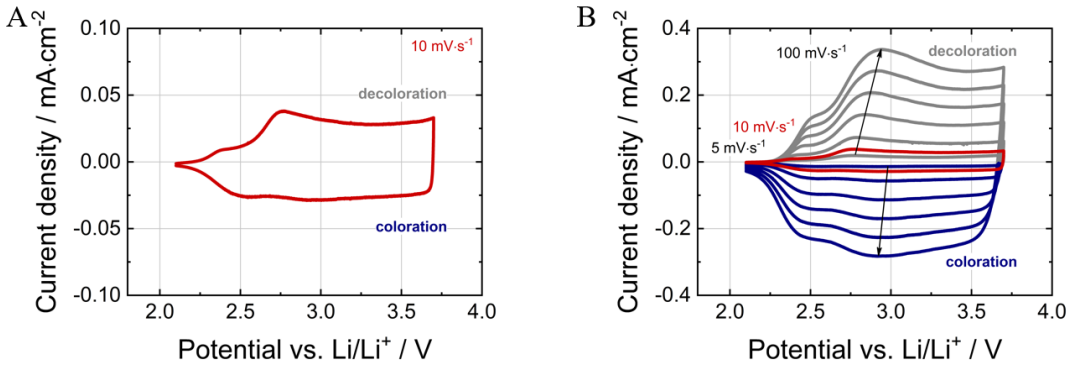

Figure 4.23: Cyclic voltammograms of the nano-PEDOT-EthC6 thin films (5 cycles) at a scan rate of $10\,\mathrm{mV\,s^{-1}}$ (A) and as a function of the scan rate ranging from $5\,\mathrm{mV\,s^{-1}}$ to $100\,\mathrm{mV\,s^{-1}}$ (B).

The nano-PEDOT-EthC6 films were further characterized in galvanostatic charging/discharging experiments. First, the redox behavior was investigated as a function of the charging/discharging rate with current densities between $1\,\mu\mathrm{A\,cm^{-2}}$ and $1000\,\mu\mathrm{A\,cm^{-2}}$. The charge/discharge curves are depicted in Figure 4.24A. They show a reversible oxidation and reduction behavior, while the coulombic efficiency is approx. 1 for all charging/discharging rates. The maximum charge density is determined after the discharge (reduction) process at 2.1 V versus Li/Li^+ and depends on the applied current density. The nano-PEDOT-EthC6 film exhibits a maximum charge density of $3.8\,\mathrm{mC\,cm^{-2}}$ at a current density of $1\,\mu\mathrm{A\,cm^{-2}}$. The high current density indicates high film thickness of the EC layers. This enables a high optical contrast and, in particular, a highly absorbing dark state. However, due to the structure of PEDOT-EthC6, the bright state exhibits color neutrality and high transmissivity. As further revealed in Figure 4.24A, the polarization over-potential increases with charge and discharge rate (current density), especially with increased charge/discharge rates. This becomes observable by a shift of the potential to higher values during charging and by a shift of the potential to lower values during discharging.

Second, cycling stability measurements were performed by means of galvanostatic charging/discharging experiments ($50\,\mu\mathrm{A\,cm^{-2}}$) as well. The individual charge and discharge curves are shown in Figure 4.24B. Over the course of 1 000 cycles, there is an almost perfect overlap of the individual curves. The identical shape of the curves along with the unchanged overpotential over the course of 1 000 cycles indicate EC thin films with high cycling stability. The results from the cycling stability measurements are further evaluated in Figure 4.24C and indicate a highly reversible redox switching behavior (coulombic efficiency above 98 %). The charge density, with values of approx. $3.5\,\mathrm{mC\,cm^{-2}}$ after charging/discharging, remains almost constant over the course of 1 000 switching cycles. The total charge retention is 98 % after 1 000 cycles. CV measurements before and after the cycling stability measurements are depicted in Figure 4.24B. The CVs overlap almost perfectly. Small deviations are due to formation processes as well as hindered diffusion and insertion of the counter anions ($TFSI^-$) during the first few cycles.

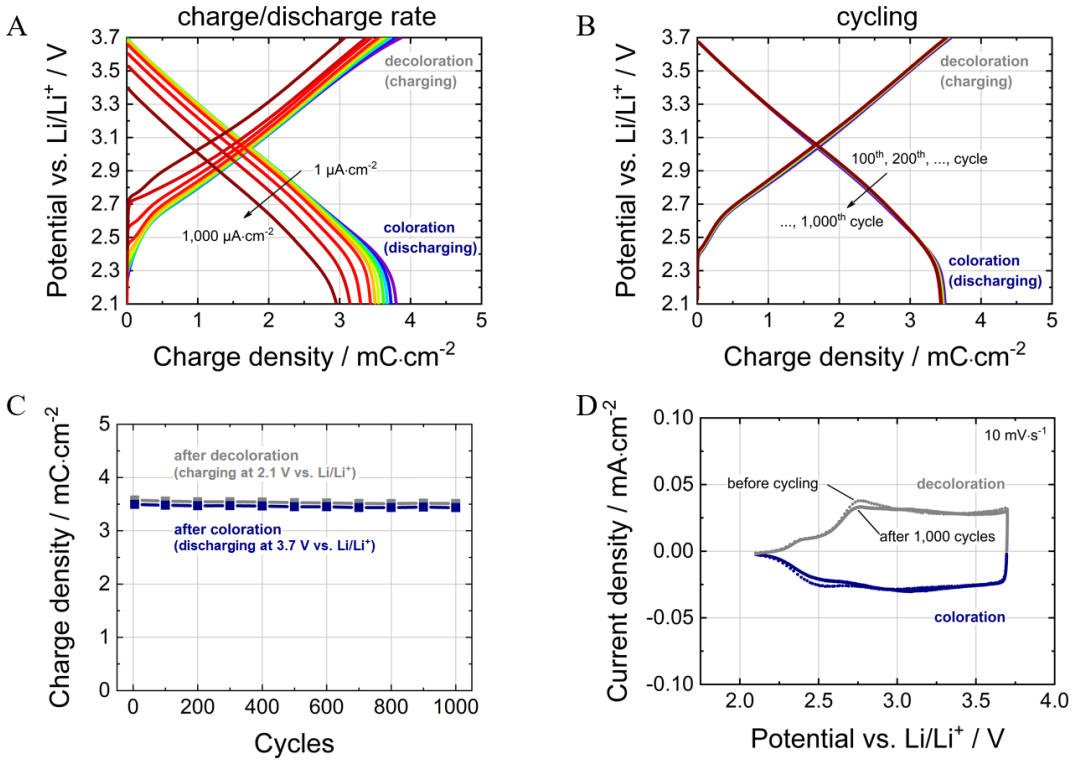

Figure 4.24: Charge/discharge experiments of the nano-PEDOT-EthC6 thin films as a function of current densities ranging from $1\,\mu A\,cm^{-2}$ to $1000\,\mu A\,cm^{-2}$ (A) and during cycling at $50\,\mu A\,cm^{-2}$ (B) as well as the charge/discharge density over the course of 1 000 cycles (C) and cyclic voltammograms before (dotted line) and after cycling (solid line).

Nano-PEDOT-EthC6 thin films prepared from the novel PEDOT-EthC6 coating dispersion exhibit similar electrochemical behavior when compared to the *in-situ* polymerized material. The cycling stability is remarkable, indicating high purity and stability of the EC thin films. This emphasizes the effective processing steps during the preparation of the PEDOT-EthC6 dispersion. In particular, the results imply that the coating dispersion consists solely of polymer and solvents (n-butanol and n-heptanol). Impurities that could affect the cycle stability, e.g. residues of the oxidizing agent, were effectively removed. The cycling stability is at a remarkably high level and indicates high purity and stability of the EC thin films. In this context, the preparation and purification of the PEDOT-EthC6 coating dispersion has advantages when compared to the complex aqueous rinsing process of the *in-situ* polymerized thin films.[21] In conclusion, a novel polymerization approach has been demonstrated with the EDOT-EthC6 monomer, combining the advantages of *in-situ* polymerization and standard cross-coupling polymerization followed by re-dispersion. The resultant PEDOT-EthC6 nanoparticles form dispersions having prolonged shelf life and characteristics compatible with high-throughput coating and printing processes on flexible, conductive substrates. Nano-PEDOT-EthC6 thin films deposited according to the new procedure achieve similar EC properties concerning cycling stability and color neutrality in the bright state when compared to thin films resulting from the previously developed *in-situ* polymerization process.

5 Conclusion and Outlook

The aforementioned drawback of most ECPs, the lack of a highly transmissive and fully colorless bright state, was targeted by the evaluation of a series of sidechain modified EDOT derivatives, bearing a terminal double bond in the lateral sidechain. Especially the EDOT-EthC6 compound, showed enhanced EC properties in terms of a highly transmissive and color neutral bright state and was accessed by a simple and straightforward synthesis. The EC thin film production was scaled-up to the pilot-line scale via a customized large-area and high-throughput R2R process. Thus, it was demonstrates that the incorporation of a sidechain with a terminal double bond yields a material with a performance that surpasses any other PEDOT-related material described in the literature.

The novel PEDOT-EthC6 thin films were further successfully incorporated into ECDs with complementary-switching electrodes. The PEDOT-EthC6 polymer on PET-ITO functions as the cathodically-coloring working electrode and PB on PET-ITO as an anodically-coloring counter electrode. Combined with a solid polymer electrolyte, the ECDs show enhanced EC properties in terms of coloration efficiency, transmittance and color neutrality in the bright state, cycling stability and reversibility. The ECD assembly was scaled-up to a maximum size of 45 x 65 cm^2 (active area) via a customized large-area S2S lamination process. The unique materials and the large-scale processing provide excellent prospects for the commercialization of high-quality flexible see-through ECDs.

For practical applications, it is crucially important that the mentioned EDOT-EthC6/PB ECDs show a performance that is constant in time under demanding environmental conditions and over many cycles of operation. The EDOT-EthC6/PB ECDs were submitted to conscious environmental aging tests under a humid atmosphere (90% rH). The observed irreversible reduction of PET-ITO was attributed to the electrode potentials in combination with moisture ingress into the ECDs.

By incorporation of auxiliary reference electrodes (lithium), knowledge on the actual electrode potentials in the environment of the ECDs was gathered. This allowed the driving voltage window to be adjusted in an unbalanced cell configuration (charge density ratio) to an extent in which irreversible ITO reduction no longer occurs. A detailed investigation of ECDs with the optimized cell configuration (charge density ratio < 1) showed that the overall device performance with regard to visible light transmittance change and response time is not hindered and that the cycling stability under humid atmospheres (90% rH) is significantly improved.

Apart from the avoidance of appropriate electrode potentials necessary for ITO reduction in humid atmospheres, appropriate electrode and device fabrication processes were investigated in order to counteract the influence of moisture and the resulting failure mechanisms regarding the EDOT-EthC6/PB ECDs. Therefore, a dispersion polymerization process in organic media of the EDOT-EthC6 monomer was developed. The PEDOT-EthC6 nanoparticles, arising during an oxidative polymerization, form a stable organic dispersion giving access to straightforward printing and coating processes. The deposited PEDOT-EthC6 thin films show comparable EC properties regarding the *in-situ* polymerized material.

Ultimately, this doctoral thesis creates a basis, with the help of scientific methodology, for assessing the requirements for ECDs themselves and the methods and processes used to manufacture them concerning long-term performance and stability. The basic conclusion for the investigated EC-system is that the less moisture is involved, the better is the long-term cycling stability of ECDs. At the same time, this work also showes that ECDs can tolerate certain amounts of water through measures such as suitable control of the operational voltages and still show excellent EC properties and long-term stability. However, in order to achieve the absolutely optimal performance, a dry processing of the ECDs and appropriate sealing methods are necessary.

Nevertheless, the more advanced the structure and components of an ECD are, and the more requirements to the corresponding manufacturing process have to be met, the higher are the expected costs of the technology. In this context, it is important to specify the trade-off between performance and costs regarding the corresponding application-derived requirements for the appropriate device structure and process. To precise this, indoor applications, for example in the context of increasing digitization, demand far fewer requirements with regard to environmental influences. In the architectural and automotive sector, an EC system is exposed to completely different requirements, which is why more advanced measures and therefore other costs are to be expected here.

The ongoing research in addition to the results presented in this work is targeted at even prolonged cycling tests under different environmental influence. The influence of moisture to ECDs is only one factor posing serious stability problems to ECDs. Especially concerning architectural or automotive applications, factors like solar radiation, oxygen and air contaminants as well as thermal exposure, thermal shock or cycling have to be considered. In addition to the understanding of the degradation mechanisms, suitable solutions to counteract device degradation must be developed and implemented. In addition to the best possible performance of the ECDs, the compatibility with existing and future manufacturing processes must always be kept in mind. If crucial progress is made here in the foreseeable future, there is a good chance for EC systems to penetrate the market in the architectural, interior design and automotive sector in a quick and broad way.

6 Summary

6.1 Summary (ENG)

The present work builds on a conjugated electrochromic polymer with a highly transmissive and colorless bright state and its application in electrochromic devices. The main body of this work focuses on the investigation of the influence of moisture on electrochromic devices and solutions to overcome possible degradation of these devices due to moisture ingress.

Firstly, a series of EDOT derivatives with a terminal double bond in the lateral sidechain to potentially achieve a highly transmissive and fully colorless bright state was investigated. All of the EDOT derivatives were electrochemically polymerized and characterized by means of (*in-situ*) spectroelectrochemistry. The results highlight the dramatic influence of the terminal double bond on the improved visible light transmittance and color neutrality in the bright state. After detailed evaluation and comparison, the best performing compound, which contains a hexenyl sidechain (PEDOT-EthC6), was scaled-up by changing the deposition technique from an electrochemical to a chemical *in-situ* polymerization process on a R2R-pilot line in an industrially relevant environment. The R2R-processed PEDOT-EthC6 half-cells were characterized in detail and provide enhanced electrochromic properties in terms of visible light transmittance and color neutrality in the bright state as well as short response times, improved contrast ratio, coloration efficiency and cycling stability (10 000 cycles). The results of the thin film characterization are summerized in Tab. 6.1.[21]

In a second step, the novel PEDOT-EthC6 electrochromic polymer was combined with a Prussian Blue counter electrode and a solid polymer electrolyte to form an all-solid-sate ECDs based on complementary switching electrodes and PET-ITO as flexible substrates. The fabricated ECDs were optically and (spectro-)electrochemically characterized. Excellent functionality of the S2S-processed flexible ECDs was maintained throughout 10 000 switching cycles under laboratory conditions. The ECDs offer enhanced electrochromic properties in terms of visible light transmittance change and color neutrality in the bright state as well as contrast ratio, coloration efficiency, cycling stability and fast response times. The results of the device characterization are summerized in Tab. 6.1. Furthermore, the final device assembly was transferred from a S2S-process to a continuous R2R-lamination process.[238]

In a third step, the PEDOT-EthC6/PB-based ECDs were submitted to conscious environmental aging tests. The emphasis of the research presented in this work, was mainly put at the influence of moisture and possible failure mechanisms regarding the PEDOT-EthC6/PB-based ECDs. An intense brown coloration of the electrodes was observed while cycling the ECDs in humid atmospheres (90% rH) as a major degradation phenomenon. The brown coloration and a thereby accompanied loss of conductivity of the PET-ITO substrates was related to significant degradation of the ITO layers, inserted as the conductive layers in the flexible ECDs. A dissolution of the ITO thin films and formation of metallic indium particles on the surface of the ITO layers was observed that harmed the cycling stability enormously. The conductive layers of the aged ECDs were investigated by XRD, UV-Vis, SEM and (spectro-)electrochemical measurements and validated the supposed irreversible reduction of the ITO layers.[279]

In the absence of reasonable alternatives to PET-ITO for flexible (R2R-processed) ECDs, it is also important to investigate measures to avoid the degradation of ECDs. This is primarily associated with the avoidance of appropriate electrode potentials necessary for ITO reduction in humid atmospheres. As an intrinsic action point, the electrode potentials were investigated via electrochemical measurements in a three-electrode set-up of an all-solid-state ECD. Extensive knowledge on the electrode potentials allowed the voltage-induced degradation of the ITO in flexible ECDs to be avoided through the implementation of an unbalanced electrode configuration (charge density ratio of working and counter electrode). It was possible to narrow the overall operational voltage window to an extent in which irreversible ITO reduction no longer occurs. The unbalanced electrode configuration lead to an improved cycling stability without harming other characteristics such as response time and light transmittance change and allows ECD operation in the presence of humidity.[279]

The avoidance of the mentioned degradation phenomena is further associated with appropriate sealing methods and materials as well as appropriate electrode and device fabrication processes. Since a variety of sealing materials is commercially available, due to the commercial launch of organic photovoltaic (OPV) and light emitting diodes (OLEDs), the focus in the present work was put to water-free electrode fabrication. As an extrinsic action point, a novel preparation method of a nanoscale PEDOT-EthC6 dispersion based on organic solvents is presented here in a final step. The water-free processing method gives access to straightforward printing and coating processes on flexible PET-ITO substrates and thus represents a promising and simplified alternative to the established $PEDOT{:}PSS$. The resulting nano-PEDOT-EthC6 thin films exhibit enhanced color neutrality and transmissivity in the bright state and are comparable to the properties of the *in-situ* polymerized PEDOT-EthC6 thin films.[280]

Table 6.1: Electrochromic properties of the PEDOT-EthC6 and Prussian Blue half cells and the resulting electrochromic full cell (PEDOT-EthC6/PB).

half cells	charge density q / mC cm^{-2}	max. absorbance wavelength λ_{max} / nm	operating potential vs. Li/Li^+ U_{dark} | U_{bright} / V	color values L* | a* | b*	visible light transmittance $\tau_{v,dark}$ | $\tau_{v,bright}$ / %	transmittance at λ_{max} T_{dark} | T_{bright} / %	contrast ratio at λ_{max} CR	coloration efficiency at λ_{max} η / cm^2 C^{-1}
PEDOT-EthC6	3.5	626	2.1	29.7 | 17.0 | -58.2	4.4	0.8	71.9	530
			3.7	83.8 | -4.3 | -4.1	62.8	57.5		
Prussian Blue	4.5	683	3.6	85.9 | -13.0 | -13.7	65.5	41.9	2.3	78
			2.4	97.5 | -1.4 | 1.9	93.9	94.3		
full cell			operating voltage V_{dark} | V_{bright} / V					
PEDOT-EthC6 / Prussian Blue	(3.5)[a]	630	-1.4	26.8 | 12.8 | -52.9	3.7	0.5	93.4	(563)[a]
			1.8	77.9 | -5.9 | -0.6	52.7	46.7		

[a]Assumption that the available charge density of the full cell is equal to the charge density of the half cell with lower charge density (theoretical value).

6.2 Zusammenfassung (DE)

Die vorliegende Arbeit beruht auf einem konjugierten elektrochromen Polymer mit hochtransmissivem und farblosem Hellzustand sowie dessen Anwendung in elektrochromen Elementen. Der Hauptteil dieser Arbeit konzentriert sich auf den Einfluss von Feuchtigkeit auf elektrochrome Elemente sowie Lösungen, um einer möglichen Degradation dieser Systeme aufgrund der Einwirkung von Feuchtigkeit entgegenzuwirken.

In einem ersten Schritt wurde eine Reihe von EDOT-Derivaten mit terminalen Doppelbindung in einer lateralen Seitenkette untersucht, um einen hoch-transmissiven und vollständig farblosen Hellzustand zu erreichen. Alle EDOT-Derivate wurden elektrochemisch polymerisiert und mittels (*in-situ*) spektroelektrochemischer Messungen charakterisiert. Die Ergebnisse unterstreichen den dramatischen Einfluss der terminalen Doppelbindung auf die verbesserte Transmission und Farbneutralität im Hellzustand. Nach einer detaillierten Bewertung und entsprechendem Vergleich wurden die Dünnschichten der Verbindung mit den besten Eigenschaften, welche eine Hexenylseitenkette (PEDOT-EthC6) enthält, hochskaliert. Dazu wurde die elektrochemische Abscheidung durch einen chemischen *in-situ*-Polymerisationsprozess ersetzt. Dies ermöglicht die Abscheidung elektrochromer Dünnschichten im großen Maßstab auf einer R2R-Beschichtungsanlage. Die mittels R2R-Beschichtung abgeschiedenen PEDOT-EthC6-Dünnschichten wurden daraufhin detailliert charakterisiert und zeigen verbesserte elektrochrome Eigenschaften hinsichtlich visueller Transmission und Farbneutralität im Hellzustand, kurze Schaltzeiten, ein verbessertes Kontrastverhältnis sowie verbesserte Färbeeffizienz und Zyklenstabilität (10 000 Zyklen). Die Ergebnisse der Dünnschichtcharakterisierung sind in Tab. 6.2 zusammengefasst.[21]

Im zweiten Schritt wurden PEDOT-EthC6-Halbzellen mit Preußisch Blau-Gegenelektroden und einem festen Polymerelektrolyten kombiniert und ein Festkörper- ECD auf Basis koplementär-färbender Elektroden und flexiblen PET-ITO-Substraten realisiert. Die hergestellten ECDs wurden optisch und (spektro-)elektrochemisch charakterisiert. Die Funktionalität der S2S-assemblierten flexiblen ECDs wurde über 10 000 Schaltzyklen unter Laborbedingungen getestet. Die ECDs bieten verbesserte elektrochrome Eigenschaften hinsichtlich der visuellen Transmission und Farbneutralität im Hellzustand sowie des Kontrastverhältnisses, der Färbeeffizienz, Zyklenstabilität und Schaltzeit. Die Ergebnisse der Charakterisierung sind in Tab. 6.2 zusammengefasst. Darüber hinaus wurde die S2S-Laminierung der ECDs in einen kontinuierlichen R2R-Laminierprozess übertragen.[238]

Dann wurden die PEDOT-EthC6/PB-basierten ECDs kontrollierten Alterungstests unterzogen. Der Schwerpunkt dieser Arbeit lag hauptsächlich auf dem Einfluss von Feuchtigkeit und den daraus resultierenden Degradationsmechanismen des PEDOT-EthC6/PB-Systems. Während die ECDs in feuchter Atmosphäre (90 % rH) zyklisiert wurden, konnte eine intensive Braunfärbung der Elektroden beobachtet werden. Die braune Färbung und ein damit einhergehender Verlust der Leitfähigkeit wurde auf eine signifikante Degradation der ITO-Schichten zurückgeführt, die als leitfähige Schichten in den flexiblen ECDs Verwendung fanden. Die Auflösung der ITO-Dünnschichten sowie die Bildung von metallischen Indiumpartikeln auf der Oberfläche der ITO-Schichten wurde beobachtet und als Ursache für die verminderte Zyklenstabilität herangezogen. Die leitfähigen Schichten der gealterten ECDs wurden durch XRD-, UV-Vis-, REM- und (spektro-)elektrochemische Messungen untersucht und die vermutete irreversible Reduktion der ITO- Schichten bestätigt.[279]

Mangels Alternativen zu PET-ITO für flexible (R2R-prozessierte) ECDs ist es wichtig, Maßnahmen zur Vermeidung der Degradation von ECDs zu untersuchen. Dies ist in erster Linie mit der Vermeidung geeigneter Elektrodenpotentiale verbunden, die für die Reduktion von ITO in feuchter Atmosphäre erforderlich sind. Als intrinsische Maßnahme wurden die Elektrodenpotentiale durch elektrochemische Messungen in einem Drei-Elektroden-Aufbau eines Festkörper-ECD untersucht. Aufgrund der umfassende Kenntnis der Elektrodenpotentiale konnte die spannungsinduzierte Degradation der enthaltenen ITO-Schichten durch die Implementierung einer unbalancierten Elektrodenkonfiguration (Ladungsdichteverhältnis von Arbeits- und Gegenelektrode) vermieden werden. Es war dadurch möglich, das gesamte Spannungsfenster zum Betrieb des ECD so weit einzuschränken, dass keine irreversible ITO-Reduktion mehr auftrat. Die unbalancierte Elektrodenkonfiguration führt zu einer verbesserten Zyklenstabilität, ohne andere Eigenschaften wie Schaltzeit oder visuellen Transmissionshub zu beeinträchtigen und ermöglicht daher den Betrieb von ECDs auch in feuchter Atmosphäre.[279]

Die Vermeidung der genannten Degradationsphänomene ist ferner mit geeigneten Versiegelungsverfahren und -materialien sowie geeigneten Elektroden- und Assemblierungsverfahren möglich. Da aufgrund der kommerziellen Einführung von organischer Photovoltaik (OPV) und organischer Leuchtdioden (OLEDs) eine Vielzahl von Versiegelungsmaterialien kommerziell erhältlich ist, lag der Schwerpunkt der vorliegenden Arbeit auf der Herstellung wasserfreier Elektroden. Als extrinsische Maßnahme wurde in einem letzten Schritt eine neuartige Herstellungsmethode für eine nanoskaligen PEDOT-EthC6-Dispersion auf Basis organischer Lösungsmittel entwickelt. Die wasserfreie Verarbeitungsmethode ermöglicht einfache Druck- und Beschichtungsprozesse auf flexiblen PET-ITO-Substraten und stellt somit eine vielversprechende und vereinfachte Alternative zu etabliertem $PEDOT{:}PSS$ dar. Die resultierenden PEDOT-EthC6-Schichten zeigen im Hellzustand ebenfalls eine verbesserte Farbneutralität sowie visuelle Transmission und sind vergleichbar mit den Eigenschaften der *in-situ*-polymerisierten PEDOT-EthC6-Schichten.[280]

Tabelle 6.2: Elektrochrome Eigenschaften der PEDOT-EthC6 und Preußisch Blau Halbzellen sowie der daraus resultierenden PEDOT-EthC6/Preußisch Blau Vollzelle (PEDOT-EthC6/PB).

Halbzelle	Ladungs-dichte q / $mC\,cm^{-2}$	Wellenlänge der max. Absorption λ_{max} / nm	Schalt-Potential gegen Li/Li^+ U_{dunkel} | U_{hell} / V	Farbwerte L* | a* | b*	visuelle Licht-transmission $\tau_{v,dunkel}$ | $\tau_{v,hell}$ / %	Transmission bei λ_{max} T_{dunkel} | T_{hell} / %	Kontrast-verhältnis bei λ_{max} CR	Färbe-effizienz bei λ_{max} η / $cm^2\,C^{-1}$
PEDOT-EthC6	3.5	626	2.1	29.7 | 17.0 | -58.2	4.4	0.8	71.9	530
			3.7	83.8 | -4.3 | -4.1	62.8	57.5		
Preußisch Blau	4.5	683	3.6	85.9 | -13.0 | -13.7	65.5	41.9	2.3	78
			2.4	97.5 | -1.4 | 1.9	93.9	94.3		
Vollzelle			Schalt-spannung V_{dunkel} | V_{hell} / V					
PEDOT-EthC6 / Preußisch Blau	(3.5)[a]	630	-1.4	26.8 | 12.8 | -52.9	3.7	0.5	93.4	(563)[a]
			1.8	77.9 | -5.9 | -0.6	52.7	46.7		

[a]Annahme, dass die verfügbare Ladungsdichte der Vollzelle gleich der Ladungsdichte der Halbzelle mit geringerer Ladungsdichte ist (theoretischer Wert).

Bibliography

[1] S. H. Schneider, *Science* **1989**, *243*, 771–781.

[2] *Klimawandel in Deutschland: Entwicklung, Folgen, Risiken und Perspektiven*, (Eds.: G. Brasseur, D. Jacob, S. Schuck-Zöller), Springer Spektrum, Berlin, **2017**.

[3] M. Hauck, C. Leuschner, J. Homeier, *Klimawandel und Vegetation - Eine globale Übersicht*, 1. Auflage, Springer Spektrum, Berlin, **2019**.

[4] Umweltbundesamt, Nationaler Inventarbericht zum Deutschen Treibhausgasinventar 1990 - 2018, **2020**.

[5] M. Detsi, A. Manolitsis, I. Atsonios, I. Mandilaras, M. Founti, *Energies* **2020**, *13*, 3020.

[6] C. A. Balaras, K. Droutsa, E. Dascalaki, S. Kontoyiannidis, *Energy and Buildings* **2005**, *37*, 429–442.

[7] R. Baetens, B. P. Jelle, A. Gustavsen, *Solar Energy Materials and Solar Cells* **2010**, *94*, 87–105.

[8] M. C. Finnegan, L. Z. Solomon, *The Journal of Social Psychology* **1981**, *115*, 291–292.

[9] P. Leather, M. Pyrgas, Di Beale, L. C., *Environment and Behavior* **1998**, *30*, 739–762.

[10] C. E. Ochoa, M. B. Aries, E. J. van Loenen, J. L. M. Hensen, *Applied Energy* **2012**, *95*, 238–245.

[11] N. L. Sbar, L. Podbelski, H. M. Yang, B. Pease, *International Journal of Sustainable Built Environment* **2012**, *1*, 125–139.

[12] R. Liang, Y. Sun, M. Aburas, R. Wilson, Y. Wu, *Energy and Buildings* **2018**, *176*, 216–231.

[13] S. Papaefthimiou, *Advances in Building Energy Research* **2010**, *4*, 77–126.

[14] U. Posset, M. Harsch, A. Rougier, B. Herbig, G. Schottner, G. Sextl, *RSC Advances* **2012**, *2*, 5990–5996.

[15] R. D. Rauh, *Electrochimica Acta* **1999**, *44*, 3165–3176.

[16] W. J. Hee, M. A. Alghoul, B. Bakhtyar, O. Elayeb, M. A. Shameri, M. S. Alrubaih, K. Sopian, *Renewable and Sustainable Energy Reviews* **2015**, *42*, 323–343.

[17] *Electrochromic Materials and Devices*, (Eds.: R. J. Mortimer, D. R. Rosseinsky, P. M. S. Monk), Wiley-VCH, Weinheim, Germany, **2015**.

[18] S. D. Rezaei, S. Shannigrahi, S. Ramakrishna, *Solar Energy Materials and Solar Cells* **2017**, *159*, 26–51.

[19] C. G. Granqvist, Bayrak P. İ., G. A. Niklasson, *Surface and Coatings Technology* **2018**, *336*, 133–138.

[20] D. Rosseinsky, R. J. Mortimer, *Advanced Materials* **2001**, *13*, 782–793.

[21] S. Macher, M. Schott, M. Sassi, I. Facchinetti, R. Ruffo, G. Patriarca, L. Beverina, U. Posset, G. A. Giffin, P. Löbmann, *Advanced Functional Materials* **2020**, *30*, 1906254.

[22] C. M. Lampert, *Materials Today* **2004**, *7*, 28–35.

[23] C. H. Stoessel in *Optical Thin Films And Coatings*, (Eds.: A. Piegari, F. Flory), Elsevier Science, Burlington, **2013**, pp. 718–740.

[24] *Optical Thin Films And Coatings: From Materials To Applications*, (Eds.: A. Piegari, F. Flory), Elsevier Science, Burlington, **2013**.

[25] G. J. Marshall, C. P. Mahony, M. J. Rhodes, S. R. Daniewicz, N. Tsolas, S. M. Thompson, *Engineering* **2019**, *5*, 954–969.

[26] N. I. Jaksic, C. Salahifar, *Solar Energy Materials and Solar Cells* **2003**, *79*, 409–423.

[27] R. B. Farrington, R. Anderson, D. M. Blake, S. D. Burch, M. R. Cuddy, M. A. Keyser, J. P. Rugh, *National Renwable Energy Laboratory* **1999**.

[28] R. B. Farrington, D. L. Brodt, S. D. Burch, M. A. Keyser, *National Renewable Energy Laboratory* **1999**.

[29] N. R. Lynam in Large-Area Chromogenics: Materials and Devices for Transmittance Control, (Eds.: C. M. Lampert, C.-G. Granqvist), SPIE, **2017**, p. 1030404.

[30] C. M. Lampert, C.-G. Granqvist, Eds., Large-Area Chromogenics: Materials and Devices for Transmittance Control, SPIE, **2017**.

[31] C. M. Lampert, A. Agrawal, C. Baertlien, J. Nagai, *Solar Energy Materials and Solar Cells* **1999**, *56*, 449–463.

[32] J. M. Bell, I. L. Skryabin, *Solar Energy Materials and Solar Cells* **1999**, *56*, 437–448.

[33] J. Nagai, G. D. McMeeking, Y. Saitoh, *Solar Energy Materials and Solar Cells* **1999**, *56*, 309–319.

[34] C. Daniel, *Journal of The Minerals Metals and Materials Society* **2008**, *60*, 43–48.

[35] J. Li, C. Daniel, D. Wood, *Journal of Power Sources* **2011**, *196*, 2452–2460.

[36] J. Li, C. Daniel, S. J. An, D. Wood, *MRS Advances* **2016**, *1*, 1029–1035.

[37] R. J. Mortimer, *Annual Reviews* **2011**, 241–268.

[38] P. M. S. Monk, R. J. Mortimer, D. R. Rosseinsky, *Electrochromism and Electrochromic Devices*, Cambridge Univ. Press, Cambridge, **2007**.

[39] T. Leichtweiss, Dissertation, Justus-Liebig-Universität, Gießen, **2010**.

[40] J. Jensen, F. C. Krebs, *Advanced Materials* **2014**, *26*, 1–4.

[41] R. J. Mortimer, *Chemical Society Reviews* **1997**, *26*, 147–156.

[42] R. J. Mortimer, *Electrochimica Acta* **1999**, *44*, 2971–2981.

[43] Gentex Corporation, www.gentex.com.

[44] A. Case, *Calm Technology: Principles and Patterns for Non-Intrusive Design*, O' Reilly Media, USA, **2015**.

[45] H. Müller, A. Colley, J. Häkkilä, W. Jensen, M. Löchtefeld, Eds., Using Electrochromic Displays to Display Ambient Information and Notifications, The 2019 ACM International Joint Conference on Pervasive and Ubiquitous Computing and the 2019 ACM International, London, UK, **2019**.

[46] W. Jensen, A. Colley, J. Häkkilä, C. Pinheiro, M. Löchtefeld, *Advances in Human-Computer Interaction* **2019**, *2019*, 1–14.

[47] N. Kobayashi in *Handbook of Visual Display Technology*, *Vol. 23*, (Eds.: J. Chen, W. Cranton, M. Fihn), Springer, Berlin, Heidelberg, **2015**, pp. 1–13.

[48] W. M. Kline, R. G. Lorenzini, G. A. Sotzing, *Coloration Technology* **2014**, *130*, 73–80.

[49] A. Piccolo, F. Simone, *Journal of Building Engineering* **2015**, *3*, 94–103.

[50] J. Al Dakheel, K. Tabet Aoul, *Energies* **2017**, *10*, 1672.

[51] S. Attia, S. Bilir, T. Safy, C. Struck, R. Loonen, F. Goia, *Energy and Buildings* **2018**, *179*, 165–182.

[52] C. Louet, S. Cantin, J.-P. Dudon, P.-H. Aubert, F. Vidal, C. Chevrot, *Solar Energy Materials and Solar Cells* **2015**, 141–151.

[53] P. M. S. Monk, *The Viologens*, Wiley, Chichester, UK, **1998**.

[54] A. L. Eh, A. W. M. Tan, X. Cheng, S. Magdassi, P. S. Lee, *Energy Technology* **2018**, *6*, 33–45.

[55] C. G. Granqvist, E. Avendaño, A. Azens, *Thin Solid Films* **2003**, *442*, 201–211.

[56] J. Jensen, M. Hösel, A. L. Dyer, F. C. Krebs, *Advanced Functional Materials* **2015**, *25*, 2073–2090.

[57] H. Wang, M. Barrett, B. Duane, J. Gu, F. Zenhausern, *Materials Science and Engineering: B* **2018**, *228*, 167–174.

[58] A. W. Czanderna, D. K. Benson, G. J. Jorgensen, J. G. Zhang, C. E. Tracy, S. K. Deb, *Solar Energy Materials and Solar Cells* **1999**, *56*, 419–436.

[59] A. Cochet, Dissertation, Julius-Maximilians-Universität, Würzburg, **2008**.

[60] A. I. Hofmann, W. T. T. Smaal, M. Mumtaz, D. Katsigiannopoulos, C. Brochon, F. Schütze, O. R. Hild, E. Cloutet, G. Hadziioannou, *Angewandte Chemie* **2015**, *127*, 8626–8630.

[61] A. A. Karyakin, *Electroanalysis* **2001**, *13*, 813–819.

[62] K. M. Lee, H. Tanaka, A. Takahashi, K. H. Kim, M. Kawamura, Y. Abe, T. Kawamoto, *Electrochimica Acta* **2015**, *163*, 288–295.

[63] C. A. Nguyen, S. Xiong, J. Ma, X. Lu, P. S. Lee, *Physical Chemistry Chemical Physics* **2011**, *13*, 13319–13326.

[64] L. Su, Z. L. Hong Wang, *Supramolecular Science* **1998**, *5*, 657–659.

[65] R. C. Agrawal, G. P. Pandey, *Journal of Physics D: Applied Physics* **2008**, *41*, 223001.

[66] S. B. Aziz, T. J. Woo, M. Kadir, H. M. Ahmed, *Journal of Science: Advanced Materials and Devices* **2018**, *3*, 1–17.

[67] C. Julien, A. Mauger, A. Vijh, K. Zaghib, *Lithium Batteries: Science and Technology*, Springer, Cham, Germany, **2016**.

[68] F. B. Dias, L. Plomp, J. B. J. Veldhuis, *Journal of Power Sources* **2000**, *88*, 169–191.

[69] Q. Li, J. Chen, L. Fan, X. Kong, Y. Lu, *Green Energy and Environment* **2016**, *1*, 18–42.

[70] T. Placke, O. Fromm, S. F. Lux, P. Bieker, S. Rothermel, *Journal of The Electrochemical Society* **2012**, *159*, A1755–A1765.

[71] I. Rey, J. C. Lassègues, J. Grondin, L. Servant, *Electrochimica Acta* **1998**, *43*, 1505–1510.

[72] Y. Tominaga, K. Yamazaki, V. Nanthana, *Journal of The Electrochemical Society* **2015**, *162*, A3133–A3136.

[73] S. Y. Hong, Y. Kim, Y. Park, A. Choi, N.-S. Choi, K. T. Lee, *Energy and Environmental Science* **2013**, *6*, 2067.

[74] H. Kim, G. Yoon, K. Lim, K. Kang, *Chemical Communication* **2016**, *52*, 12618–12621.

[75] S. P. Ong, V. L. Chevrier, G. Hautier, A. Jain, C. Moore, S. Kim, X. Ma, G. Ceder, *Energy and Environmental Science* **2011**, *4*, 3680.

[76] X. Zhao, X. Zhang, D. Wu, H. Zhang, F. Ding, Z. Zhou, *Journal of Materials Chemistry A* **2016**, *4*, 16606–16611.

[77] V. Di Noto, S. Lavina, G. A. Giffin, E. Negro, B. Scrosati, *Electrochimica Acta* **2011**, *57*, 4–13.

[78] G. A. Giffin, A. Moretti, S. Jeong, S. Passerini, *The Journal of Physical Chemistry C* **2014**, *118*, 9966–9973.

[79] G. A. Giffin, *Journal of Materials Chemistry A* **2016**, *4*, 13378–13389.

[80] S. Jeremias, G. A. Giffin, A. Moretti, S. Jeong, S. Passerini, *The Journal of Physical Chemistry C* **2014**, *118*, 28361–28368.

[81] T.-Y. Wu, W.-B. Li, C.-B. Kuo, C.-F. Chou, J.-W. Liao, H.-R. Chen, *International Journal of Electrochemical Science* **2013**, *8*, 10720–10732.

[82] K. Xu, *Chemical reviews* **2004**, *104*, 4303–4417.

[83] Byker, H. J., Gentex Cooperation (1990) Single-compartment, self-erasing, solution-phase electrochromic devices, solutions for use therein and uses thereof. US Patent 4,902,108.

[84] H. J. Byker, Ed., Proceedings of the Symposium on Electrochromic Materials II, The Electrochemical Society Inc., pp. 3-13, **1994**.

[85] A. Gonçalves, C. Costa, S. Pereira, N. Correia, M. M. Silva, P. C. Barbosa, L. C. Rodrigues, I. Henriques, R. Martins, E. Fortunato, *Polymers for Advanced Technologies* **2012**, *23*, 791–795.

[86] C. A. Nguyen, S. Xiong, J. Ma, X. Lu, P. S. Lee, *The Journal of Physical Chemistry B* **2009**, *113*, 8006–8010.

[87] W. H. Meyer, *Advanced Materials* **1998**, *10*, 439–448.

[88] A. M. Soutar, D. R. Rosseinsky, W. Freeman, X. Zhang, X. How, H. Jiang, X. Zeng, X. Miao, *Solar Energy Materials and Solar Cells* **2012**, *100*, 268–270.

[89] G. P. T. Ganesh, R. Ravi, B. Deb, *Solar Energy Materials and Solar Cells* **2015**, *140*, 17–24.

[90] A. M. Andersson, C. G. Granqvist, J. R. Stevens, *Applied Optics* **1989**, *28*, 3295–3302.

[91] J. E. Weston, B. C. H. Steele, *Solid State ionics* **1982**, *7*, 81–88.

[92] A. M. Stephan, K. S. Nahm, *Polymer* **2006**, *47*, 5952–5964.

[93] A. M. Haregewoin, A. S. Wotango, B.-J. Hwang, *Energy and Environmental Science* **2016**, *9*, 1955–1988.

[94] C. G. Granqvist, *Handbook of Inorganic Electrochromic Oxides*, Elsevier, Amsterdam, **1995**.

[95] M. Schott, Dissertation, Julius-Maximilians-Universität, Würzburg, **2015**.

[96] C. G. Granqvist, *Solar Energy Materials and Solar Cells* **2007**, *91*, 1529–1598.

[97] *Handbook of Transparent Conductors*, (Eds.: D. S. Ginley, H. Hosono, D. C. Paine), Springer, New York, USA, **2010**.

[98] K. Ellmer, *Nature Photonics* **2012**, *6*, 809–817.

[99] A. Kumar, C. Zhou, *ACS nano* **2010**, *4*, 11–14.

[100] T. Minami, *Semiconductor Science and Technology* **2005**, *20*, S35–S44.

[101] T. Minami, *Thin Solid Films* **2008**, *516*, 5822–5828.

[102] M. Hövel, B. Gompf, M. Dressel, *Physical Review B* **2010**, *81*, 2014.

[103] P. C. Lansåker, J. Backholm, G. A. Niklasson, C. G. Granqvist, *Thin Solid Films* **2009**, *518*, 1225–1229.

[104] G. B. Smith, G. A. Niklasson, J. S. E. M. Svensson, C. G. Granqvist, *Journal of Applied Physics* **1986**, *59*, 571–581.

[105] X. Fang, C. L. Mak, J. Dai, K. Li, H. Ye, C. W. Leung, *ACS Applied Materials and Interfaces* **2014**, *6*, 15743–15752.

[106] C. Guillén, J. Herrero, *Thin Solid Films* **2011**, *520*, 1–17.

[107] Y. S. Kim, J. H. Park, D. H. Choi, H. S. Jang, J. H. Lee, H. J. Park, J. I. Choi, D. H. Ju, J. Y. Lee, D. Kim, *Applied Surface Science* **2007**, *254*, 1524–1527.

[108] H. J. Park, J. H. Park, J. I. Choi, J. Y. Lee, J. H. Chae, D. Kim, *Vacuum* **2008**, *83*, 448–450.

[109] A. Aliprandi, T. Moreira, C. Anichini, M.-A. Stoeckel, M. Eredia, U. Sassi, M. Bruna, C. Pinheiro, C. A. T. Laia, S. Bonacchi, P. Samorì, *Advanced Materials* **2017**, *29*.

[110] D. S. Hecht, L. Hu, G. Irvin, *Advanced Materials* **2011**, *23*, 1482–1513.

[111] H. Hosseinzadeh Khaligh, K. Liew, Y. Han, N. M. Abukhdeir, I. A. Goldthorpe, *Solar Energy Materials and Solar Cells* **2015**, *132*, 337–341.

[112] L. Gomes, A. Branco, T. Moreira, F. Feliciano, C. Pinheiro, C. Costa, *Solar Energy Materials and Solar Cells* **2016**, *144*, 631–640.

[113] C. G. Granqvist, A. A. Hultaker, *Thin Solid Films* **2002**, *411*, 1–5.

[114] Groenendaal, L. B.:, Jonas, F., D. Freitag, *Advanced Materials* **2000**, *12*, 481–494.

[115] Y.-H. Ha, N. Nikolov, S. K. Pollack, J. Mastrangelo, B. D. Martin, R. Shashidhar, *Advanced Functional Materials* **2004**, *14*, 615–622.

[116] M. d. Keersmaecker, A. W. Lang, A. M. Österholm, J. R. Reynolds, *ACS Applied Materials and Interfaces* **2018**, *10*, 31568–31579.

[117] X. Guo, X. Liu, F. Lin, H. Li, Y. Fan, N. Zhang, *Scientific reports* **2015**, *5*, 10569.

[118] P. R. Somani, S. Radhakrishnan, *Materials Chemistry and Physics* **2002**, *77*, 117–133.

[119] S. K. Deb, *Solar Energy Materials and Solar Cells* **1992**, *25*, 327–338.

[120] S. K. Deb, *Solar Energy Materials and Solar Cells* **1995**, *39*, 191–201.

[121] W. Estrada, A. M. Andersson, C. G. Granqvist, *Journal of Applied Physics* **1988**, *64*, 3678–3683.

[122] C. G. Granqvist, *Electrochimica Acta* **1999**, *44*, 3005–3015.

[123] S. Passerini, B. Scrosati, A. Gorenstein, A. M. Andersson, C. G. Granqvist, *Journal of The Electrochemical Society* **1989**, *136*, 3394–3395.

[124] J. Svensson, C. G. Granqvist, *Applied Physics Letters* **1986**, *49*, 1566–1568.

[125] J. B. Goodenough, *Progress in Solid State Chemistry* **1971**, *5*, 145–399.

[126] C. G. Granqvist, *Solid State ionics* **1994**, *70-71*, 678–685.

[127] J. N. Behera, D. M. D'Alessandro, N. Soheilnia, J. R. Long, *Chemistry of Materials* **2009**, *21*, 1922–1926.

[128] M. Fan, S. Kao, T. Chang, R. Vittal, K. Ho, *Solar Energy Materials and Solar Cells* **2016**, *145*, 35–41.

[129] K. Itaya, T. Ataka, S. Toshima, *Journal of the American Chemical Society* **1982**, *104*, 4767–4772.

[130] T. Liao, W. Chen, H. Liao, L. Chen, *Solar Energy Materials and Solar Cells* **2016**, *145*, 26–34.

[131] V. D. Neff, *Journal of The Electrochemical Society* **1978**, *125*, 886–887.

[132] M. B. Robin, *Inorganic Chemistry* **1962**, *1*, 337–342.

[133] X. Shen, S. Wu, Y. Liu, K. Wang, Z. Xu, W. Liu, *Journal of colloid and interface science* **2009**, *329*, 188–195.

[134] C. L. Bird, A. T. Kuhn, *Chemical Society Reviews* **1981**, *10*, 49.

[135] R. G. Compton, A. M. Waller, P. M. S. Monk, D. R. Rosseinsky, *Journal of the Chemical Society Faraday Transactions* **1990**, *86*, 2583–2586.

[136] R. J. Jasinski, *Journal of The Electrochemical Society* **1977**, *124*, 637.

[137] F. Han, M. Higuchi, D. G. Kurth, *Journal of the American Chemical Society* **2008**, *130*, 2073–2081.

[138] B. Chen, S. Kao, C. Hu, M. Higuchi, K. Ho, Y. Liao, *ACS Applied Materials and Interfaces* **2015**, *7*, 25069–25076.

[139] F. S. Han, M. Higuchi, D. G. Kurth, *Advanced Materials* **2007**, *19*, 3928–3931.

[140] M. Higuchi, *Journal of Materials Chemistry C* **2014**, *2*, 9331–9341.

[141] M. D. Hossain, T. Sato, M. Higuchi, *Chemistry an Asian journal* **2013**, *8*, 76–79.

[142] L. Hsiao, T. Chang, H. Lu, Y. Wang, Y. Lu, K. Ho, M. Higuchi, *Journal of Materials Chemistry C* **2019**, *7*, 7554–7562.

[143] C. Hu, T. Sato, J. Zhang, S. Moriyama, M. Higuchi, *ACS Applied Materials and Interfaces* **2014**, *6*, 9118–9125.

[144] L. Niklaus, M. Schott, Mihelcic, M. Jerman, I. Posset, U. Sextl, G., *Solar Energy Materials and Solar Cells* **2019**, *200*, 110002.

[145] S. Pai, M. Moos, M. H. Schreck, C. Lambert, D. G. Kurth, *Inorganic Chemistry* **2017**, *56*, 1418–1432.

[146] S. Pai, M. Schott, L. Niklaus, U. Posset, D. G. Kurth, *Journal of Materials Chemistry C* **2018**, *6*, 3310–3321.

[147] A. Schiffrin, M. Capsoni, G. Farahi, C. Wang, C. Krull, M. Castelli, T. Roussy, K. A. Cochrane, Y. Yin, N. V. Medhekar, M. Fuhrer, A. Q. Shaw, W. Ji, S. A. Burke, *ACS nano* **2018**, *12*, 6545–6553.

[148] M. Schott, W. Szczerba, D. G. Kurth, *Langmuir* **2014**, *30*, 10721–10727.

[149] M. Schott, H. Lorrmann, W. Szczerba, M. Beck, D. G. Kurth, *Solar Energy Materials and Solar Cells* **0126**, *2014*, 68–73.

[150] M. Schott, W. Szczerba, U. Posset, A. S. Vuk, M. Beck, H. Riesemeier, A. F. Thünemann, D. G. Kurth, *Solar Energy Materials & Solar Cells* **2016**, *147*, 61–67.

[151] M. Schott, L. Niklaus, J. Clade, U. Posset, *Solar Energy Materials and Solar Cells* **2019**, *200*, 110001.

[152] W. Szczerba, M. Schott, H. Riesemeier, A. F. Thünemann, D. G. Kurth, *Physical Chemistry Chemical Physics* **2014**, *16*, 19694–19701.

[153] A. Winter, U. S. Schubert, *Chemical Society Reviews* **2016**, *45*, 5311–5357.

[154] P. Aguirre-Etcheverry, D. O'Hare, *Chemical reviews* **2010**, *110*, 4839–4864.

[155] V. Balzani, A. Juris, M. Venturi, S. Campagna, S. Serroni, *Chemical reviews* **1996**, *96*, 759–834.

[156] D. M. D'Alessandro, F. R. Keene, *Chemical Society Reviews* **2006**, *35*, 424–440.

[157] N. S. Hush, *Coordination Chemistry Reviews* **1985**, *64*, 135–157.

[158] W. Kaim, G. K. Lahiri, *Angewandte Chemie (International ed. in English)* **2007**, *46*, 1778–1796.

[159] W. Kaim, *Inorganic Chemistry* **2011**, *50*, 9752–9765.

[160] W. Kaim, *Coordination Chemistry Reviews* **2011**, *255*, 2503–2513.

[161] C. Yao, J. Yao, Y. Zhong, *Inorganic Chemistry* **2011**, *50*, 6847–6849.

[162] P. M. Beaujuge, S. Ellinger, J. R. Reynolds, *Nature materials* **2008**, *7*, 795–799.

[163] A. M. Österholm, D. E. Shen, J. A. Kerszulis, R. H. Bulloch, M. Kuepfert, A. L. Dyer, J. R. Reynolds, *ACS Applied Polymer Materials and Interfaces* **2015**, *7*, 1413–1421.

[164] A. M. Österholm, D. E. Shen, D. S. Gottfried, J. R. Reynolds, *Advanced Materials Technologies* **2016**, *1*, 1600063.

[165] S. Duluard, B. Ouvrard, A. Celik-Cochet, G. Campet, U. Posset, G. Schottner, M.-H. Delville, *The Journal of Physical Chemistry B* **2010**, *114*, 7445–7451.

[166] S. Duluard, A. Celik-Cochet, I. Saadeddin, A. Labouret, G. Campet, G. Schottner, U. Posset, M.-H. Delville, *New Journal of Chemistry* **2011**, *35*, 2314.

[167] P. M. Beaujuge, J. R. Reynolds, *Chemical reviews* **2010**, *110*, 268–320.

[168] J. L. Brédas, G. B. Street, B. Thémans, J. M. André, *The Journal of Chemical Physics* **1985**, *83*, 1323–1329.

[169] J. L. Brédas, *The Journal of Chemical Physics* **1985**, *82*, 3808–3811.

[170] C. K. Chiang, C. R. Fincher, Y. W. Park, A. J. Heeger, H. Shirakawa, E. J. Louis, S. C. Gau, A. G. MacDiarmid, *Physical Review Letters* **1977**, *39*, 1098–1101.

[171] M. Sassi, M. M. Salamone, R. Ruffo, G. E. Patriarca, C. M. Mari, G. A. Pagani, U. Posset, L. Beverina, *Advanced Functional Materials* **2016**, *26*, 5240–5246.

[172] A. J. Heeger, *Reviews of Modern Physics* **2001**, *73*, 681–700.

[173] H. Shirakawa, *Reviews of Modern Physics* **2001**, *73*, 713–718.

[174] A. G. MacDiarmid, *Reviews of Modern Physics* **2001**, *73*, 701–712.

[175] A. Elschner, S. Kirchmeyer, W. Lövenich, U. Merker, K. Reuter, *PEDOT: Principles and Applications of an Intrinsically Conductive Polymer*, CRC Press, Boca Raton, **2011**.

[176] G. Inzelt, *Journal of Solid State Electrochemistry* **2017**, *21*, 1965–1975.

[177] S. Kirchmeyer, K. Reuter, *Journal of Materials Chemistry* **2005**, *15*, 2077.

[178] R. Hoffmann, *Angewandte Chemie International Edition* **1987**, *26*, 846–878.

[179] H. S. Nalwa, *Handbook of Organic Conductive Molecules and Polymers*, Wiley, Chichester, UK, **1997**.

[180] R. Gross, A. Marx, *Festkörperphysik*, de Gruyter, Oldenburg, **2012**.

[181] S. Macher, Masterarbeit, Julius-Maximilians-Universität, Würzburg, **2017**.

[182] Reynolds, J. R., Thompson, B. C., T. A. Skotheim, *Handbook of Conducting Polymers*, CRC Press, Boca Raton, USA, **2019**.

[183] M. Rehahn, *Chemie in unserer Zeit* **2003**, *37*, 18–30.

[184] P. W. Atkins, J. d. Paula, *Physikalische Chemie*, Wiley-VCH, Weinheim, **2006**.

[185] I. Zozoulenko, A. Singh, S. K. Singh, V. Gueskine, X. Crispin, M. Berggren, *ACS Applied Polymer Materials* **2019**, *1*, 83–94.

[186] W. J. Feast, J. Tsibouklis, K. L. Pouwer, L. Groenendaal, E. W. Meijer, *Polymer* **1996**, *37*, 5017–5047.

[187] J. Roncali, *Chemical reviews* **1997**, *97*, 173–206.

[188] J. Roncali, *Chemical reviews* **1992**, *92*, 711–738.

[189] D. M. de Leeuw, M. M. J. Simenon, A. R. Brown, R. E. F. Einerhand, *Synthetic Metals* **1997**, *87*, 53–59.

[190] T. Yasuda, Y. Sakai, S. Aramaki, T. Yamamoto, *Chemistry of Materials* **2005**, *17*, 6060–6068.

[191] P. Audebert, S. Sadki, F. Miomandre, G. Clavier, *Electrochemistry Communications* **2004**, *6*, 144–147.

[192] U. Salzner, *The Journal of Physical Chemistry B* **2002**, *106*, 9214–9220.

[193] U. Salzner, M. E. Köse, *The Journal of Physical Chemistry B* **2002**, *106*, 9221–9226.

[194] S. Ellinger, K. R. Graham, P. Shi, R. T. Farley, T. T. Steckler, R. N. Brookins, P. Taranekar, J. Mei, L. A. Padilha, T. R. Ensley, H. Hu, S. Webster, D. J. Hagan, E. W. van Stryland, K. S. Schanze, J. R. Reynolds, *Chemistry of Materials* **2011**, *23*, 3805–3817.

[195] C. M. Amb, A. L. Dyer, J. R. Reynolds, *Chemistry of Materials* **2011**, *23*, 397–415.

[196] J. A. Kerszulis, C. M. Amb, A. L. Dyer, J. R. Reynolds, *Macromolecules* **2014**, *47*, 5462–5469.

[197] J. A. Kerszulis, K. E. Johnson, M. Kuepfert, D. Khoshabo, A. L. Dyer, J. R. Reynolds, *Journal of Physical Chemistry B* **2015**, *3*, 3211–3218.

[198] A. Kumar, D. M. Welsh, M. C. Morvant, F. Piroux, K. A. Abboud, J. R. Reynolds, *Chemistry of Materials* **1998**, *10*, 896–902.

[199] R. M. Walczak, J. R. Reynolds, *Advanced Materials* **2006**, *18*, 1121–1131.

[200] C. L. Gaupp, K. Zong, P. Schottland, B. C. Thompson, C. A. Thomas, J. R. Reynolds, *Macromolecules* **2000**, *33*, 1132–1133.

[201] P. Schottland, K. Zong, C. L. Gaupp, B. C. Thompson, C. A. Thomas, I. Giurgiu, R. Hickman, K. A. Abboud, J. R. Reynolds, *Macromolecules* **2000**, *33*, 7051–7061.

[202] C. A. Thomas, K. Zong, P. Schottland, J. R. Reynolds, *Advanced Materials* **2000**, *12*, 222–225.

[203] C. Arbizzani, A. Bongini, M. Mastragostino, A. Zanelli, G. Barbarella, M. Zambianchi, *Advanced Materials* **1995**, *7*, 571–574.

[204] M.-N. Collomb-Dunand-Sauthier, S. Langlois, E. Genies, *Journal of Applied Electrochemistry* **1994**, *24*.

[205] I. Osaka, R. D. McCullough, *Accounts of Chemical Research* **2008**, *41*, 1202–1214.

[206] M. L. Blohm, J. E. Pickett, P. C. van Dort, *Macromolecules* **1993**, *26*, 2704–2710.

[207] M. Martinez, J. R. Reynolds, S. Basak, D. A. Black, D. S. Marynick, M. Pomerantz, *Journal of Polymer Science Part B: Polymer Physics* **1988**, *26*, 911–920.

[208] M. Sassi, M. M. Salamone, R. Ruffo, C. M. Mari, G. A. Pagani, L. Beverina, *Advanced Materials* **2012**, *24*, 2004–2008.

[209] F. C. Krebs, *Nature materials* **2008**, *7*, 766–767.

[210] S. Hassab, D. E. Shen, A. M. Österholm, M. Da Rocha, G. Song, Y. Alesanco, A. Vinuales, A. Rougier, J. R. Reynolds, J. Padilla, *Solar Energy Materials and Solar Cells* **2018**, *185*, 54–60.

[211] C. L. Gaupp, D. M. Welsh, J. R. Reynolds, *Macromolecular Rapid Communications* **2002**, *23*, 885–889.

[212] R. M. Walczak, J. S. Cowart, J. R. Reynolds, *Journal of Materials Chemistry* **2007**, *17*, 254–260.

[213] G. Gunbas, L. Toppare, *Chemical Communication* **2012**, *48*, 1083–1101.

[214] S. Miyanishi, K. Tajima, K. Hashimoto, *Macromolecules* **2009**, *42*, 1610–1618.

[215] D. Bagnis, L. Beverina, H. Huang, F. Silvestri, Y. Yao, H. Yan, G. A. Pagani, T. J. Marks, A. Facchetti, *Journal of the American Chemical Society* **2010**, *132*, 4074–4075.

[216] H. J. Buser, D. Schwarzenbach, W. Petter, A. Ludi, *Inorganic Chemistry* **1977**, *16*, 2704–2710.

[217] M. J. Piernas Muñoz, E. Castillo Martínez, *Prussian Blue Based Batteries*, Springer International Publishing, Cham, **2018**.

[218] A. Paolella, C. Faure, V. Timoshevskii, S. Marras, G. Bertoni, A. Guerfi, A. Vijh, M. Armand, K. Zaghib, *Journal of Materials Chemistry A* **2017**, *5*, 18919–18932.

[219] X. Wu, M. Shao, C. Wu, J. Qian, Y. Cao, X. Ai, H. Yang, *ACS Applied Polymer Materials and Interfaces* **2016**, *8*, 23706–23712.

[220] M. Wozar, Masterarbeit, Julius-Maximilians-Universität, Würzburg, **2019**.

[221] M. Schott, Diplomarbeit, Julius-Maximilians-Universität, Würzburg, **2010**.

[222] K. Itaya, I. Uchida, *Inorganic Chemistry* **1986**, *25*, 389–392.

[223] T. Dumas, D. Guillaumont, P. Moisy, D. K. Shuh, T. Tyliszczak, P. L. Solari, C. Den Auwer, *Chemical Communication* **2018**, *54*, 12206–12209.

[224] F. S. Hegner, J. R. Galán-Mascarós, N. López, *Inorganic Chemistry* **2016**, *55*, 12851–12862.

[225] K. Nassau, *The Physics and Chemistry of Color: The Fifteen Causes of Color*, Wiley, New York, **2001**.

[226] F. Grandjean, L. Samain, G. J. Long, *Dalton transactions* **2016**, *45*, 18018–18044.

[227] R. J. Mortimer, D. R. Rosseinsky, *Dalton transactions* **1984**, 2059.

[228] R. Huggins, *Energy Storage: Fundamentals, Materials and Applications*, Springer International Publishing, Cham, **2016**.

[229] A. Roig, J. Navarro, J. J. Garcia, F. Vicente, *Electrochimica Acta* **1994**, *39*, 437–442.

[230] A. Viehbeck, *Journal of The Electrochemical Society* **1985**, *132*, 1369.

[231] DIN EN 410:2011-04, Glas im Bauwesen: Bestimmung der lichttechnischen und strahlungsphysikalischen Kenngrößen von Verglasungen.

[232] M. Richter, *Einführung in die Farbmetrik*, de Gruyter, Berlin, **1976**.

[233] DIN 52347:1987-12, Prüfung von Glas und Kunststoffen; Verschleißprüfung; Reibradverfahren mit Streulichtmessung.

[234] H. J. Byker, Brief History of Electrochromics, DecoChrom Open Conference: Bringing Electrochromics to New Markets and Products, Lisbon, **25.06.2019**.

[235] K. C. Ho, T. G. Rukavina, C. B. Greenberg, *Journal of The Electrochemical Society* **1994**, *141*, 2061.

[236] T.-S. Tung, K.-C. Ho, *Solar Energy Materials and Solar Cells* **2006**, *90*, 521–537.

[237] P. C. Barbosa, L. C. Rodrigues, M. M. Silva, M. J. Smith, A. J. Parola, F. Pina, C. Pinheiro, *Electrochimica Acta*, *55*, 1495–1502.

[238] S. Macher, M. Schott, M. Dontigny, A. Guerfi, K. Zaghib, U. Posset, P. Löbmann, *Advanced Materials Technologies* **2021**, *6*, 2000836.

[239] F. M. Miachalak, J. R. Owen, *Solid State ionics* **1996**, *86-88*, 965–970.

[240] V. S. Bagotzky, A. M. Skundin, *Chemical Power Sources*, Academic Press, New York, London, **1980**.

[241] P. Arora, R. E. White, *Journal of The Electrochemical Society* **1998**, *145*, 3647–3668.

[242] D. E. Stilwell, K. H. Park, M. H. Miles, *Journal of Applied Electrochemistry* **19325-33192**, *22*.

[243] G. V. Zhuang, H. Yang, B. Blizanac, P. N. Ross, JR., *Electrochemical and Solid State Letters* **2005**, *8*, A441–A445.

[244] X. Xing, C. Wang, X. Liu, L. Qin, E. Wang, F. Zhang, *Electrochimica Acta* **2017**, *253*, 530–535.

[245] R.-T. Wen, M. A. Arvizu, G. A. Niklasson, C. G. Granqvist, *Surface and Coatings Technology* **2015**, *278*, 121–125.

[246] R. H. Bulloch, J. R. Reynolds, *Journal of Materials Chemistry C* **2016**, *4*, 603–610.

[247] J. Jensen, M. V. Madsen, F. C. Krebs, *The Journal of Physical Chemistry C* **2013**, *1*, 4826.

[248] M. Day, D. M. Wiles, *Journal of Applied Polymer Science* **1972**, *16*, 203–215.

[249] P. Gijsman, G. Meijers, G. Vitarelli, *Polymer Degradation and Stability* **1999**, *65*, 433–441.

[250] S. Holdcroft, *Macromolecules* **1991**, *24*, 4834–4838.

[251] M. S. A. Abdou, S. Holdcroft, *Macromolecules* **1993**, *26*, 2954–2962.

[252] M. S. A. Abdou, G. A. Diaz-Guijada, M. I. Arroyo, S. Holdcroft, *Chemistry of Materials* **1991**, *3*, 1003–1006.

[253] H. Hintz, H.-J. Egelhaaf, L. Lüer, J. Hauch, H. Peisert, T. Chassé, *Chemistry of Materials* **2011**, *23*, 145–154.

[254] M. Koch, R. Nicolaescu, P. V. Kamat, *The Journal of Physical Chemistry C* **2009**, *113*, 11507–11513.

[255] M. Manceau, A. Rivaton, J. Gardette, *Macromolecular Rapid Communications* **2008**, *29*, 1823–1827.

[256] M. Manceau, A. Rivaton, J. Gardette, S. Guillerez, N. Lemaître, *Polymer Degradation and Stability* **2009**, *94*, 898–907.

[257] H. Hintz, H.-J. Egelhaaf, H. Peisert, T. Chassé, *Polymer Degradation and Stability* **2010**, *95*, 818–825.

[258] M. V. Madsen, T. Tromholt, A. Böttiger, J. W. Andreasen, K. Norrman, F. C. Krebs, *Polymer Degradation and Stability* **2012**, *97*, 2412–2417.

[259] G. Barbarella, M. Zambianchi, A. Bongini, L. Antolini, *Advanced Materials* **1993**, *5*, 834–839.

[260] M. Manceau, E. Bundgaard, J. E. Carlé, O. Hagemann, M. Helgesen, R. Søndergaard, M. Jørgensen, F. C. Krebs, *Journal of Materials Chemistry* **2011**, *21*, 4132.

[261] M. Metger, B. Strehle, S. Solchenbach, H. A. Gasteiger, *Journal of The Electrochemical Society* **2016**, *163*, A798–A809.

[262] C. Yang, J. Chen, T. Qing, X. Fan, W. Sun, A. v. Cresce, M. S. Ding, O. Borodin, J. Vatamanu, M. A. Schroeder, N. Eidson, C. Wang, K. Xu, *Joule* **2017**, *1*, 122–132.

[263] H. Kim, J. Hong, K. Park, H. Kim, S. Kim, K. Kang, *Chemical reviews* **2014**, *114*, 11788–11827.

[264] Q. Yang, W. Wang, H. Li, J. Zhang, F. Kang, B. Li, *Electrochimica Acta* **2018**, *270*, 96–103.

[265] S. Han, *Scientific reports* **2019**, *9*, 5555–5565.

[266] S. Koneshan, J. C. Rasaiah, R. M. Lynden-Bell, S. H. Lee, *The Journal of Physical Chemistry B* **1998**, *102*, 4193–4204.

[267] S. H. Lee, J. C. Rasaiah, *The Journal of Chemical Physics* **1994**, *101*, 6964–6974.

[268] S. H. Lee, J. C. Rasaiah, *The Journal of Physical Chemistry* **1996**, *100*, 1420–1425.

[269] W. Rudolph, M. H. Brooker, C. C. Pye, *The Journal of Physical Chemistry* **1995**, *99*, 3793–3797.

[270] *Hydrolysis of Metal Ions*, (Eds.: P. L. Brown, C. Ekberg), Wiley-VCH, Weinheim, **2016**.

[271] H. H. Loeffler, B. M. Rode, *The Journal of Chemical Physics* **2002**, *117*, 110–117.

[272] J. R. Newsome, G. W. Neilson, J. E. Enderby, *Journal of Physics C: Solid State Physics* **1980**, *13*, L923–L926.

[273] N. Yoshinari, S. Yamashita, Y. Fukuda, Y. Nakazawa, T. Konno, *Chemical science* **2019**, *10*, 587–593.

[274] Y. Li, Y. Lu, P. Adelhelm, M. Titirici, Y. Hu, *Chemical Society Reviews* **2019**, *48*, 4655–4687.

[275] R. W. Impey, P. A. Madden, I. R. McDonald, *The Journal of Physical Chemistry* **1983**, *87*, 5071–5083.

[276] K. P. Jensen, W. L. Jorgensen, *Journal of chemical theory and computation* **2006**, *2*, 1499–1509.

[277] J. Mähler, I. Persson, *Inorganic Chemistry* **2012**, *51*, 425–438.

[278] J. He, L. You, J. Mei, *ACS Applied Materials and Interfaces* **2017**, *9*, 34122–34130.

[279] S. Macher, M. Rumpel, M. Schott, U. Posset, G. A. Giffin, P. Löbmann, *ACS Applied Materials and Interfaces* **2020**, *12*, 36695–36705.

[280] S. Macher, M. Sassi, L. Beverina, U. Posset, M. Schott, G. A. Giffin, P. Löbmann, *ChemElectroChem* **2021**.

[281] R. Ruffo, A. Celik-Cochet, U. Posset, C. M. Mari, G. Schottner, *Solar Energy Materials and Solar Cells* **2008**, *92*, 140–145.

[282] L. Groenendaal, G. Zotti, P.-H. Aubert, S. M. Waybright, J. R. Reynolds, *Advanced Materials* **2003**, *15*, 855–879.

[283] A. Kraft, M. Rottmann, K.-H. Heckner, *Solar Energy Materials and Solar Cells* **2006**, *90*, 469–476.

[284] D. E. Shen, A. M. Österholm, J. R. Reynolds, *Journal of Materials Chemistry C* **2015**, *3*, 9715–9725.

[285] H. W. Heuer, R. Wehrmann, S. Kirchmeyer, *Advanced Functional Materials* **2002**, *12*, 89–94.

[286] D. R. Rosseinsky, L. Glasser, H. D. Brooke Jenkins, *Journal of the American Chemical Society* **2004**, *126*, 10472–10477.

[287] M. J. Piernas Munoz, E. Castillo Martínez, *Prussian Blue Based Batteries*, Springer Nature, Cham, Switzerland, **2018**.

[288] K. Jüttner, W. J. Lorenz, *Materials Science Forum* **1989**, *44-45*, 191–204.

[289] A. Zeng, E. Liu, I. F. Annergren, S. N. Tan, S. Zhang, P. Hing, J. Gao, *Diamond and Related Materials* **2002**, *11*, 160–168.

[290] J. C. Wojdel, I. d. P. R. Moreira, S. T. Bromley, F. Illas, *Journal of Materials Chemistry* **2009**, *19*, 2032–2036.

[291] J. Agrisuelas, J. J. García-Jareno, D. Gimenez-Romero, F. Vicente, *The Journal of Physical Chemistry C* **2009**, *113*, 8438–8446.

[292] L. Beverina, G. A. Pagani, M. Sassi, *Chemical Communication* **2014**, *50*, 5413–5430.

[293] A. Kraft, H. Henning, A. Herbst, K.-H. Heckner, *Journal of Electroanalytical Chemistry* **1994**, *365*, 191–196.

[294] C. C. Plá Cid, E. R. Spada, M. L. Sartorelli, *Applied Surface Science* **2013**, *273*, 603–606.

[295] G. Folcher, H. Cachet, M. Froment, J. Bruneaux, *Thin Solid Films* **1997**, *301*, 242–248.

[296] J. E. A. M. van den Meerakker, W. R. ter Veen, *Journal of The Electrochemical Society* **1992**, *139*, 385–390.

[297] L. Liu, S. Yellinek, I. Valdinger, A. Donval, D. Mandler, *Electrochimica Acta* **2015**, *176*, 1374–1381.

[298] E. Matveeva, *Journal of The Electrochemical Society* **2005**, *152*, H138–H145.

[299] T. S. Bejitual, K. Ramji, A. J. Kessman, K. A. Sierros, D. R. Cairns, *Materials Chemistry and Physics* **2012**, *132*, 395–401.

[300] W. S. Leung, Y. C. Chan, S. M. Lui, *Microelectronic Engineering* **2013**, *101*, 1–7.

[301] Y.-N. Kim, S.-M. Jeong, M.-S. Jeon, H.-G. Shin, J.-K. Song, H.-S. Lee, *Journal of Electroceramics* **2006**, *17*, 955–958.

[302] J.-H. Lan, J. Kanicki, *Thin Solid Films* **1997**, *304*, 123–129.

[303] S. Gardonio, L. Gregoratti, D. Scaini, C. Castellarin-Cudia, P. Dudin, P. Melpignano, V. Biondo, R. Zamboni, S. Caria, M. Kiskinova, *Organic Electronics* **2008**, *9*, 253–261.

[304] E. R. Spada, F. R. de Paula, C. C. Plá Cid, G. Candiotto, R. M. Faria, M. L. Sartorelli, *Electrochimica Acta* **2013**, *108*, 520–524.

[305] N. Nadaud, N. Lequeux, M. Nanot, J. Jové, T. Roisnel, *Journal of Solid State Chemistry* **1998**, *135*, 140–148.

[306] J. Ahmad, K. Bazaka, L. J. Anderson, R. D. White, M. V. Jacob, *Renewable and Sustainable Energy Reviews* **2013**, *27*, 104–117.

[307] S. Lee, J.-H. Han, S.-H. Lee, G.-H. Baek, J.-S. Park, *The Journal of The Minerals Metals and Materials Society* **2018**, *71*, 197–211.

[308] D. Yu, Y.-Q. Yang, Z. Chen, Y. Tao, Y.-F. Liu, *Optics Communications* **2016**, *362*.

[309] W. T. Neo, Q. Ye, S.-J. Chua, J. Xu, *Journal of Materials Chemistry C* **2016**, *4*, 7364–7376.

[310] K. E. Aasmundtveit, E. J. Samuelsen, L. A. A. Pettersson, O. Inganäs, T. Johansson, R. Feidenhans'l, *Synthetic Metals* **1999**, *101*, 561–564.

[311] L. A. A. Pettersson, F. Carlsson, O. Inganäs, H. Arwin, *Thin Solid Films* **1998**, *313-314*, 356–361.

[312] L. A. A. Pettersson, T. Johansson, F. Carlsson, H. Arwin, O. Inganäs, *Synthetic Metals* **1999**, *101*, 198–199.

[313] D. M. de Leeuw, E. J. Lous, *Synthetic Metals* **1994**, *65*, 45–53.

[314] T. Johansson, L. A. A. Pettersson, O. Inganäs, *Synthetic Metals* **2002**, *129*, 269–274.

[315] S. Garreau, G. Louam, S. Lefrant, J. P. Buisson, G. Froyer, *Synthetic Metals* **1999**, *101*, 312–313.

[316] C. A. T. Laia, P. López-Cornejo, S. M. B. Costa, J. d'Oliveira, J. M. G. Martinho, *Langmuir* **1998**, *14*, 3531–3537.

Acknowledgement

First and foremost I want to thank Prof. Dr. Peer Löbmann for the scientific supervision of this Ph.D. work. I appreciate all his contributions of time, ideas and support to make my Ph.D. project successful. The numerous discussions on a scientific and personal level will always be remembered as an enriching and pleasing exchange. I am also thankful for the excellent example he has provided as a sincere scientist and professor.

For this dissertation I would like to thank my reviewers Prof. Dr. Peer Löbmann and Prof. Dr. Christoph Lambert for their time and interest in my research.

My full and special thanks go to Dr. Uwe Posset and Dr. Marco Schott for the willingness to take over the technical supervision of my Ph.D. work. I appreciate all their differentiated comments and expedient discussions, which have given me a critical access to my Ph.D. project. The enthusiasm they both have for their research was contagious and motivational for me, even during tough times in my Ph.D pursuit.

The members of the *Fraunhofer Research and Development Center for Electromobility* have contributed immensely to my personal and professional time during my Ph.D. work. The group has been a source of friendship, valuable advice and collaboration. I am especially grateful to Christine Müller, Annalena Götz, Vilija Anfimovaite, Ajana Gebel and Hendrik Bohn for all the active support in the laboratory. To Lukas Niklaus and all the other anonymous electrochemists for their support and constant willingness to discuss the electrochemical measurements. To Elena Fleder, Werner Stracke and Manfred Römer for the numerous SEM images and to Matthias Rumpel for the thin film XRD measurements.

I would also like to thank my students Moritz Wozar, Hendrik Bohn and Tim Schembri, who contributed to my Ph.D. as a part of their master thesis and internships, for their work and support.

My specials thanks go to Prof. Dr. Luca Beverina, Dr. Mauro Sassi and all other colleagues at the *University of Milano-Bicocca* for the great support and cooperation with regard to the sidechain-modified PEDOT derivatives on which this Ph.D. work is based on. I further thank Dr. Abdelbast Guerfi and colleagues of *Hydro-Québec's Research Institute (IREQ)* for supplying the polymer electrolyte used in this Ph.D. project as well as Dr. Lubomír Kubáč and *Center for Organic Chemistry (COC)* for supplying the precursor materials used in this work.

I gratefully acknowledge the funding sources that made my Ph.D. project possible. I was funded by the European Union's Horizon 2020 Research and Innovation Program under grant agreement no. 760973 (DecoChrom) and the Bavarian State Ministry of Econonmic Affairs and Media, Energy and Technology (Fraunhofer Research and Developement Center for Electromobility). I further thank Prof. Dr. Gerhard Sextl and Dr. Henning Lorrmann for enabling my Ph.D. at the *Fraunhofer Institute for Silicate Research ISC* and the *Fraunhofer Research and Development Center for Electromobility* in Würzburg.

Lastly, I would like to thank my family and friends for all their emotional support and encouragement. For Tim Sauermann who was a great support in designing the 3D figures. For Myles Rooney who took over the proofreading as a scientist and native speaker. For my parents who supported me in all my pursuits, especially for making my studies and the subsequent Ph.D. possible. And for my loving, supportive, encouraging, cheering and patient wife Katharina whose faithful support during the final stages of this Ph.D. is so appreciated.

Würzburg, March 12, 2021 Sven Macher

Appendixes

- Publications
- Individual Contribution to Articles
- Sebstständikeitserklärung

Publications

Articles

1. Macher, S., Schott, M., Sassi, M., Facchinetti, I., Ruffo, R., Patriarca, G., Beverina, L., Posset, U., Giffin, G. A., Löbmann, P., New Roll-to-Roll Processable PEDOT-Based Polymer with Colorless Bleached State for Flexible Electrochromic Devices, *Advanced Functional Materials* **2020**, 30, 1906254,

2. Macher, S., Schott, M., Dontigny, M., Guerfi, A., Zaghib, K., Posset, U., Löbmann, P., Large-Area Complementary Switching Electrochromic Devices on Flexible Polymer Substrates with High Optical Contrast and Enhanced Cycling Stability, *Advanced Materials Technologies* **2021**, 6, 2000836,

3. Macher, S., Rumpel, M., Schott, M., Posset, U., Giffin, G. A., Löbmann, P., Avoiding Voltage-Induced Degradation in PET-ITO-Based Flexible Electrochromic Devices, *ACS Applied Materials & Interfaces* **2020**, 12, 32, 36695-36705,

4. Macher, S., Sassi, M., Beverina, L., Posset, U., Schott, M., Giffin, G. A., Löbmann, P., Electrochromic Polymer Ink Derived from a Sidechain Modified EDOT for Electrochromic Devices with Colorless Bright State, *ChemElectroChem* **2021**, 8, 726-734.

Patents

1. Macher, S., Posset, U., Beverina, L., Sassi, M., Schott, M., Colloidal Coating Dispersion, **2020**, European Patent, EP3654094 A1,

2. Macher, S., Posset, U., Beverina, L., Sassi, M., Schott, M., Colloidal Coating Dispersion, **2020**, US Patent, US2020/0157418 A1.

Conferences

1. Macher, S., Farbveränderliche Oberflächen im Innenarchitekturbereich, *SMART MATERIALS Symposium*, **2017**, Bünde, Deutschland, *oral presentation*,

2. Macher, S., Schott, M., Sassi, M., Ruffo, R., Facchinetti, I., Patriarca, G., Beverina, L., Posset, U., Löbmann, P., Roll-to-Roll Processed PEDOT-Based Polymer for Flexible Electrochromic Devices, 14^{th} *International Symposium on Functional π-Electron Systems*, **2019**, Berlin, Deutschland, *poster presentation*,

3. Macher, S., Posset, U., Sassi, M., Beverina, L., Kubáč, L., Schott, M., Löbmann, P., Nanoscale Polymer Dispersions Derived from Substituted 3,4-Ethylene Dioxythiophene (EDOT) Derivatives for Flexible Electrochromic Devices, *Particle Based Materials Symposium*, **2019**, Ulm, Deutschland, *poster presentation*,

4. Macher, S., R2R Coating of Electrochromic Polymer Thin Films, 18^{th} *International Coating Symposium*, **2019**, Dormagen, Deutschland, *oral presentation*,

5. Macher, S., Long-term Performance and Durability of Electrochromic Glazing, *Energy Efficient Technologies for Building Envelopes Symposium*, **2020**, Dresden, Deutschland, *oral presentation*,

6. Macher, S., Schott, M., Sassi, M., Ruffo, R., Beverina, L., Posset, U., Löbmann, P., New Roll-to-Roll Processable PEDOT-Based Polymer with Colorless Bleached State for Flexible Electrochromic Devices, *The* 14^{th} *International Meeting on Electrochromism (IME-14)*, **2020**, Atlanta, Georgia, USA, *oral presentation and travel-award* - postponed indefinitely due to COVID19 pandemic.

Personal Contribution to Articles

The present "cumulative dissertation" is a shortened version of the obtained results and is based on the following publications. The individual contribution of each co-author for each publication is shown below and in the following forms.

- Macher, S., Schott, M., Sassi, M., Facchinetti, I., Ruffo, R., Patriarca, G., Beverina, L., Posset, U., Giffin, G. A., Löbmann, P., New Roll-to-Roll Processable PEDOT-Based Polymer with Colorless Bleached State for Flexible Electrochromic Devices, *Advanced Functional Materials* **2020**, 30, 1906254.

  All presented work on the characterization of the PEDOT-EthC6 derivative (main part) as well as the assembly and characterization of the proof-of-concept ECD was carried out by S. Macher. The synthesis, electropolymerization and characterization of the sidechain-modified EDOT derivatives was performed by Dr. M. Sassi, I. Facchinetti, Dr. R. Ruffo, G. Patriarca and Prof. Dr. L. Beverina. The *in-situ* polymerization process was developed and performed by Dr. U. Posset, Dr. M. Schott and S. Macher. The composition and coordination of this publication was carried out by S. Macher. Dr. G. A. Giffin and Prof. Dr. P. Löbmann carried out correction work and linguistic proof reading.

- Macher, S., Schott, M., Dontigny, M., Guerfi, A., Zaghib, K., Posset, U., Löbmann, P., Large-area Electrochromic Devices on Flexible Polymer Substrates with High Optical Contrast and Enhanced Cycling Stability, *Advanced Materials Technologies* **2021**, 6, 2000836.

  All presented work on the characterization of the PEDOT-EthC6/PB devices (main part) as well as the assembly of the laborartory-size ECD was carried out by S. Macher. The developement of the HQ674 solid polymer electrolyte was performed by M. Dontigny, Dr. A. Guerfi and Dr. K. Zaghib. The S2S and R2R lamination processes for ECD assembly was developed and optimized by M. Dontigny, Dr. M. Schott, Dr. U. Posset and S. Macher. The composition and coordination of this publication was carried out by Prof. Dr. P. Löbmann and S. Macher. Dr. U. Posset carried out correction work and linguistic proof reading.

- Macher, S., Rumpel, M., Schott, M., Posset, U., Giffin, G. A., Löbmann, P., Avoiding Voltage-Induced Degradation in PET-ITO-Based Flexible Electrochromic Devices, *ACS Applied Materials & Interfaces* **2020**, 12, 32, 36695-36705.

  All presented work on the assembly as well as the optical and (spectro-)electrochemical characterization of the PEDOT-EthC6 based ECDs was carried out by S. Macher. The XRD measurements were performed by M. Rumpel. The composition and coordination of this publication was carried out by S. Macher. Dr. M. Schott, Dr. U. Posset and Prof. Dr. P. Löbmann carried out correction work. Dr. G. A. Giffin was responsible for the linguistic proof reading.

- Macher, S., Sassi, M., Beverina, L., Posset, U., Schott, M., Giffin, G. A., Löbmann, P., Electrochromic Polymer Ink Derived from a Sidechain Modified EDOT for Electrochromic Devices with Colorless Bright State, *ChemElectroChem* **2021**, 8, 726-734.

  All presented work on the characterization of the PEDOT-EthC6-based coating dispersion (main part) was carried out by S. Macher. Dr. U. Posset, Dr. M. Sassi and Prof. Dr. L. Beverina also contributed to the development of the synthesis of the PEDOT-EthC6-based coating dispersion with their numerous ideas and advice. The composition and coordination of this publication was carried out by S. Macher. Dr. M. Schott, Dr. G. A. Giffin and Prof. Dr. P. Löbmann carried out correction work and linguistic proof reading.

- Macher, S., Posset, U., Beverina, L., Sassi, M., Schott, M., Colloidal Coating Dispersion, **2020**, European Patent, EP3654094 A1.

  S. Macher (30%), U. Posset (15%), M. Schott (5%), L. Beverina (25%), and M. Sassi (25%) contributed to the invention (shares according to invention). The patent application was essentially written by S. Macher and U. Posset.

Julius-Maximilians-
UNIVERSITÄT
WÜRZBURG

Fakultät für
CHEMIE UND
PHARMAZIE

Erklärung zur Autorenschaft

New Roll-to-Roll Processable PEDOT-Based Polymer with Colorless Bleached State for Flexible Electrochromic Devices, Sven Macher, Marco Schott, Mauro Sassi, Irene Facchinetti, Riccardo Ruffo, Giorgio Patriarca, Luca Beverina, Uwe Posset, Guinevere A. Giffin, Peer Löbmann, Advanced Functional Materials, 2020, 30, 1906254

Detaillierte Darstellung der Anteile an der Veröffentlichung (in %)
Angabe Autoren/innen (ggf. Haupt- / Ko- / korrespondierende/r Autor/in) mit Vorname Nachname (Initialen)

Sven Macher, Hauptautor (SM), Marco Schott, korrespondierender Autor (MSch), Mauro Sassi (MSas), Irene Facchinetti (IF), Riccardo Ruffo (RR), Giorgio Patriarca (GP), Luca Beverina (LB), Uwe Posset (UP), Guinevere A. Giffin (GG), Peer Löbmann (PL)

Autor	SM	MSch	MSas	IF	RR	GP	LB	UP	GG	PL		∑ in Prozent
Entwicklung/Synthese Monomere			3%				7%					10%
Charakterisierung Polymere (Labor)			5%	2%	5%	2%	1%					15%
Entwicklung Beschichtung (Technikum)		5%						10%				15%
Charakterisierung Beschichtung (Technikum)	12%	5%						3%				20%
Assemblierung ECD	3%	2%										5%
Charakterisierung ECD	5%											5%
Verfassen der Veröffentlichung	15%	3%					2%					20%
Korrektur der Veröffentlichung									4%	4%		8%
Koordination der Veröffentlichung	2%											2%
Summe	**37%**	**15%**	**8%**	**2%**	**5%**	**2%**	**10%**	**13%**	**4%**	**4%**		**100%**

Erklärung zur Autorenschaft

Large-area Electrochromic Devices on Flexible Polymer Substrates with High Optical Contrast and Enhanced Cycling Stability, Sven Macher, Marco Schott, Martin Dontigny, Abdelbast Guerfi, Karim Zaghib, Uwe Posset, Peer Löbmann, Advanced Materials Technologies, 2020, XX, XXXXXXX.

Detaillierte Darstellung der Anteile an der Veröffentlichung (in %)
Angabe Autoren/innen (ggf. Haupt- / Ko- / korrespondierende/r Autor/in) mit Vorname Nachname (Initialen)

Sven Macher, Hauptautor (SM), Marco Schott, korrespondierender Autor (MSch), Martin Dontigny (MD), Abdelbast Guerfi (AG), Karim Zaghib (KZ), Uwe Posset (UP), Peer Löbmann (PL)

Autor	SM	MSch	MD	AG	KZ	UP	PL					∑ in Prozent
Elektrolyt-Entwicklung				6%	4%							10%
ECD-Assemblierung (Labor)	6%	8%	4%			7%						25%
ECD-Assemblierung (Technikum)		2%				3%						5%
ECD-Charakterisierung (optisch)	10%											10%
ECD-Charakterisierung (elektrochemisch)	10%											10%
ECD-Charakterisierung (Stabilität)	10%											10%
Verfassen der Veröffentlichung	12%						8%					20%
Korrektur der Veröffentlichung		4%				4%						8%
Koordination der Veröffentlichung	2%											2%
Summe	**50%**	**14%**	**4%**	**6%**	**4%**	**14%**	**8%**					**100%**

Julius-Maximilians-
UNIVERSITÄT
WÜRZBURG

Fakultät für
CHEMIE UND
PHARMAZIE

Erklärung zur Autorenschaft

Avoiding Voltage-Induced Degradation in PET-ITO-Based Flexible Electrochromic Devices, Sven Macher, Matthias Rumpel, Marco Schott, Uwe Posset, Guinevere A. Giffin, Peer Löbmann, ACS Applied Materials & Interfaces, 12, 32, 36695–36705.

Detaillierte Darstellung der Anteile an der Veröffentlichung (in %)
Angabe Autoren/innen (ggf. Haupt- / Ko- / korrespondierende/r Autor/in) mit Vorname Nachname (Initialen)

Sven Macher, Hauptautor (SM), Matthias Rumpel (MR), Marco Schott, korrespondierender Autor (MSch), Uwe Posset (UP), Guinevere A. Giffin (GG), Peer Löbmann (PL)

Autor	SM	MR	MSch	UP	GG	PL						∑ in Prozent
Systematische Alterung	10%											10%
Charakterisierung nach Alterung	15%	2%	3%									20%
ECD mit Referenzelektrode	8%			2%								10%
Optimierung ECD	5%		3%	2%								10%
Systematische Alterung optimiertes ECD	10%											10%
Charakterisierung nach Alterung opt. ECD	8%	2%										10%
Verfassen der Veröffentlichung	20%											20%
Korrektur der Veröffentlichung					4%	4%						8%
Koordination der Veröffentlichung	2%											2%
Summe	**78%**	**4%**	**6%**	**4%**	**4%**	**4%**						**100%**

Erklärung zur Autorenschaft

Electrochromic Polymer Ink Derived from a Sidechain-Modified EDOT for Electrochromic Devices with Colorless Bright State, Sven Macher, Mauro Sassi, Luca Beverina, Uwe Posset, Marco Schott, Guinevere A. Giffin, Peer Löbmann, ChemElectroChem, 2021, 8, 726-734.

Detaillierte Darstellung der Anteile an der Veröffentlichung (in %)
Angabe Autoren/innen (ggf. Haupt- / Ko- / korrespondierende/r Autor/in) mit Vorname Nachname (Initialen)

Sven Macher, Hauptautor (SM), Mauro Sassi (MSas), Luca Beverina (LB), Uwe Posset (UP), Marco Schott, korrespondierender Autor (MSch), Guinevere A. Giffin (GG), Peer Löbmann (PL)

Autor	SM	MSas	LB	UP	MSch	GG	PL					∑ in Prozent
Synthese u. Präparation EC-Dispersion	10%	5%	5%	5%								25%
Beschichtung EC-Dispersion	10%											10%
Charakterisierung Schichten (optisch)	10%		5%									15%
Charakterisierung Schichten (elektrochem.)	8%	2%										10%
Charakterisierung Schichten (Stabilität)	10%											10%
Verfassen der Veröffentlichung	12%			5%	3%							20%
Korrektur der Veröffentlichung					4%	2%	2%					8%
Koordination der Veröffentlichung	2%											2%
Summe	**62%**	**7%**	**10%**	**10%**	**7%**	**2%**	**2%**					**100%**

Julius-Maximilians-
UNIVERSITÄT
WÜRZBURG

Fakultät für
CHEMIE UND
PHARMAZIE

Erklärung zur Autorenschaft

Colloidal Coating Dispersion, Sven Macher, Mauro Sassi, Luca Beverina, Uwe Posset, Marco Schott, 2020, Europäisches Patent, EP 3 654 094 A1.

Detaillierte Darstellung der Anteile an der Veröffentlichung (in %)
Angabe Autoren/innen (ggf. Haupt- / Ko- / korrespondierende/r Autor/in) mit Vorname Nachname (Initialen)

Sven Macher, Hauptautor (SM), Mauro Sassi (MSas), Luca Beverina (LB), Uwe Posset (UP), Marco Schott, korrespondierender Autor (MSch)

Autor	SM	MSas	LB	UP	MScht							∑ in Prozent
Anteil gemäß Erfindungsmeldung	20%	18%	18%	10%	4%							70%
Verfassen der Veröffentlichung	15%			5%								20%
Korrektur der Veröffentlichung				8%								8%
Koordination der Veröffentlichung	2%											2%
Summe	**37%**	**18%**	**18%**	**23%**	**4%**							**100%**

Selbstständigkeitserklärung

Hiermit erkläre ich, dass ich die vorliegende Arbeit selbständig verfasst und keine anderen als die angegebenen Quellen und Hilfsmittel verwendet und die Arbeit keiner anderen Prüfungsbehörde unter Erlangung eines akademischen Grades vorgelegt habe.

In dieser Dissertation werden Ergebnisse der Masterarbeit "*Systematische Untersuchung des reversiblen Photobleaching-Effekts von elektrochromen Preußisch Blau-Dünnschichten*" von Moritz Wozar (Universität Würzburg, Fakultät für Chemie und Pharmazie, 2019) genutzt. Diese Arbeiten wurden unter der Anleitung von Herrn Prof. Dr. Peer Löbmann und mir durchgeführt. Die Datenanalyse und wissenschaftliche Interpretation der Ergebnisse fand in enger Diskussion mit Moritz Wozar statt. Er hat der Weiterverwendung der von ihm erhaltenen Daten zugestimmt.

Weiterhin werden in dieser Dissertation Ergebnisse der Praktikumsarbeiten "*Internship Report for the Lecture 'Elektrochemische Energiespeicher und -wandler'*" von Hendrik Bohn (Universität Würzburg, Fakultät für Chemie und Pharmazie, 2019) und "*Untersuchung von Elektrolyten zur Verbesserung der Zyklenstabilität elektrochromer Elemente unter feuchten Umgebungsbedingungen*" von Tim Schembri (Universität Würzburg, Fakultät für Chemie und Pharmazie, 2020) genutzt. Diese Arbeiten wurden ebenfalls unter der Anleitung von Herrn Prof. Dr. Peer Löbmann und mir durchgeführt. Die Datenanalyse und wissenschaftliche Interpretation der Ergebnisse fand in enger Diskussion mit Hendrik Bohn und Tim Schembri statt. Sie haben der Weiterverwendung der von ihnen erhaltenen Daten zugestimmt.

Würzburg, 12. März 2021 Sven Macher